98-61

Seismic investigation of a salt dissolution feature in Kansas

by

Ana C. Villella
B. S., West Georgia College, 1994

Submitted to the Department of
Geology and the Faculty of
the Graduate School of the University
of Kansas in partial fulfillment of
the requirements for the degree of
Master of Science

_____
Chairman

_____

_____

_____
Department Chairman

Date submitted: _____

To Vilma, Nino and Alessandro for all their love and support.

Acknowledgments

Contents

Abstract 6
Introduction 7
Geologic Background 9
Evaporite Deposits 15
Salt dissolution processes and formation of sinkholes 17
Subsidence caused by oil and gas operations in Kansas 20
Panning Sinkhole 24
Crawford and Witt Sinkholes 28
History of the French "A" no.1 well 33
Seismic Acquisition 39
Seismic Processing 42
Shot domain processing 48
CMP domain processing 56
Experimental low fold 3-D survey 68
Synthetic Seismogram 69
Seismic Interpretation 73
Structural Interpretation 82
Conclusions 89
References 92
Appendix A 95
Appendix B 96
Appendix C 97

Illustrations

Figures

1. Local setting of the French Sink 8
2. Stratigraphic chart of the Lower Permian in Kansas 11
3. Stratigraphic interpretation, synthetic seismogram and gamma-ray log. 12
4. Interstratal salt karst diagram 19
5. Location of sinkholes in central Kansas 23
6. Sequence of events in the formation of the Panning Sinkhole 25
7. Sequence of events in the formation of the Panning Sinkhole 26
8. Cross-section through the Witt and Crawford Sinks 30
9. CMP stack along I-70 32
10. Schematic section of the French "A" no. 1 well 34
11. Aerial photograph of the study site 35
12. Photograph of the French site 37
13. Photograph of the French site 38
14. Photograph of vibrator truck 40
15. Contour map of the study site 43
16. Block diagram of the study site 44

17. Processing flow chart for the first acquisition survey 46
18. Processing flow chart for the second acquisition survey 47
19. FK spectrum of shot gather 1078 49
20. FK spectrum of shot gather 2340 50
21. Mute zones applied to shot gather 2340 53
22. Example of using noise adaptive filtering 55
23. Example of spectral balancing shot gather 2340 57
24. Stacking velocity field from line1, trip1 59
25. Stacking velocity field from line2, trip1 60
26. Stacking velocity field from line3, trip1 61
27. Stacking velocity field from line1, trip2 62
28. Stacking velocity field from line2, trip2 63
29. NMO corrected CMP gather 4230 64
30. Gamma-ray and sonic logs form the French and Staub wells 70
31. Interpreted CMP stack from line1, trip1 74
32. Interpreted CMP stack from line2, trip1 75
33. Interpreted CMP stack from line3, trip1 76
34. Interpreted CMP stack from line1, trip2 77
35. Interpreted CMP stack from line2, trip2 78
36. Stress regime around a cavern in horizontal strata 84
37. Shear and compressional stresses on a sagging beam 85
38. Classification of common rocks according to strength 88

Plates

1. CMP Stack from line1, trip1
2. CMP Stack from line2, trip1
3. CMP Stack from line3, trip1
4. CMP Stack from line1, trip2
5. CMP Stack from line2, trip2
6. True-Fold map from line1, trip1
7. True-Fold map from line2, trip1
8. True-Fold map from line3, trip1
9. True-Fold map from line1, trip2
10. True-Fold map from line2, trip2
11. CMP Stack from line1, trip2
12. True-Fold map from line1, trip2
13. CMP Stack from line2, trip2
14. True-Fold map from line2, trip2

Abstract

Shallow seismic reflection techniques successfully delineated the main structural and stratigraphic features of a salt dissolution sinkhole formed in the vicinity of a disposal well. The French sinkhole formed by gradual subsidence of a surface area of approximately 15,000 m^2 in the North St. John oil field in central Kansas. Subsidence resulted from deformation and failure of rock units overlying a solution opening formed by dissolution of the Permian-Hutchinson Salt member found approximately 400m deep at the study site. High resolution seismic images reveal important information on the mechanisms of formation of the French sinkhole and map dissolution altered zones for appraisal of the development of the structure.

Five 2-D seismic reflection profiles were acquired and processed to generate common-mid-point (CMP) stack sections of the area of interest. Processing flow was consistent with standard seismic reflection investigations focusing in the careful removal of coherent noise before stacking. True-fold maps of the CMP stacks and fold decimation studies were key in evaluating changes in signal-to-noise ratio as a function of geology or a function of fold content. A synthetic seismogram was used to aid in the stratigraphic interpretation of the final CMP stacks. A low-fold, minimal deployment 3-D survey was carried out to evaluate the feasibility and potential of the technique in shallow site characterization.

Reflections from key stratigraphic horizons reveal precursory plastic deformation and failure of units confined to a tension dome centered at the well location and extending from within the salt interval to the surface. This dome resulted from changes in the stress regime after dissolution of the salt interval by unsaturated brines flowing through a faulty well casing which formed an open cavity. Continuous access of unsaturated brines to the salt through the wellbore and pathways opened by failure within the tension dome result in the present dissolution front extending outward from the center of the structure a distance of approximately 250 m. The source of unsaturated brines is attributed to both disposal practices and groundwater.

Ana Villella, M. S.
Department of Geology, 1998
University of Kansas

Introduction

Sinkholes represent a common hazard to property and safety the world over and can be initiated by natural or induced dissolution processes. Understanding the processes by which sinkholes form is key in minimizing the impact and risks associated with their formation and is essential in preventing their occurrence. Shallow high resolution seismic investigations have proven successful in imaging salt dissolution sinkholes in central Kansas and other parts of the world (Steeples et al., 1986, Knapp et al., 1989, Miller et al., 1997). The high resolution potential of the seismic data in this study enables imaging of important structural features controlling mechanisms of sinkhole development.

Petroleum activities in central Kansas, in particular brine disposal in shallow and deep well systems, have been responsible for localized dissolution of the Hutchinson Salt which underlies a significant portion of south central Kansas and north central Oklahoma (figure 1). Drilling of wells through the salt section with early and modern rotary tools using unsaturated mud with respect to chlorides results in contained borehole enlargement not known to cause surface subsidence. Inadequate or faulty casing which fails to isolate the salt interval from shallower aquifers and disposal brines are the

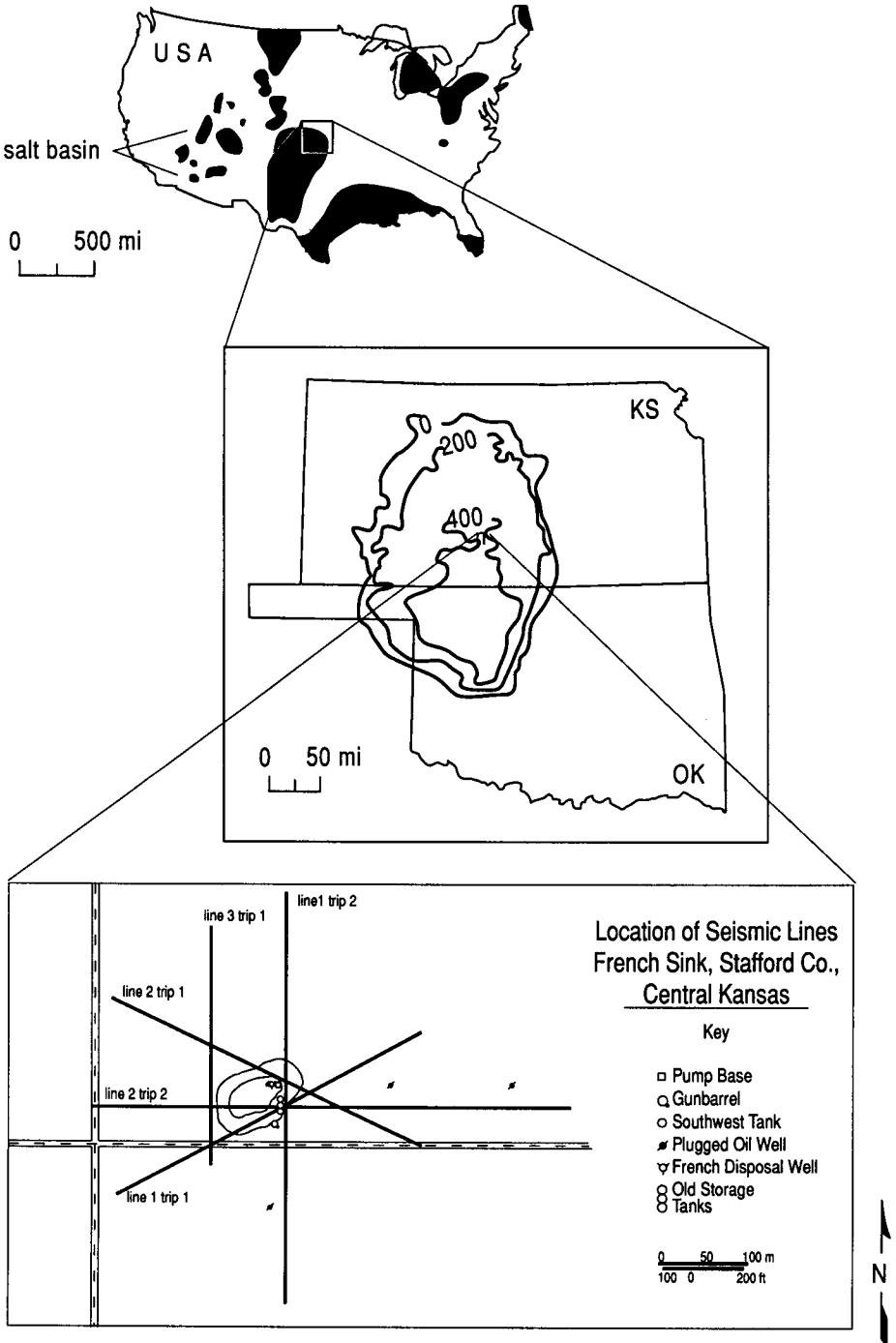

Figure 1. Site map showing relative locations of (a) major salt basins in the United States (Ege, 1984) with (b) a generalized isopach map of the Hutchinson Salt Member in Kansas and Oklahoma (Walters, 1977), and (c) the relative location of the seismic reflection lines to the sinkhole, SW 1/4, Section 17, T23 S, R13 W, Stafford County.

main causes for uncontrolled salt dissolution which can culminate with sinkhole development and surface subsidence.

The French sinkhole which formed around the French "A" no.1 disposal well in south central Kansas is the focus of this study. Prominent reflections from shallow Permian redbed sequences, the Stone Corral Anhydrite and from anhydrides within the Hutchinson Salt provide a distinct image of the subsurface at the French site. Previous seismic reflection investigations around oil wells in central Kansas have depicted bed offset and reflector drape as indications of rock deformation and failure above dissolution voids within the Hutchinson Salt (Knapp et al., 1989, Miller et al., 1995). The high resolution potential of the CMP stacks from the French site depicts a particular structural setting of a tension dome centered on the disposal well which controls the deformation features observed at the previous studies.

Geologic Background

The stratigraphic units that are the target of this seismic study are Lower Permian and include (Norton, 1939): the Chase Group, the Sumner Group, and the Nippewalla Group (figure 2). These units are interpreted from a gamma ray and laterolog survey obtained at the time of drilling of the French #1 A well (figure 3). The type log for Stafford County used to aid in the lithologic and stratigraphic interpretation of the French site is provided in Appendix A. The close match between the French well logs and the type log eased the identification of lithostratigraphic units and improved the reliability of the interpretations presented here. The similarity between these logs can be attributed to the proximity between the wells as well as to the lateral continuity of the Permian deposits in central Kansas.

The Chase Group is the deepest unit of interest and consists of approximately 102m of marine limestones, dolomites, shales and siltstones (Watney et al., 1988). The top of the Chase Group is found at 570m of depth at the study site and is marked by the presence of cherty limestones. The Chase Group deposits formed in a basin open to the sea which covered most of south central Kansas during the Lower Permian.

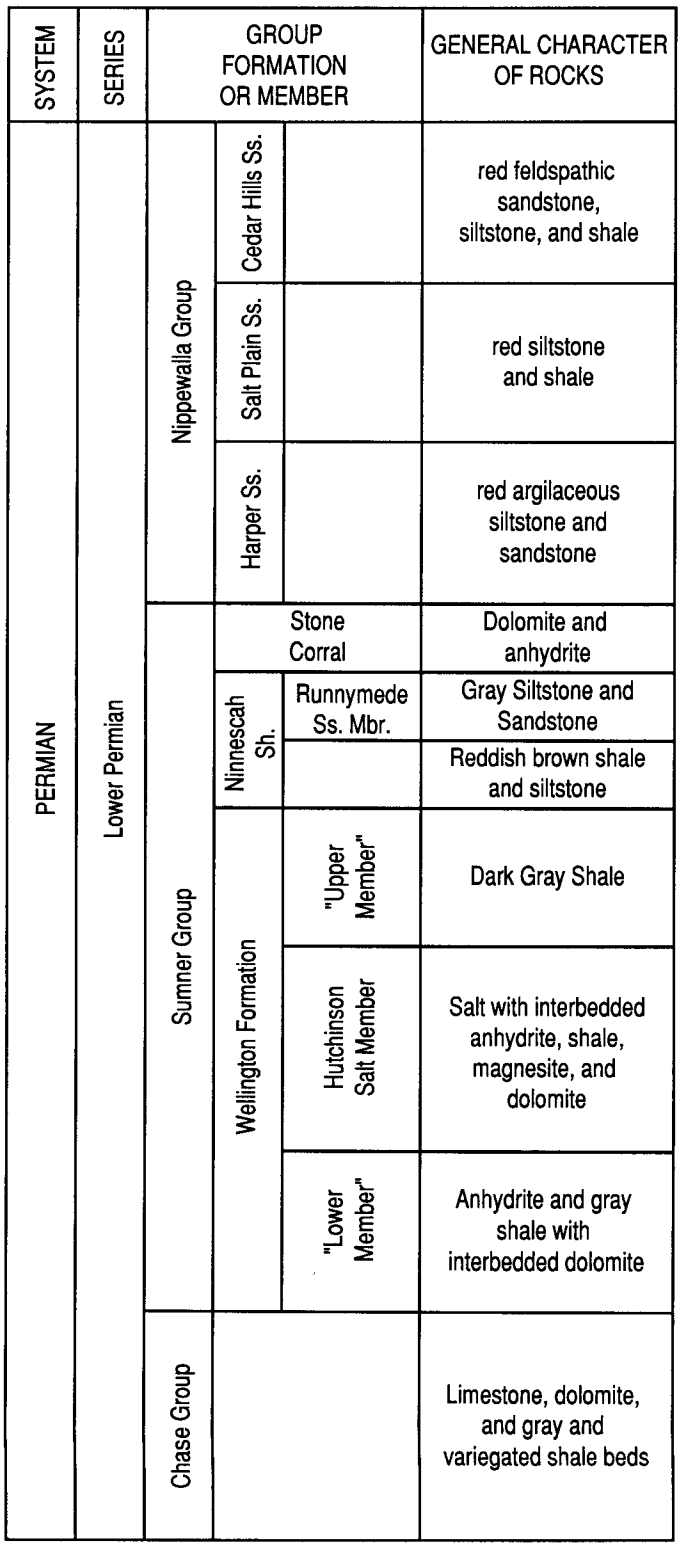

Figure 2. Simplified stratigraphic chart of the Lower Permian in Kansas. Modified from Watney et al., 1988.

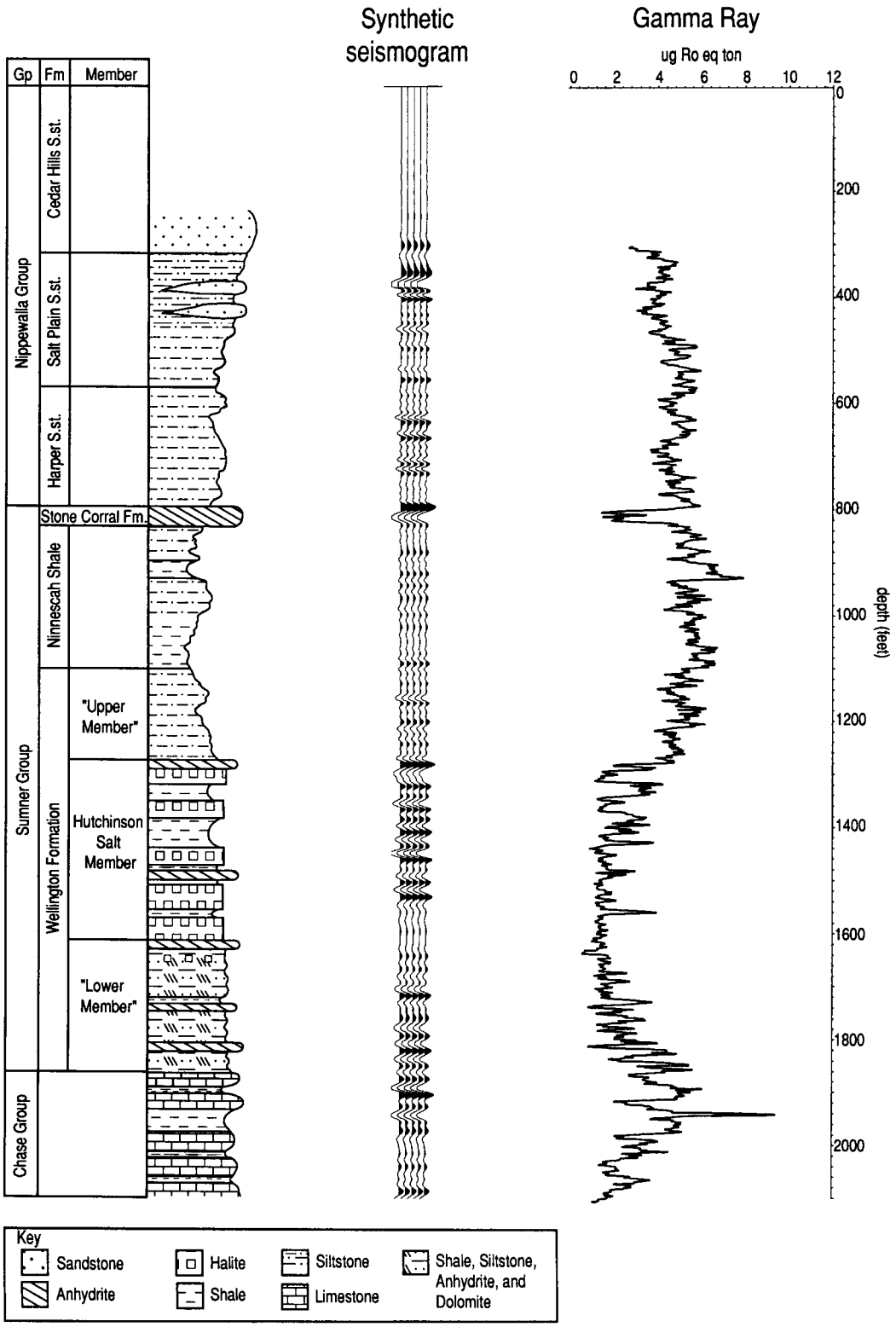

Figure 3. Stratigraphic interpretation (left), synthetic seismogram (center) and gamma-ray curve (right) of the French well.

The Sumner Group is the focus of this study and consists of the Wellington Formation, the Ninnescah Shale and the Stone Corral Formation. The Wellington Formation marks the transition from the marine deposits of the Chase Group to the redbed evaporites of the Ninnescah Shale and Stone Corral Formation. The Wellington Formation is about 265m thick and is comprised of an unnamed lower and upper member with the Hutchinson Salt Member in between them. The lower member is found at 492m of depth and is composed of anhydrite and gray shale with interbedded dolomite. The contact between this member and the overlying Hutchinson Salt is gradational. The Hutchinson Salt Member is a stratigraphic succession of halite, shale, minor anhydrite and dolomite/magnesite (Watney et al., 1988) about 100m thick at the French site. A gradational transition exists between the Hutchinson Salt and the dark gray shales of the unnamed upper member of the Wellington Formation.

Overlying the Wellington Formation is the Ninnescah Formation, followed by the Stone Corral Formation. These two uppermost units of the Sumner Group combined represent the onset of arid conditions during the Lower Permian. The Ninnescah Formation is formed by a succession of disconformable red-brown shales and siltstones and is found at about 256m deep. The Stone Corral Formation is found at the depth of 244m and consists of dolomites and anhydrites.

The shallowest units of interest for this study are of the Nippewalla Group which include the redbeds between the ground surface and the top of the Stone Corral Formation. The Harper Sandstone, the Salt Plain Formation and the Cedar Hills Sandstone are the formations from the Nippewalla Group that can be interpreted from the French wireline logs. The Harper Sandstone is found at 175m of depth and consists of approximately 70m of siltstone and fine sandstone. The Salt Plain Formation is characterized by a series of red shales and siltstones with a total average thickness of about 80m. The Cedar Hills Sandstone is composed of red feldspathic sandstone, siltstone and silty shale. This sandstone unit was widely used from the late1930's to the early 1950's for shallow disposal of oil field brines until deep water disposal well systems were introduced in the early 1960's (Walters, 1991).

Deeper stratigraphic units not imaged by the seismic surveys but important to this study are the "Granite Wash" and the Arbuckle Group. "Granite Wash" refers to arkosic detrital material resting on older Precambrian rocks (Zeller, 1968). These rocks range from Precambrian to Middle Pennsylvanian and are found at a depth of approximately 1356m at the French Sink site. The French #1A disposal well used the Granite Wash as the receptacle for salt water brines produced from nearby oil wells. Most of these brines came with oil produced from the unit sitting atop the Granite Wash. This unit, referred to as the Arbuckle Group, is responsible for most of

the oil production in central Kansas and is composed of Upper Cambrian and Lower Ordovician dolomites. At the French well, the top of the Arbuckle Group is found at a depth of 1210m.

Evaporite Deposits

The Hutchinson Salt Member occurs in central Kansas, northwestern Oklahoma and the northeastern portion of the Texas panhandle (figure 1), and is prone to dissolution and formation of sinkholes. Deposition of this unit occurred in a shallow basin that was sporadically open to the southwest (Watney et al., 1988) throughout the Lower Permian. Early in the history of the basin, maximum halite accumulation took place to the northeast while anhydrite deposition dominated the southwest. Progradation of halite over anhydritic sediments resulted in a NE-SW trend of the basin's depocenter. Based on subsequent facies change from evaporite to shale, progradation of shale from the basin margins towards its center can be inferred. Overall, the depositional basin is characterized by a gentle, uniform westward dip. Its eastern edge is marked by a solution front where proximity to the present land surface (less than 91m) has allowed localized natural access to groundwater (Walters, 1977).

In Kansas, the Hutchinson Salt extends over approximately 95,793Km² (Watney et al., 1988) with an average net thickness of 76m and reaching a maximum of over 152m in the northeastern part of the basin. Deposition occurred during fluctuating sea level causing numerous halite beds, 0.15 to 3m thick, to be formed interbedded with shale, minor anhydrite and dolomite/magnesite. Individual salt beds may be continuous for only a few miles despite the remarkable lateral continuity of the salt as a whole (Walters, 1977). Thin anhydrite beds within the halite succession have strong acoustic response, and were used to aid the interpretation of stacked sections in this study.

Another stratigraphic unit key to this investigation is the Stone Corral Formation. This 12m thick formation marks the top of the Sumner Group and consists of two massive anhydrite beds separated by a shale. The Stone Corral is a laterally continuous unit with widespread distribution. It is essentially horizontal at the study site and is found at a depth of 244m. This marker bed provides a readily identifiable unit for structural mapping and correlation purposes. The Stone Corral is a strong reflecting zone and has been used in the past to aid structural interpretation of seismic studies of sinkholes in central Kansas (Steeples et. al, 1986).

Salt dissolution processes and formation of sinkholes

Past and current natural dissolution of the Permian basin evaporites is responsible for the formation of sinkholes, subsidence troughs, collapse structures and evaporite karst. Human activities can also promote the development of dissolution related features, e.g. overmining salt deposits and inadequate seals between boreholes and evaporite deposits. Evaporite dissolution can occur very rapidly. This is because evaporites have the highest solubility of most common rocks, i.e. gypsum and salt being respectively 150 and 7,500 times more soluble than limestones (Martinez et al. 1998).

Halite is extremely soluble in groundwater having a solubility of 35.5 percent by weight at 25°C. Solubility increases at higher temperatures and solution is achieved by simple dissociation with no chemical reaction. The amount of salt removed in a system is simply controlled by the equilibrium solubility between formation and flowing water (White, 1988).

Four basic requirements are necessary for evaporite dissolution (Johnson, 1997):

(1) a deposit of gypsum($CaSo_4$) or salt (NaCl) through which water can flow;

(2) a supply of water unsaturated with $CaSo_4$ or NaCl;

(3) an outlet whereby the brine can escape; and

(4) energy (such as hydrostatic head or density gradient) to cause the flow of water through the system.

The main solution processes that take place in the formation of interstratal salt karst are discussed by Johnson, 1981 (figure 4). Dissolution starts after unsaturated groundwater percolates through permeable rocks and reaches salt beds in the subsurface. Dissolution is continuous for as long as brines remain unsaturated with respect to halite. Extensive dissolution occurs when a flow-through system permits a continuous source of unsaturated brines to be in contact with the salt.

Human activity can induce or enhance salt dissolution either intentionally or unintentionally. Solution mining is an example of intentional promotion of salt dissolution for the recovery of table salt or for the creation of Liquefied Petroleum Gas (LPG) storage cavities. Salt dissolution can also occur inadvertently when the construction or drilling of boreholes in or through salt beds fails to isolate the salt from borehole solutions. In both types of circumstance unexpected surface subsidence has occurred (Walters, 1977 and 1991).

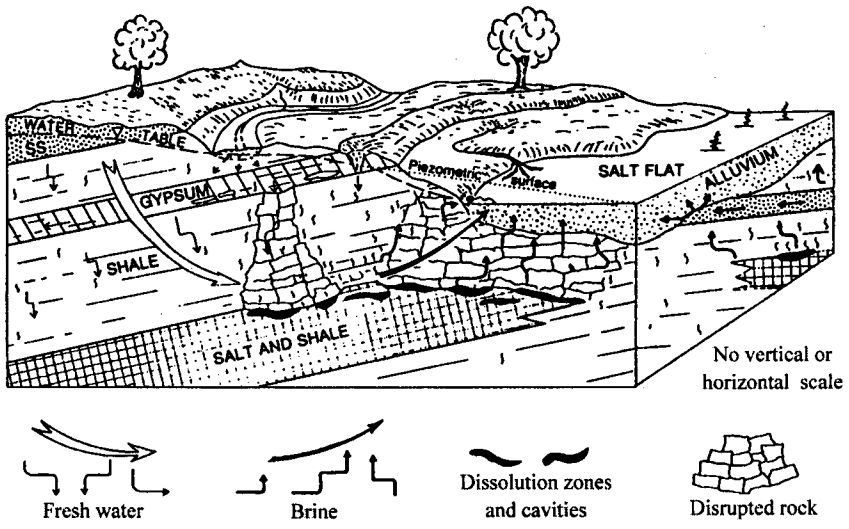

Figure 4. Interstratal salt karst in western Oklahoma (Johnson, 1981). Horizontal dimension 1-15Km; vertical dimension 30-300m.

Salt-solution mining has been a common practice in Kansas for over 100 years. Subsidence associated with this activity is rare and has been attributed to roof collapse caused by the use of the single borehole method of salt dissolution which was in practice between 1888 and 1960. Modern techniques, however, employ the use of multiple boreholes which assure surface stability by limiting roof spans. Walters (1977) gives a detailed description of five known sinkholes associated with solution mining in central Kansas. The most spectacular example is the Cargill sinkhole, which formed in three days and resulted in a crater 91m in diameter.

Subsidence caused by oil and gas operations in Kansas

Walters (1977) recognized only eight known cases of land subsidence attributed to oil and gas operations in Kansas. At the time, 80,000 oil and gas test holes had been drilled through the Hutchinson Salt, making a ratio of one land subsidence per 10,000 oil and gas test holes. In all of the cases, subsidence took place in association with deep or shallow salt water disposal (SWD) systems. Since Walters' study, a larger number of land subsidence cases is believed to be directly linked to oil production in Kansas. In Stafford County for example, eight cases of subsidence have been monitored by the Kansas Corporation Commission in the past ten years. In all of the cases,

dissolution has been caused by faulty well casings in association with disposal well systems.

Since its discovery in 1923, oil in central Kansas has been produced from aquifer reservoirs which contain large amounts of brine. Approximately 75 percent of the oil produced in the area comes from the Arbuckle dolomite reservoir which has very strong water drive.

Many wells in the Chase-Silica Oilfield in Barton and Rice counties for example produced vast quantities of water during the depletion of the Arbuckle reservoir in the 1930's. At the time, an average of 5 barrels of salt water per 1 barrel of oil were being produced in these counties, often causing wells to become unprofitable. Disposal of these brines was done in evaporation ponds in the 1930's and in SWD wells starting in the 1940's (Walters, 1991). A study from 33 Arbuckle brine analyze (Martin, 1968) from the same oil field proved brines to be unsaturated with respect to chlorides. An average of 13,780 ppm of chloride found in these samples is very low when compared to 260,000 ppm chlorides in a saturated solution. The brine samples also contain dissolved H_2S which is corrosive to metals.

Corroded or damaged casing, combined with high energy input of large volumes of unsaturated brine in SWD systems, can cause extensive salt

dissolution when brines come in contact with the salt. Similar problems are encountered where waste brines are disposed in shallow SWD wells in central Kansas. In these shallow wells, unsaturated waste is introduced to the Cretaceous Cheyenne Sandstone and the Permian Cedar Hills Sandstone aquifers which are stratigraphically above the Hutchinson Salt. These brine-bearing aquifers are not required to be isolated by surface casing the way fresh water aquifers are. Therefore, boreholes in the vicinity of these shallow SWD wells with total depth at or below the salt interval can serve as conducts for unsaturated brines to seep downward into the underlying salt, resulting in dissolution (Walters,1991).

Years of SWD practices have resulted in cases where dissolution of large quantities of salt allowed overlying strata to subside. When large cavities form, instability of the roof spans results in upward progressive collapse of the rock units above the salt, culminating in surface subsidence and the formation of sinkholes. The Panning Sinkhole and the Crawford and Witt sinks, all in central Kansas (figure 5), are examples of sinkholes associated with leaky disposal wells and because of similarities with the French Sink are briefly discussed below.

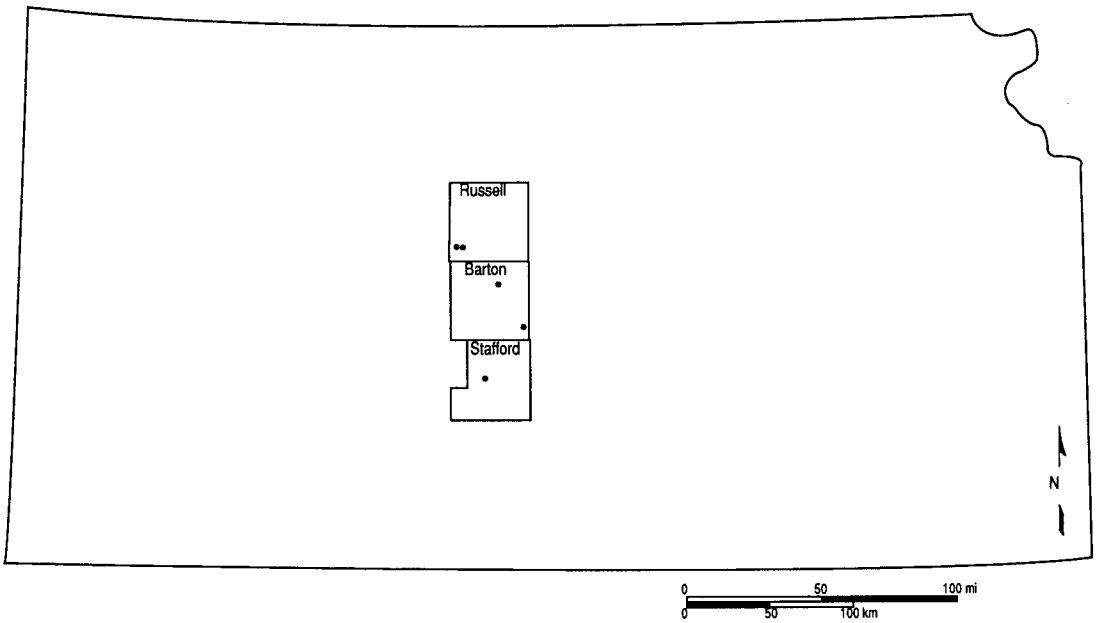

Figure 5. Location of the Witt and Crawford sinkholes (west and east respectively in Russell County) and the Panning sinkhole (Barton County) in relation to the French Sink (Stafford County).

Panning Sinkhole

The Panning Sinkhole in the Chase-Silica Oilfield in Barton County formed very rapidly, in a matter of hours, in April 1959. Its circular surface expression reached approximately 100m in diameter and 24m in depth centered around the Panning 1-A salt water disposal well. A reconstruction of the formation of this sinkhole (Walters, 1977) is based on observations and records of the well (figure 6 and figure 7).

During drilling of the Panning 1-A well in 1938, fresh water mud caused dissolution of the Hutchinson salt to a diameter of about 54 inches around the center of the well. After completion, the well produced about 100,000 barrels of oil until 1946, when oil depletion led it to be converted into a disposal well; at this time the well was deepened to a total depth of 1173m for oil brine disposal in the Granite Wash Formation. Recompletion of the well involved cementing of the salt interval but the upper 35m portion of the salt section was left open. Oil field brines were injected through a 3-inch plastic tubing for the following 3 years. No salt dissolution is believed to have occurred while the well was producing oil nor during the period in which disposal brines were being injected through the 3-inch tubing. However, in 1949 the inner tubing was removed to allow for disposal of larger amounts of brine, resulting in brines being injected down the 6-inch casing at an average of 2485 barrels of

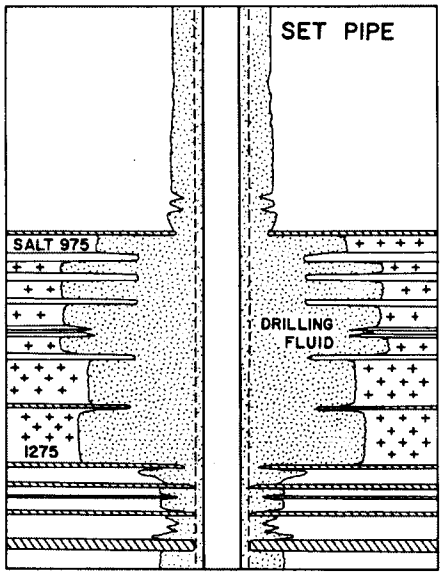

Fresh water drilling fluid dissolved salt to a diameter of 54 inches.

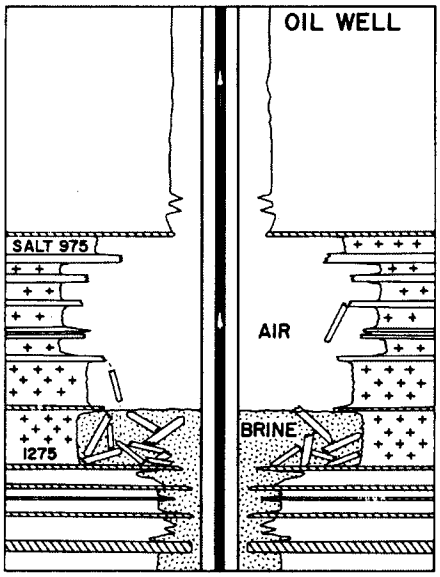

100,000 barrels of oil being produced; no salt dissolution; shale interbeds in the salt section collapsed.

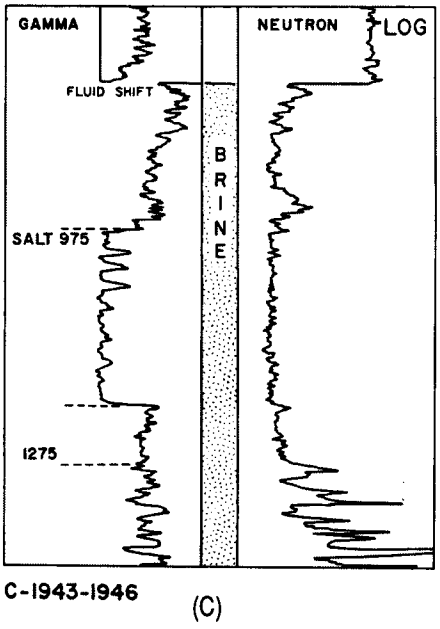

Gamma-neutron log from nearby well show the static fluid level of the Arbuckle to be 912 ft from the top of the hole. No salt dissolved. Well abandoned due to oil depletion.

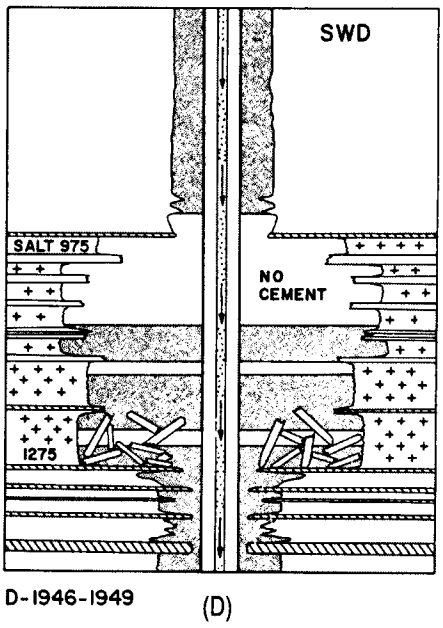

Well converted for use as a SWD by recementing the casing. No cement opposite the upper salt section; brines disposed through inner tubing; no salt dissolved.

Figure 6. Postulated sequence of events for the formation of the Panning Sinkhole (modified from Walters,1977).

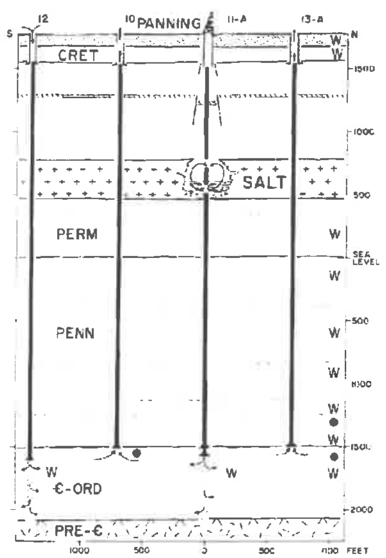

(A)

1949 - 1958. Tubing was removed from this disposal well and brine was disposed directly down the casing. Corrosion resulted in casing leaks, permitting access for 72 gpm of brine, 14,000 ppm chlorides, to circulate across the salt face, then downward into the Arbuckle aquifer. A huge cavern dissolved in the salt, no larger than 300ft in diameter. Progressive falls of shale interbeds and shale roof rocks partially filled the cavern. Successive roof falls caused the void space to gradually migrate upward to near the Stone Anhydrite, depth 465 ft (1300 ft above sea level) causing, in turn, surface subsidence, ponding of water, and tilting of the derrick.

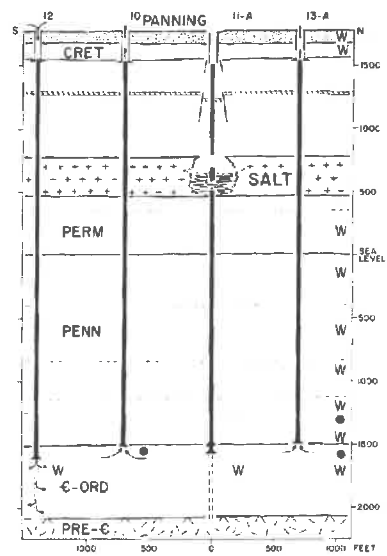

(B)

January, 1959. The Panning 11-A was abandoned but not plugged. The derrick was removed because surface subsidence caused it to tilt dangerously. With disposal brine flow discontinued, salt dissolution ceased.

	Sand		Granite
	Anhydrite	W	Water
+ + +	Salt	●	Oil
	Shale		Cement

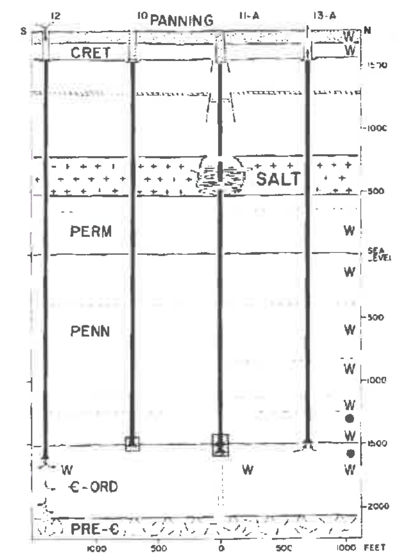

(C)

April14, 1959. The Panning 11-A was plugged with 150 sacks of cement in the surface pipe to 190 ft, and the Arbuckle was bridged. There was no other plugging. The underground void space at shallow depth was now isolated from both the near surface and the Arbuckle aquifers. Brine in the void space drained downward gradually to reach equilibrium with intermediate aquifers leaving the near surface void space unsupported by fluid and under vacuum.

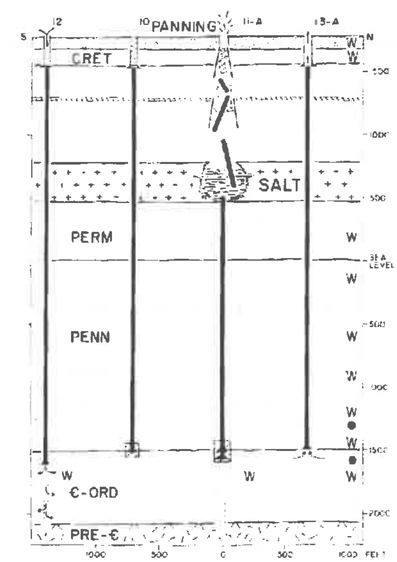

(D)

April 24, 1959. When the uppermost "keystone" bedrock at a depth of 106 ft fell into the newly drained shallow void space, the surface sinkhole formed rapidily in three hours from 9 am until noon, with some subsidence continuing until about 9 pm. As the shallow void space filled with fresh water and air, falling material such as concrete derrick corner blocks fell into the narrow aperture and compressed, them ejected, the air. The casing collapsed and fell. At first, the loose sand and gravel moved downward in a fresh water slurry at a rate faster than the flow of the aquifer, forming a deep cone shaped pit. As the void space filled, water accumulated in the surface sinkhole.

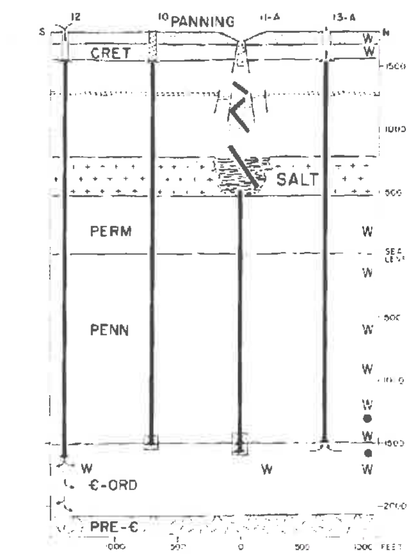

(E)

April 25, 1959 to present. The circular sinkhole diameter near 330ft, stabilized forming a fresh water pond 64 ft deep, volume near 2,000,000 ft3. In seventeen years, the surrounding fence buckled downward and inward only about 2ft on each side indicating resumption of stable subsurface conditions. Transported sand and gravel fills the shallow space voided by roof falls. The former cavern in the salt is filled and plugged with fallen Permian shale and redbeds; hence, it is thought that no further dissolution is occurring.

Figure 7. Reconstruction of events in the formation of the Panning Sinkhole (Walters, 1977).

brine per day. The chemical composition of the brines rich in H S and unsaturated with respect to chlorides (14,000ppm) caused corrosion of the casing allowing brines to circulate across the salt face. As a result, dissolution of the salt interval is believed to have formed a cavity no larger than 90m in diameter which was partially filled by falls of the overlying shale. Progressive roof failure caused the cavity to migrate upward resulting in surface subsidence. First signs of subsidence were noted in late 1957 but disposal operations continued until December 1958, when ponding of water around the well and tilting of the derrick led to the abandonment of the well. The well was plugged four months later by cementing the surface pipe to 190 ft and bridging the Arbuckle.

The Panning sinkhole formed catastrophically ten days after the plugging of the well. Termination of brine injection and plugging of the well caused the upper portion of the cavity to be devoid of brine, leaving the roof rocks unsupported by fluid. The surface expression of the sinkhole formed in only three hours, with very little to no subsidence occurring since then. Walters' model provides a thorough explanation for the formation of the Panning Sink. Photographs taken at the scene during different stages of development of the Panning Sink and the accounts of eyewitnesses provide a solid basis for the model. Valuable insight on some of the mechanisms

involved in the formation of the French Sinkhole can be gained from Walters' model.

Crawford and Witt Sinkholes

The Crawford and Witt sinkholes in the Gorham Oilfield, Russell county, central Kansas, are examples of surface subsidence associated with shallow SWD systems. During the 20 years that had passed since subsidence first started in 1957 and 1977 (Walters, 1977 and 1991), total subsidence in the Crawford sink had reached 8m while 5.2m of subsidence had occurred in the Witt sink. Approximately 533m along Interstate 70 (I-70) which crosses 52m north of the sinks were affected by ground subsidence, resulting in costly repairs.

The Crawford sink formed around two oil wells, 15m apart, that were plugged in the early 1940's, while the Witt sink formed around a single oil well plugged in 1957 (figure 8). Ponding of an area of three acres, revealed through an aerial photograph from 1957, was the first evidence of subsidence around the Crawford sink. I-70 was constructed between 1965 and 1966 but subsidence was only detected near completion of the highway. In 1967, an observation test hole was drilled between the twin Crawford wells by the

Highway Commission to investigate the subsiding ground. A comparison between the gamma-neutron log recorded at the test well and the drillers' log of the twin wells revealed 8.5m of subsidence on the top of the Nippewalla Group, 11.6m of subsidence on the Stone Corral Anhydrite and about the same amount on the top of the salt.

Other exploratory test wells drilled by the Highway Commission found that the principal source of water responsible for dissolution of the Hutchinson salt was derived from the Cheyenne and Cedar Hill Sandstones. These sandstones were used for salt-water disposal through three local wells (figure 8). Disposed brines were unsaturated with respect to sodium chloride, possessing a large capacity for dissolving salt. Wells drilled in that area are not required to have casing at the interval of these shallow brine aquifer sands. It is believed that brines from these shallow aquifers drained down along the sidewalls of boreholes in the area and gained access to the salt. Subsidence in both sinkholes has been less than 0.3 ft per year and is continuing at declining rates.

Steeples et al. (1986) led a seismic reflection investigation of the I-70 sinks using the MiniSOSIE method (Barbier et al., 1976). Seismic energy was provided by two Wacker earth tampers and nearly 4km of six-fold common-depth-point (CDP) data were acquired in the presence of heavy

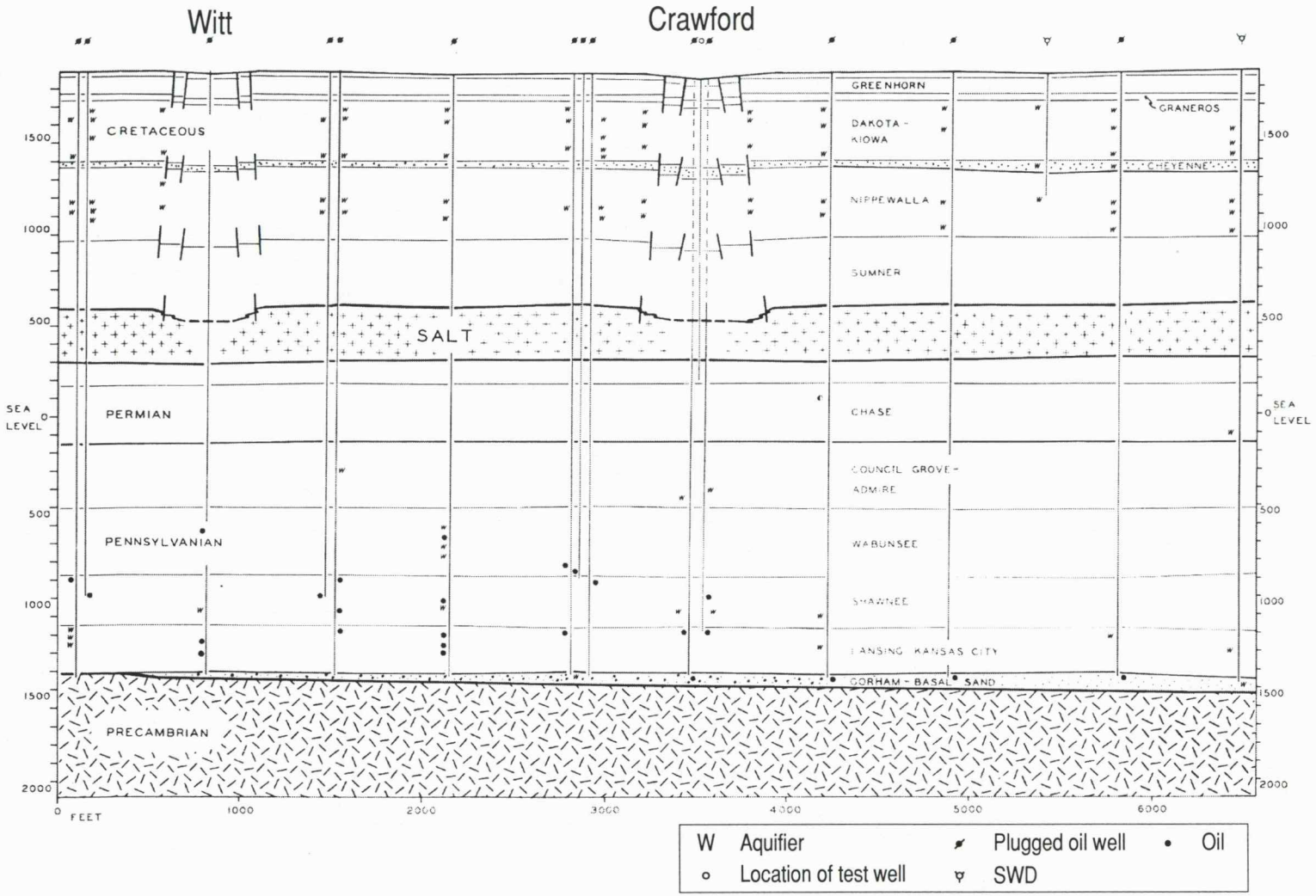

Figure 8. Cross-Section through the Witt and Crawford Sinks, Gofham Oilfield. Natural scale, no vertical exaggeration. Length of section depicted, 6500 feet (Walters, 1977).

traffic along I-70. Recorded frequencies from 80 to 120Hz from reflections from the Stone Corral Formation revealed a drop from its original position of about 15m in the Witt Sink and nearly 45m in the Crawford Sink. The structural interpretation proposed by Steeples et al. is that both sinkholes present graben-like features, bounded by sets of normal faults symmetrically placed around the center of the each sinkhole (figure 9). Steeples studies of the I-70 sinkholes (1979, 1986) impart the feasibility of the seismic reflection technique in investigating the subsurface structure of sinkholes in central Kansas. The success achieved in imaging the structure of these features can be attributed mainly to the excellent acoustic response of the Stone Corral Anhydrite.

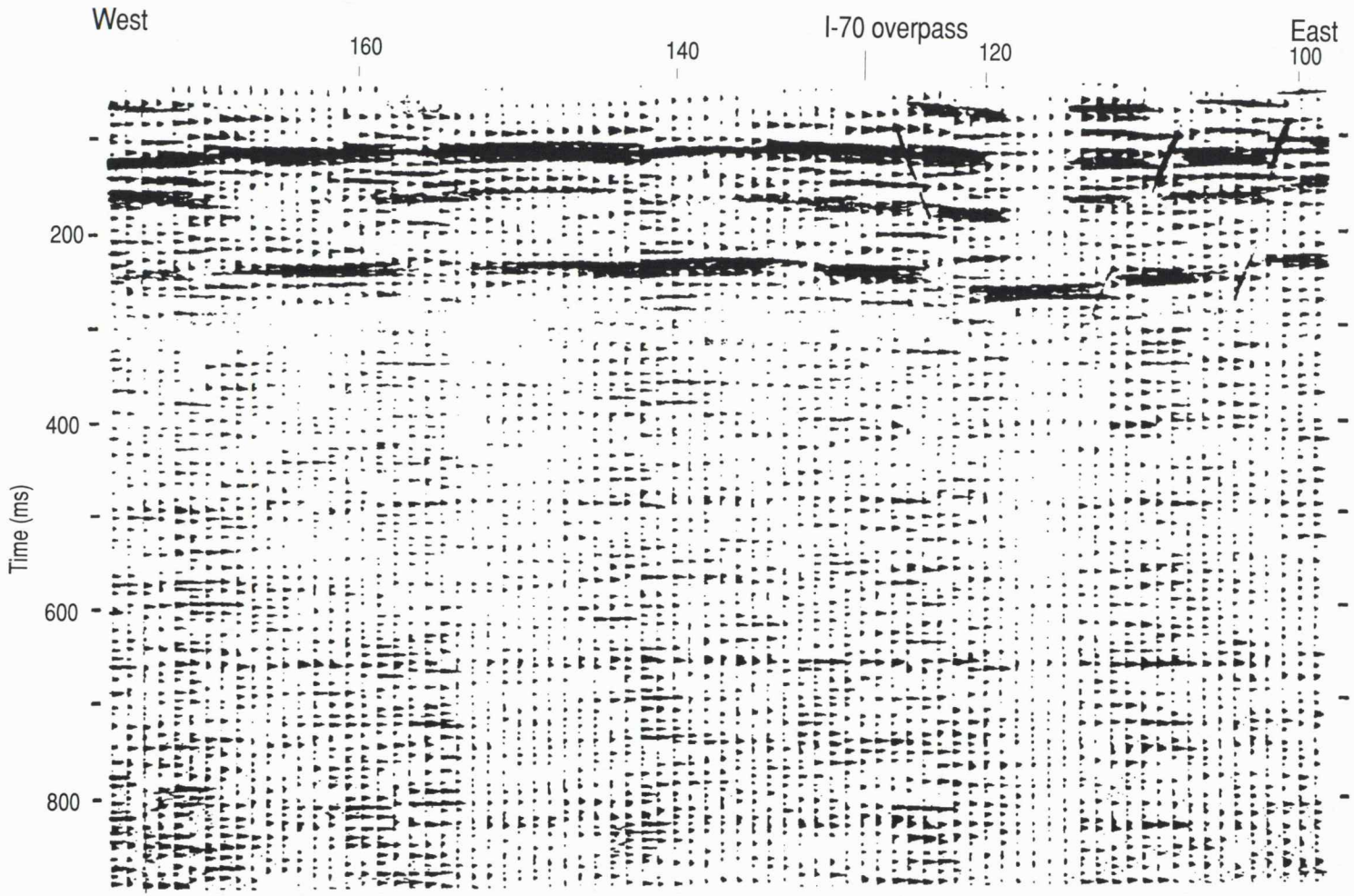

Figure 9. CMP stack section along I-70 that traverses the area between the Witt and Crawford Sink Interpretations infer the down-drop of the Stone Corral Anhydrite in the Crawford Sink (CMP 100-130, 200-300ms) due to normal faulting forming graben-like structures (Steeples et. al, 1986).

History of the French "A" no. 1 well

The French "A" no. 1 well was drilled and completed as a production well in 1955 at 100m (330ft) from the South line and 302m (990ft) from the West line of the Southwest ¼ of Section 17, Township 23 South, Range 13 West, Stafford County, Rotary style drilling was completed by D. R. Lauck Oil Co. to a total depth (TD) of 1212m (3975ft). Completion included the setting of 8 5/8" casing to 75m (245ft) with 225 sacks of cement and placement of 5 ½" production pipe to 1210 (3970ft) using 150 sacks of cement (figure 10). A drill stem test (DST) conducted in the Arbuckle from 1091m (3578ft) to TD yielded 149 barrels of oil. A gamma ray and laterolog was ran by Schlumberger from TD to 75m (245ft) of depth.

After years of use as a production well, the French "A" no. 1 was permitted in 1978 as a disposal well by the Kansas Corporation Commission (KCC). Salt water from the Schulz and Sutton producing wells (figure 11) and other nearby leases in the St. John Northwest field was disposed off in the Granite Wash Formation through the French well. Re-completion of the French to a disposal well required deepening into the Granite Wash at a depth of 1394m (4575ft). A 4" casing was used to seal of the Arbuckle and 3" fiberglass tubing was run to from the ground surface to a depth of 884m (2900ft) (in compliance with the KCC requirements) (figure 10). Brine

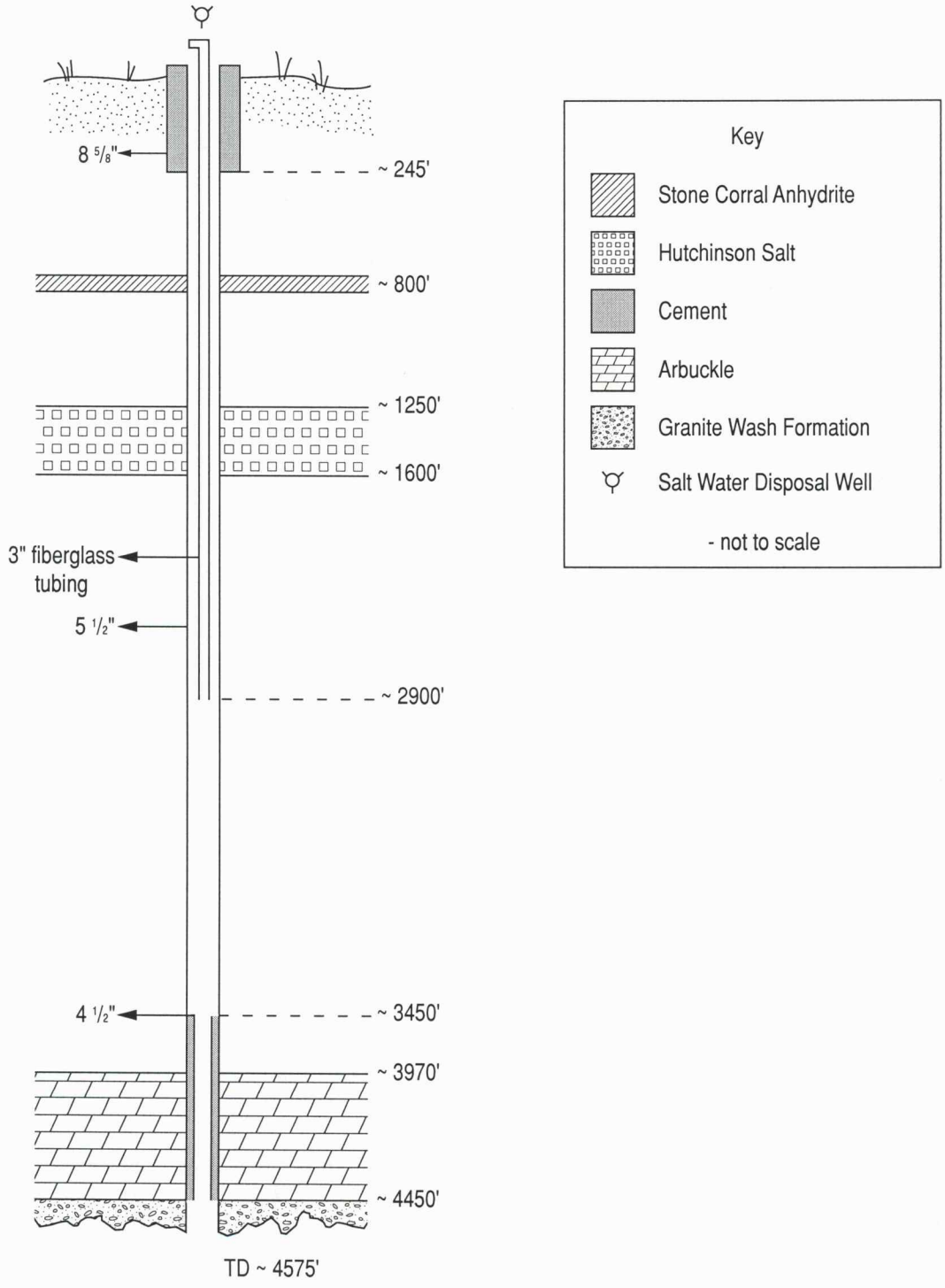

Figure 10. Schematic cross-section of the French "A" no.1 well.

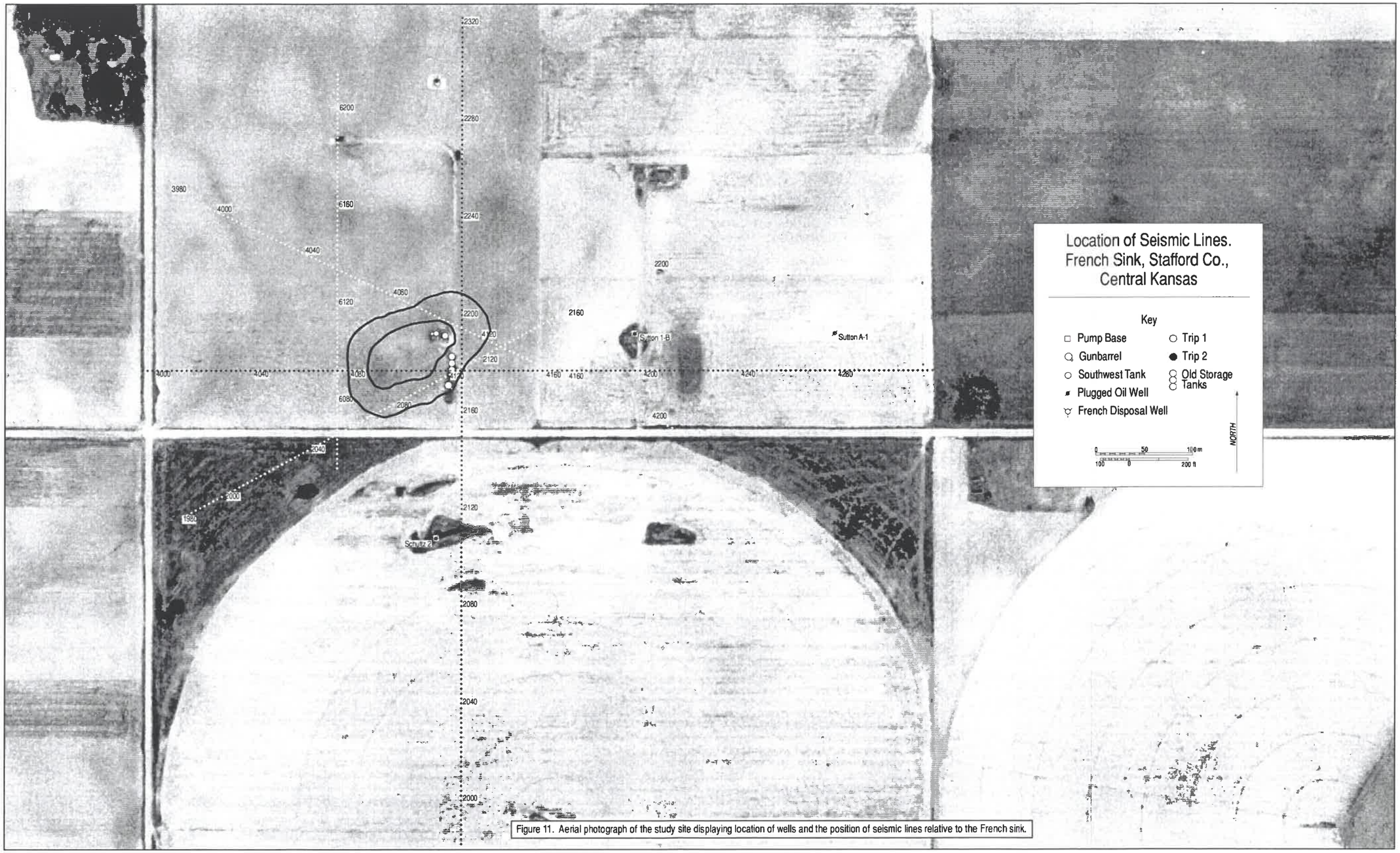

Figure 11. Aerial photograph of the study site displaying location of wells and the position of seismic lines relative to the French sink.

introduction was permitted at the well-head at a minimum of 800 barrels per day and a maximum of 1000 barrels per day under gravity pressure from a large receiving and settling tank just to the east of the well-head (figure 12). The amount and chemical composition of the disposal brines introduced over the life of the French disposal well are not known.

Subsidence at the French site was first noted in 1991. It is reported that the casing parted at a depth of 274m (900ft) with 884m (2900ft) of 3" fiberglass tubing in the hole in August 1991. Since 1991 the KCC has been monitoring subsidence at the site and has reported a gradual drop in the wellhead and pump base elevation of over 2m. The rate of subsidence at the well is currently about one foot per year. Surface subsidence influences approximately 15,000m^2 of agricultural land approximately centered on the wellhead (figure 13). Ponding of an area of approximately 5,000m^2 can produce water depths up to 1m in places restricts access to the well (figure 12).

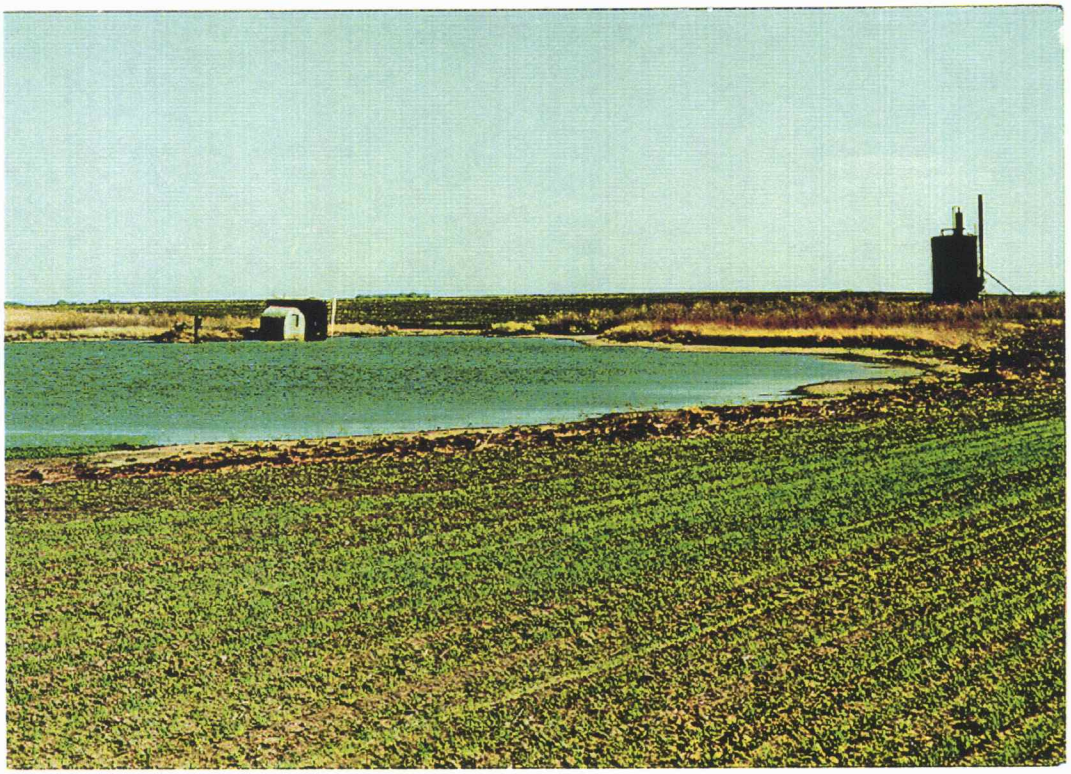

Figure 12. View of the French site looking to the northeast.

Figure 13. View of the subsidence area around the French well (looking east).

Seismic Acquisition

Seismic data for this study were acquired during two separate trips to the study site. During the preliminary site visit in 1995, three lines were deployed in a triangular pattern centered on the sinkhole (figure 11). A follow-up trip during the summer of 1997 included acquisition of two more lines. Design of these two lines was based on the results of the first trip, being oriented N-S and E-W, crossing near the subsurface center of the dissolution feature.

Acquisition parameters were defined based on a series of walkaway tests along line 1 during the first trip. Triple Mark Products L28E 40Hz geophones were deployed on 5m intervals in approximate 1m arrays. Geophones were planted into plowed fields after the top few inches of loose soil and vegetation were removed to insure good coupling. Two 48-channel, 24-bit Geometrics Strata View seismographs were linked to allow 96 channel recordings. An IVI Mini vibrator (figure 14) delivered three 10 second 30-300Hz up-sweeps recorded separately for each shot location. An initial unrecorded sweep insured the vibrator pad was well seated with good coupling at each shot point. The synthetic pilot was telemetered from the vibrator to the seismograph and recorded on the first trace of each shot

Figure 14. Vibrator truck used as a seismic source.

record. Each of the three shots per station was correlated with the pilot trace and vertically stacked.

During the first trip, lines 1 and 2 were acquired using a 96 fixed receiver spread. Shot locations were spaced at 5m intervals, with a 2.5m inline offset and approximately 15m offline offset from the receiver line. Approximately 530m of the line possesses continuous subsurface coverage with 2.5m common- mid-point (CMP) spacing. A maximum of 92 fold was recorded near the center of the spread, tapering off toward each end. Line 3 was acquired using the same methodology but was limited to only 69 recording stations by a corn field to the south of the County Line Road (figure 11). This limitation decreased the subsurface coverage to about 325m and maximum fold to 56.

The two lines collected on the second trip used end-on spreads and roll along acquisition method (Mayne, 1962). Shot stations were 2.5m inline offset and about 15m offline. A maximum of 96 fold was obtained on both lines. The N-S line from the second trip was shot over the harvested cornfield that limited the acquisition of line 3 during the first visit to the site. Lines acquired on the second survey were approximately half a mile long each. The length and positioning of these lines were designed based on the results of the first trip. They extended far enough to insure the undisturbed

subsurface around the sinkhole was imaged, extending to three nearby plugged wells (figure 11).

At the end of each trip an elevation survey was conducted using a hand level eyepiece and a measuring rod. The difference in elevation between stations was measured for each line with estimated error of + or - 0.2m for every reading taken by the surveyors. The reliability of the absolute elevation data is higher towards the beginning of each line, decreasing towards the end of the line due to accumulation of errors. Figures 15 and 16 were generated using corrected survey values and elevation information from the 7.5 minute topographic map of the study area (Appendix B). Variations in elevation as well as weathering zone thickness changes affect traveltimes and the necessary corrections to account for such variations were carried out at early stages during processing of shot gathers.

Seismic Processing

All lines were processed using ProMAX™ 2-D version 7.0, the most current release of this seismic data processing software from Landmark Graphics Inc. The platform used was a Silicon Graphics Inc. (SGI) Octane Unix workstation, running IRIX 6.4 operating system.

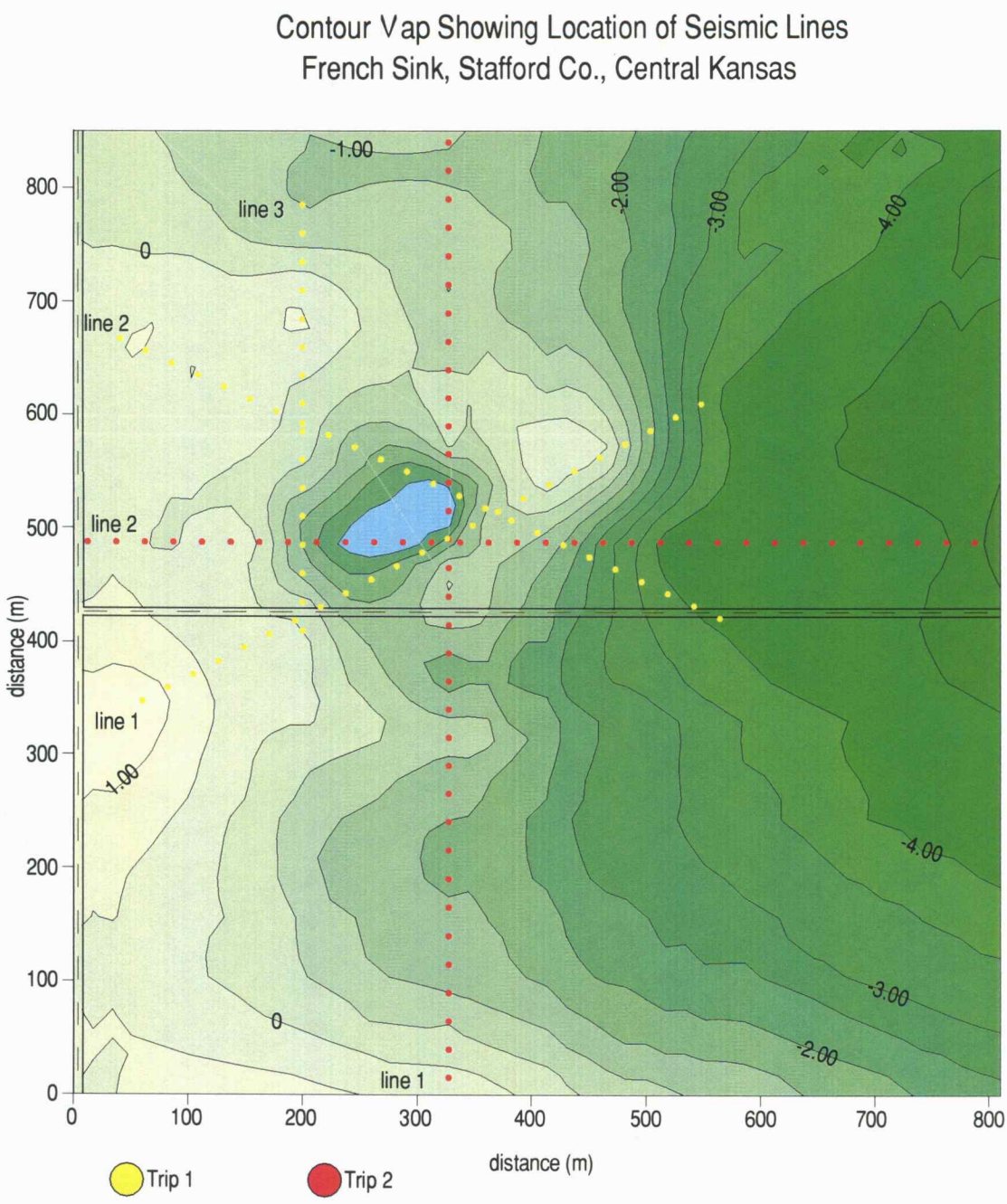

Figure 15. Contour map of the study site.

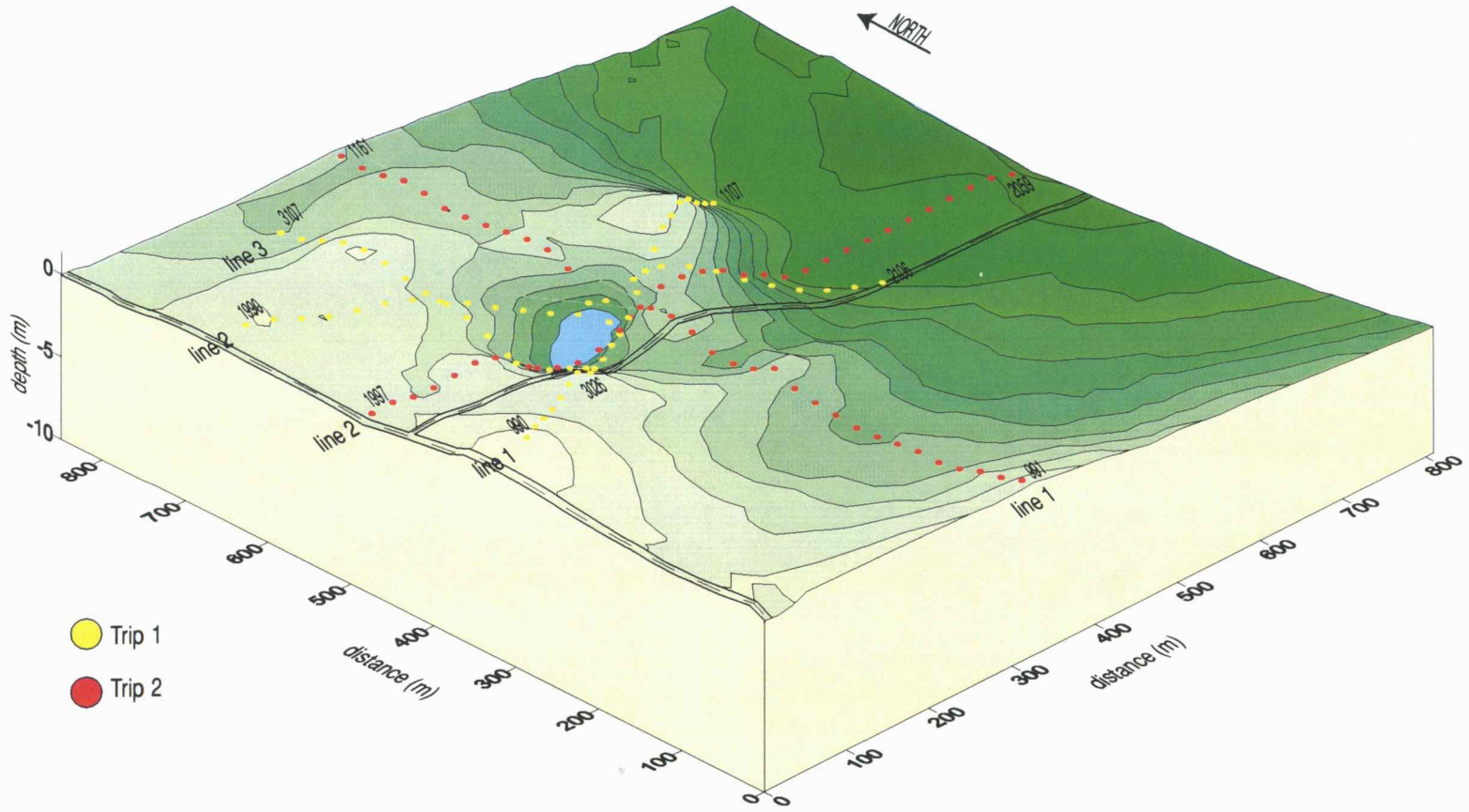

Figure 16. Block diagram from the study site.

The basic processing flow was consistent with routine 2-D shallow reflection methodologies. A summary of the steps used in processing the lines from the first and second surveys are displayed in figure 17 and figure 18 respectively.

Data acquired during the first trip were correlated on site. Three records from each shot location were cross-correlated with the pilot trace and vertically stacked during the time the vibrator moved between shot locations. Storing correlated data decreased the data volume significantly: approximately 97 percent less space is required to store a single one-second long record as opposed to three ten-seconds records of uncorrelated data per shot location. However, this procedure was not repeated during the second acquisition survey. Uncorrelated data were recorded to allow pre-processing of the second trip's data prior to vertically stacking shot gathers in an attempt to increase the signal-to-noise ratio and resolution of that survey in comparison to the previous one. The pre-correlation processing steps used in accomplishing this goal were: trace kill, frequency filtering and frequency-wavenumber (FK) filtering. Significant noise reduction was achieved as a result. However, processing time was increased considerably.

Subsequently after correlation, data were processed using techniques consistent with impulsive shallow seismic data (Steeples and Miller, 1990) to

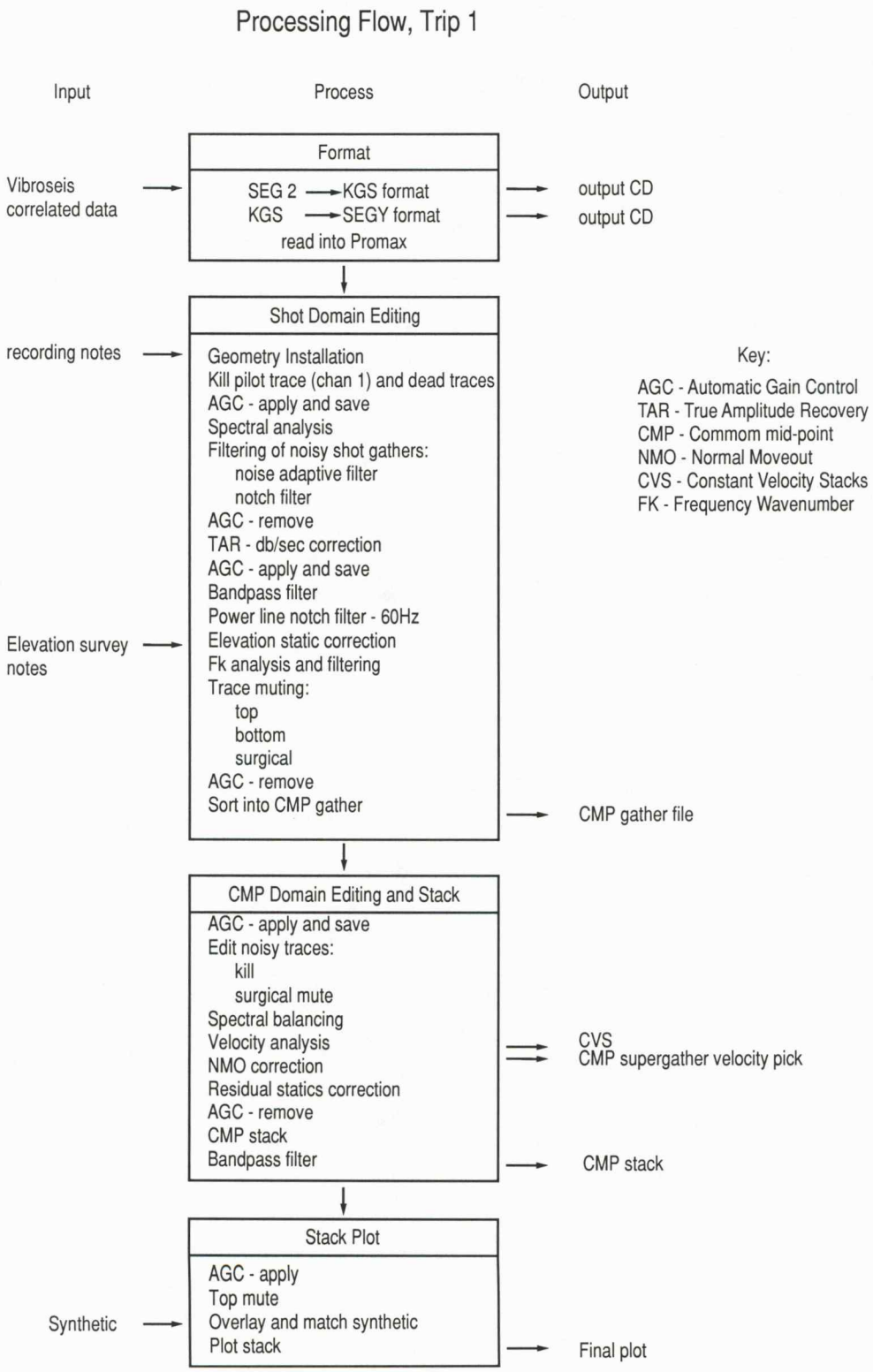

Figure 17. Processing flow for the first trip.

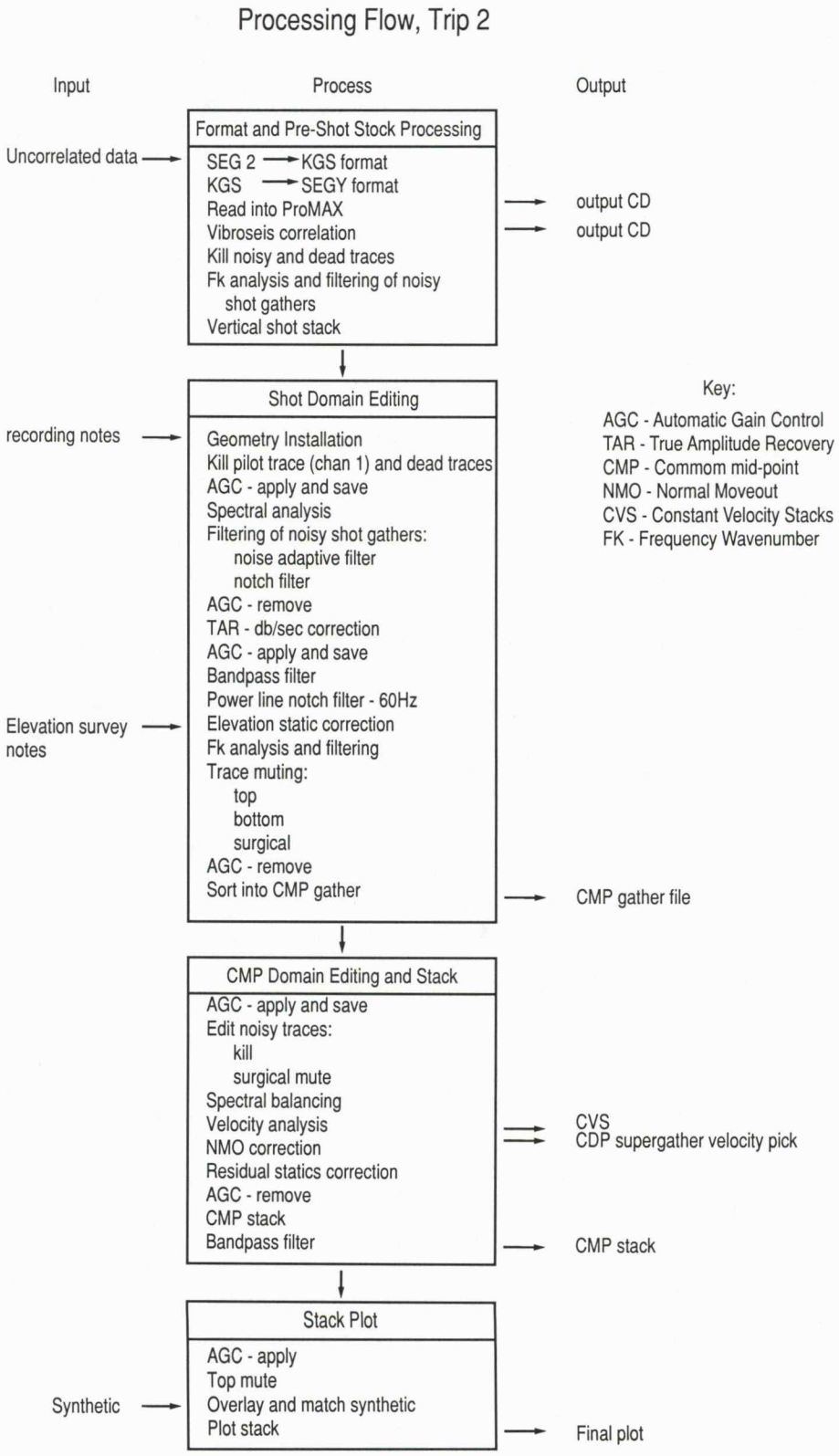

Figure 18. Processing flow for the second trip.

generate optimum CMP stacked sections. Processing steps can be divided into two main processing blocks according to the sort domain of the data: shot and CMP gathers (figure 17 and figure 18).

Shot Domain Processing

An estimated 60 percent of the total processing time was spent in the shot domain. Time, frequency and FK domain analysis of shot records was aimed at identification of noise contaminating the data. Careful attention was paid to distinctive characteristics that distinguished noise from signal in the different domains.

Coherent noises commonly found in the data sets that are not canceled with CMP stacking include power line noise, refraction arrivals, air coupled wave, groundroll and correlation noise (figure 19 and figure 20). As a result, a lot of time was dedicated to removing these types of unwanted energy from the data.

Power line noise is a constant problem thoroughly pervading most shot records. It is most apparent above the first breaks (figure 19 (A) and figure 20 (A)). The amplitude of the 60Hz noise component as well as its harmonics varies proportionally with distance between the power line and recording

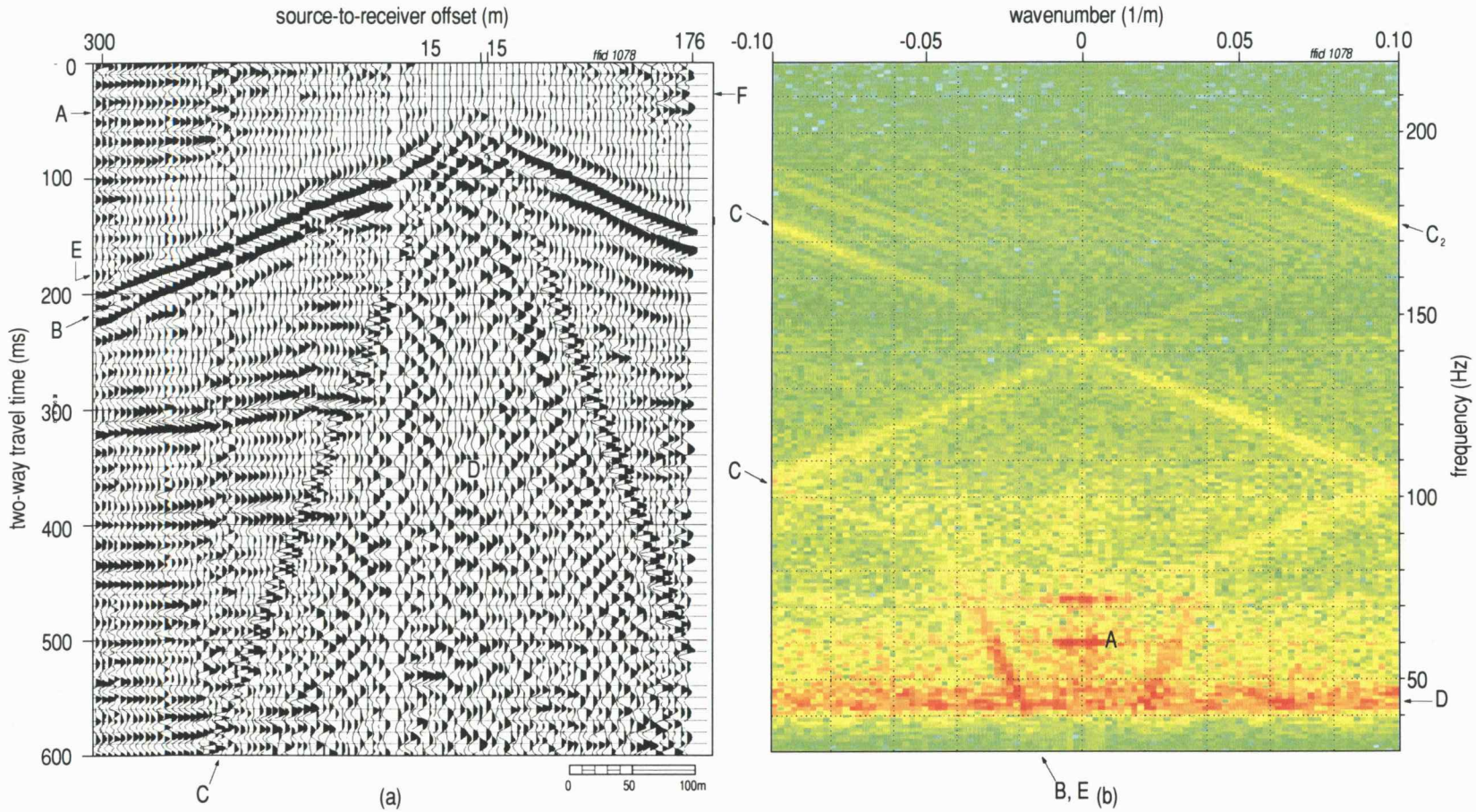

Figure 19. (a) Scaled raw shot gather from Line 1, Trip 1; (b) Fk spectrum of (a).
Noise sources:
A - 60 Hz power line noise; B - refraction; C - air coupled wave (C_1, C_2, aliased); D - ground roll;
E - corelation noise; F - random noise

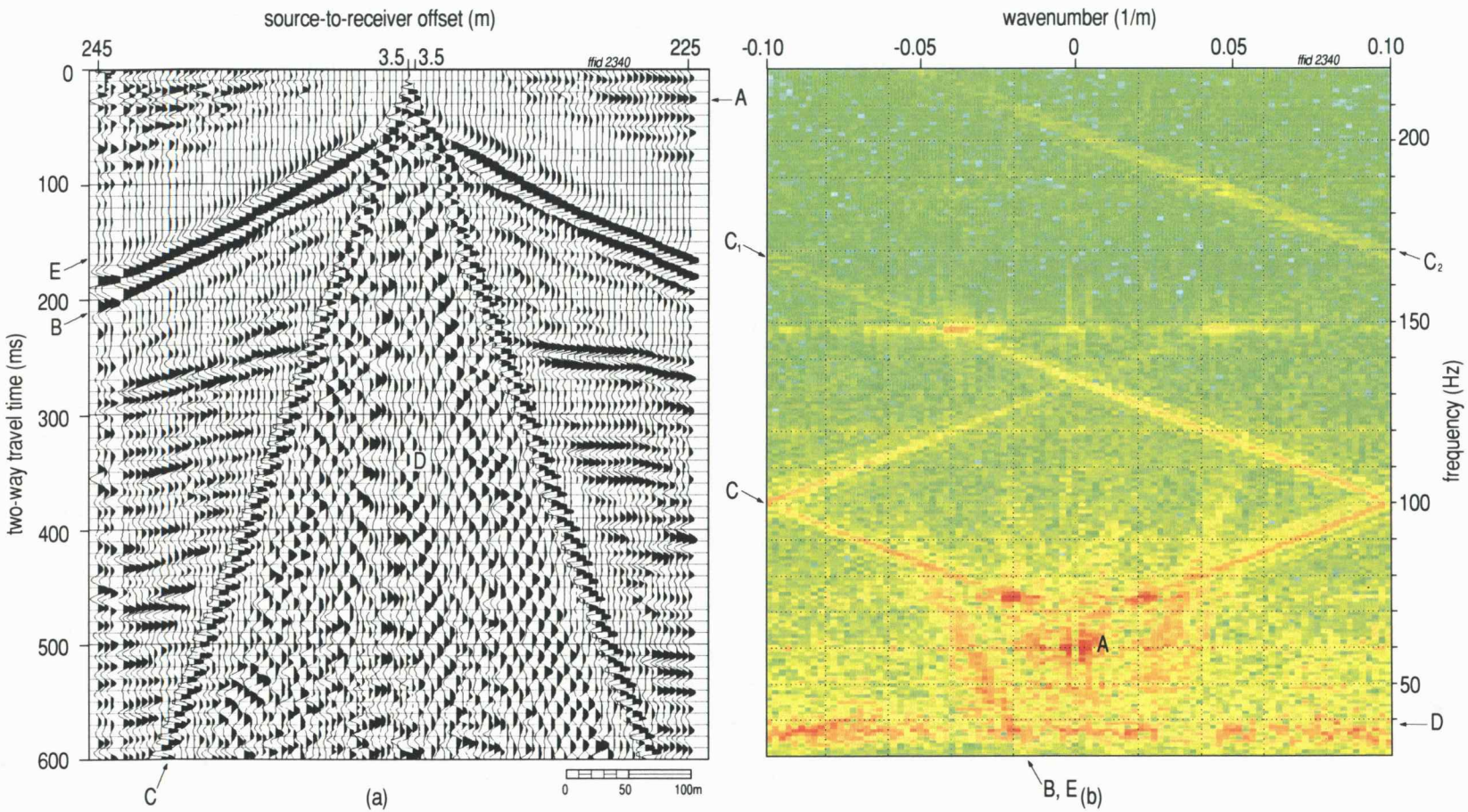

Figure 20. (a) Scaled raw shot gather from Line 2, Trip 2; (b) Fk spectrum of (a).
Noise sources:
A - 60 Hz power line noise; B - refraction; C - air coupled wave (C_1, C_2, aliased);
D - ground roll; E - correlation noise

channels. Notch filtering these monofrequencies was effective in removing them from the shot records.

Also recognizable at the time window above the first breaks is a linear noise which mimics the refraction arrivals (figure 19 (E) and figure 20 (E)). This noise is a product of the cross-correlation between the pilot trace and the recorded data and is referred here as correlation noise. The frequency and velocity content of the refracted waves and the correlation noise are the same allowing them to map in a same radial line in the FK spectrum. FK filtering of this radial component of the spectrum removed most of the correlation noise and refractions. Another measure taken to insure that the data were free of these coherent noise fronts before stack was the careful mute of the zones containing the first arrival breaks and above them. This procedure was done in the time domain (figure 21).

The air coupled wave is another example of linear coherent noise easily identifiable in the data sets (figure 19 (C) and figure 20 (C)). This air coupled energy is characterized on the shot records by a steeply dipping high frequency arrival with the velocity of sound in air (approximately 335m/sec). This velocity is considerably slower than the refraction and reflection arrivals and therefore these waves map in a distinct area in the FK domain. Frequencies above 100Hz are spatially aliased (C1 and C2) as evidenced by

having wrapped around the spectrum. This aliasing is the result of undersampling the higher frequency components of linear energy traveling at slow velocities. Careful selection and application of a bottom mute on a shot-by-shot basis successfully removed the air coupled wave from the data sets (figure 21).

Groundroll is the most dominant linear coherent noise present in the data and can be recognized on shot gathers by its low frequency and high amplitude character. Groundroll energy is scattered over a large area in the low frequency portion of the FK spectrum (figure 19-b (D) and figure 20-b (D)) because of the dispersive nature of this noise train. FK dip filtering is therefore not effective in mitigating groundroll from the data sets. Receiver arrays are commonly used to suppress groundroll in conventional oil exploration surveys. However, large arrays tend to suppress most near-surface recoverable signal spectrum as a result of the incident angle and frequency properties of the returning reflections (Knapp and Steeples, 1986); It is therefore common practice for shallow reflection data processing to mute ground roll from shot gathers (figure 21). Groundroll dominates the entire central portion of most shot records in this study with the air coupled wave acting as an envelope around it. Bottom mute zones were chosen so that both groundroll and the air coupled wave were suppressed from shot records. All shot records in this study were subjected to this muting procedure.

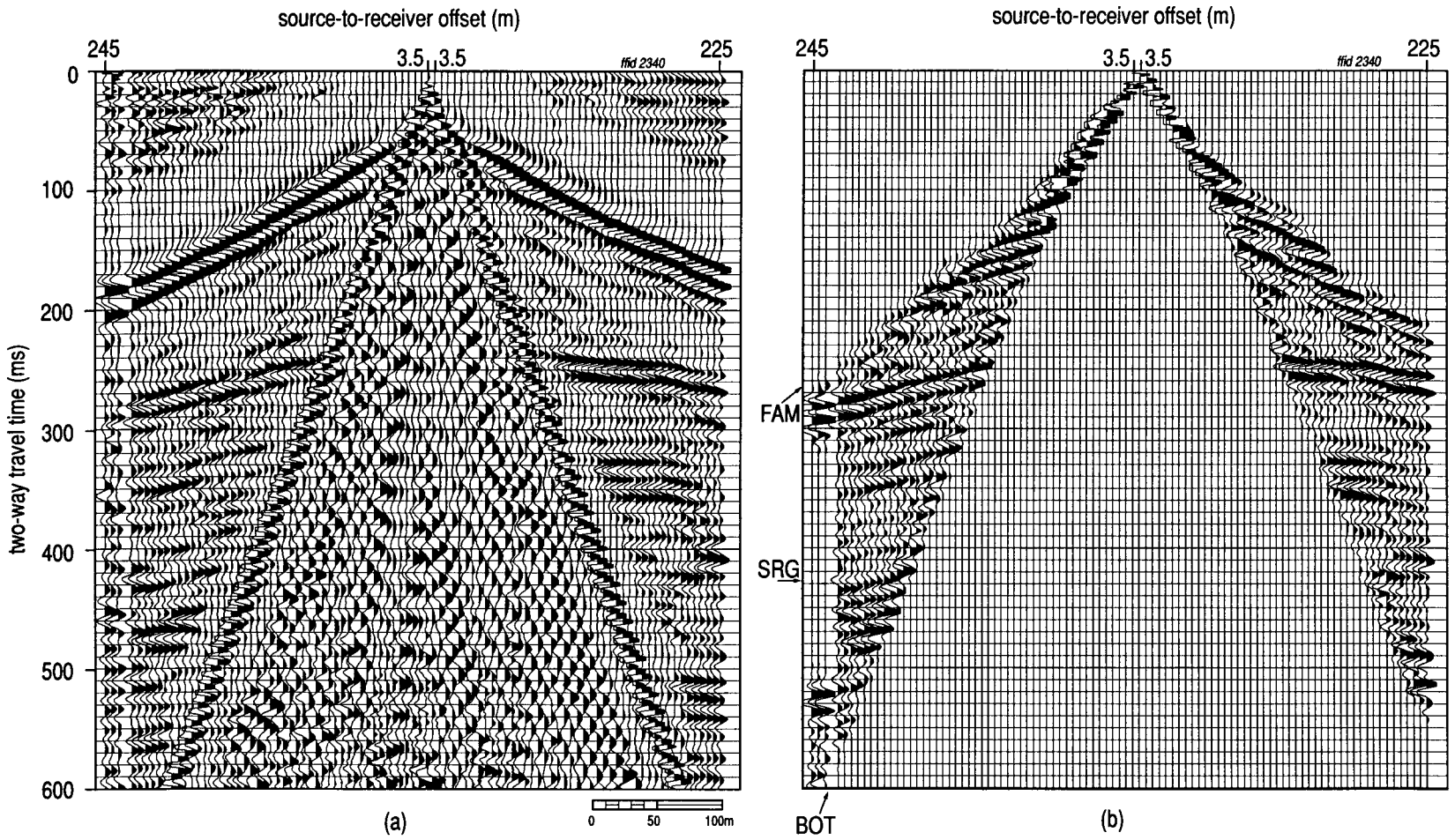

Figure 21. Mute zones: (a) Scaled raw shot gather from Line 2, Trip 2; (b) edited (a) after first arrival mute (FAM), surgical mute (SRG), and bottom mute (BOT).

Apart from the types of noise discussed above, noise derived from vehicles driving by, walking along the receiver line, airplanes flying past, all-terrain- vehicles used in data acquisition left running during recording and a pump jack located north of the sinkhole were evident on a few gathers. Surgical muting proved effective on suppressing many of these types of noise, especially when applied to selected records displaying isolated noise bursts, limited in time and space such as the noise observed in the first few traces of shot gather 2340 (figure 21). Surgical mute was used to remove noise from areas where first arrival or bottom mutes failed to suppress noise and killing a trace would have resulted in loss of valuable signal.

The previously described techniques, with the exception of mute procedures, could not remove coherent noise which was not linear. A good example is the pump jack noise observed in the last shot records of line1 trip2. Due to the location of the pump relative to the recording line, the noise energy in these records appears to have hyperbolic moveout (figure 22). This noise is continuous across the entire record and is evident in the time window before the first breaks. For this non-linear case, a noise adaptive filter was applied in the shot domain and proved quite effective in suppressing it. This adaptive filtering technique uses a time window selected by the user which contains the noise (optimally only noise) to be removed from the entire record. This window is Fourier transformed to obtain an estimate of the noise

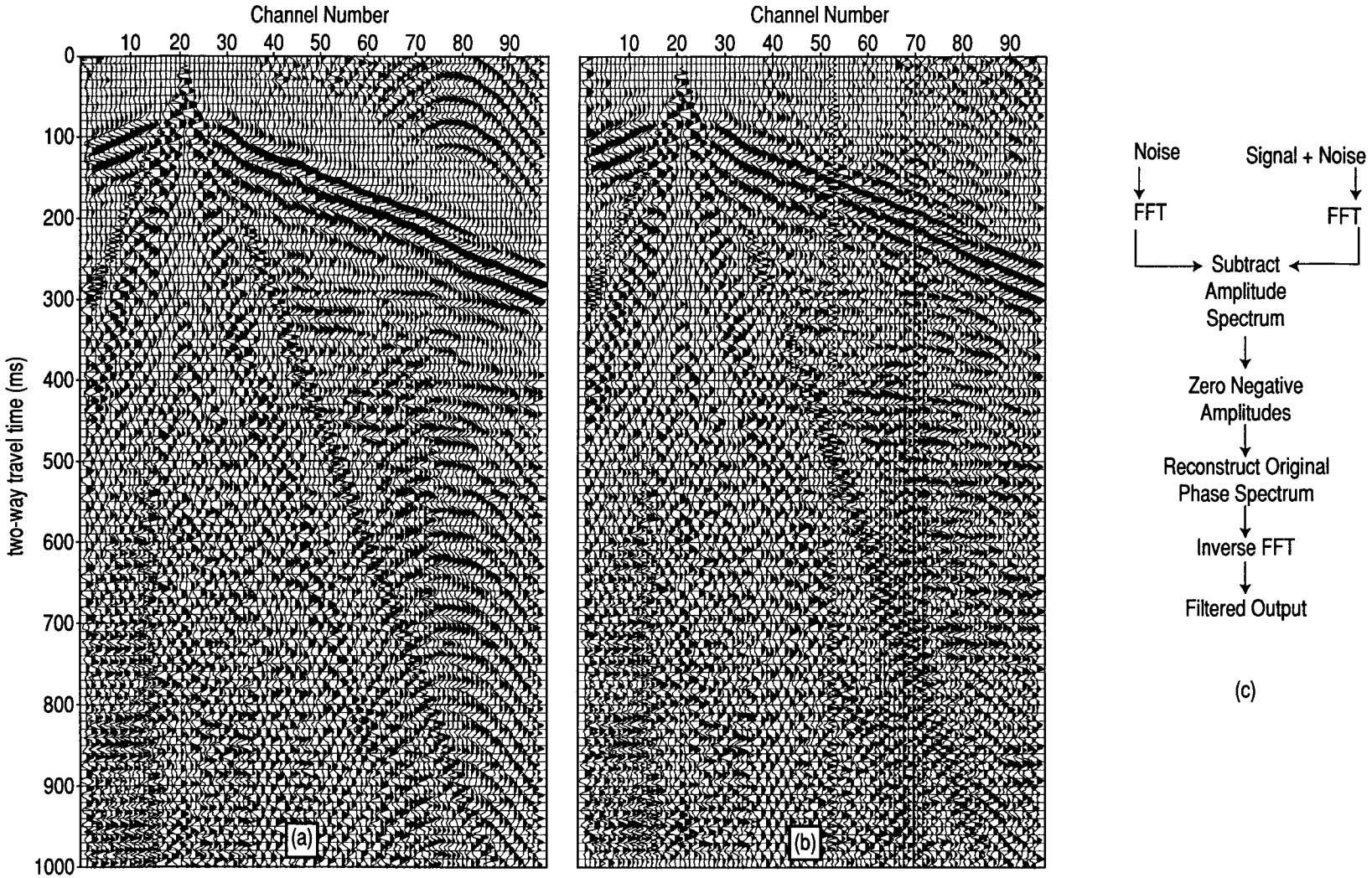

Figure 22. Noise adaptive filter; (a) original shot record showing noise with hyperbolic moveout centered at channel 78; (b) filtered output of (a) after noise adaptive filtering; (c) noise adaptive filter flow.

amplitude spectra which is then subtracted from the record. For the example of the pump jack noise, the window used to estimate the noise was above the first breaks to avoid contain any signal. This filter performs best when noise is stationary and present before the first breaks.

CMP Domain Processing

After sorting, CMP gathers were submitted to additional trace kill and surgical mute procedures to remove any noise energy that remained from the shot domain editing stage.

At this point, CMP gathers were spectrally balanced in an attempt to adjust the amplitude of different frequency components to a similar level. The band-pass envelope used to gain the spectrum components is defined by corner frequencies of 30-40-150-225Hz and proved optimal in compressing the wavelet and suppressing some of the ringy character of the data by broadening the frequency spectrum. Higher frequency components of both signal and noise were gained up, flattening the overall spectrum. A field record from line 2 of the second visit to the site illustrates the improvement achieved after spectral balancing (figure 23). The ringy character observed at 320ms in the raw shot record (a) is suppressed after spectral balancing (b).

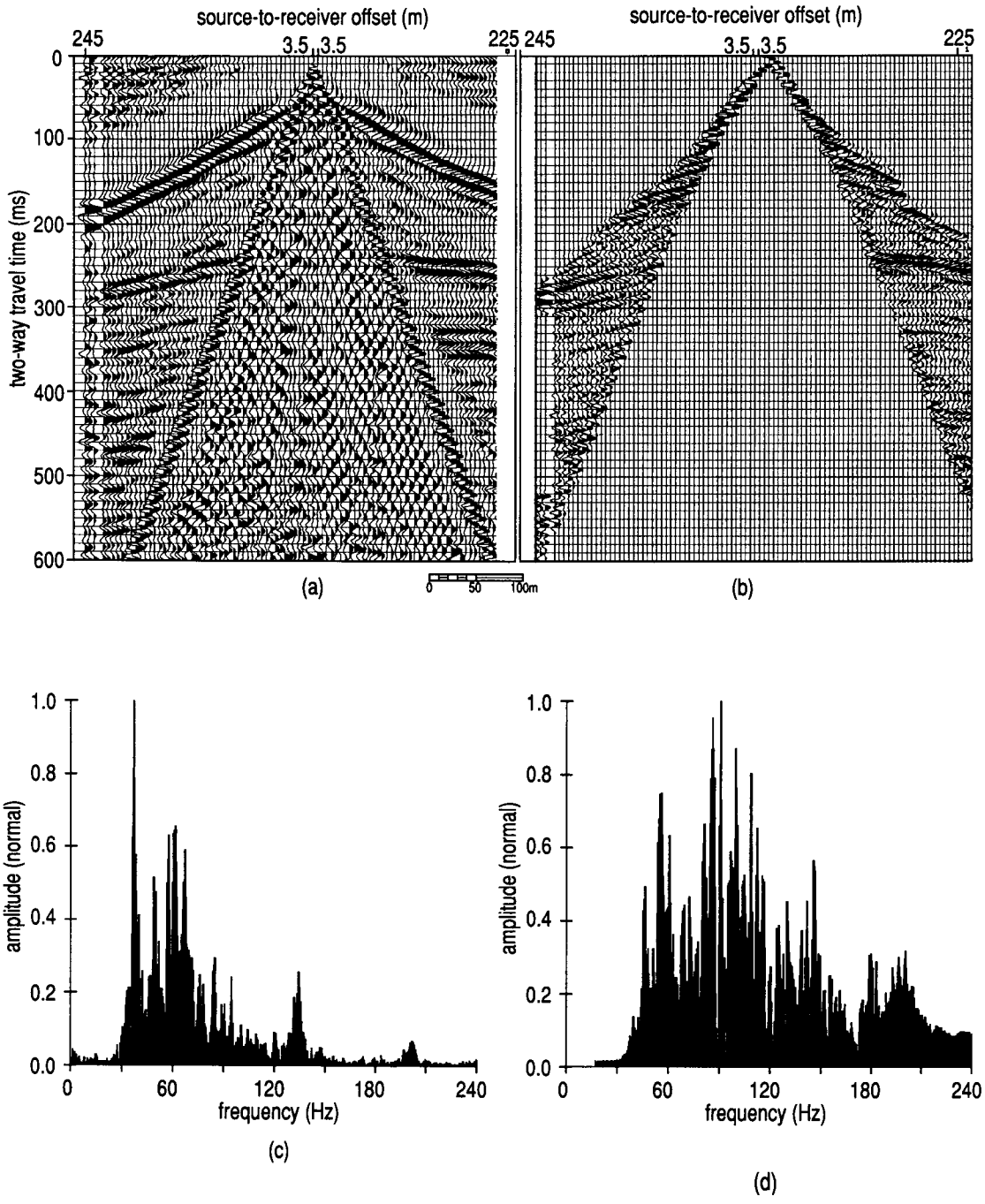

Figure 23. (a) Scaled raw data, FFID 2340, Line 2, Trip 2 ; (b) processed and spectral balanced (a); (c) frequency spectrum of (a); (d) frequency spectrum of (b).

Velocity analysis of CMP data was done it two distinct ways: velocity picking of supergathers containing 5 adjacent CMPs and constant velocity stack analysis. Comparisons between final stacks derived from both methods show similar results. The optimum stacking velocity field for each line was obtained after combining the velocity picks from both methods and smoothing the resulting field (figures 24 through 28).

CMP gathers were corrected for normal-moveout (NMO) before stack using the final velocity data discussed above. NMO correction adjusts reflection wavelets to simulate vertically incident raypaths. Stretch mute was carefully selected to prevent wavelet distortion and amplitude and frequency spectrum degradation, especially at large offsets (Miller, 1992). Examples of two NMO corrected gathers are shown in figure 29.

Stacking of CMP gathers after NMO correction yielded a single stacked trace per CMP location. The final stacked sections are shown in plate 1 through plate 5. Nominal fold decreases towards the end of the sections resulting in a lower signal-to-noise ratio at the edges of the survey. The sloping edges of these sections are produced by bottom mute operations and lack of far-offset traces at these CMP locations.

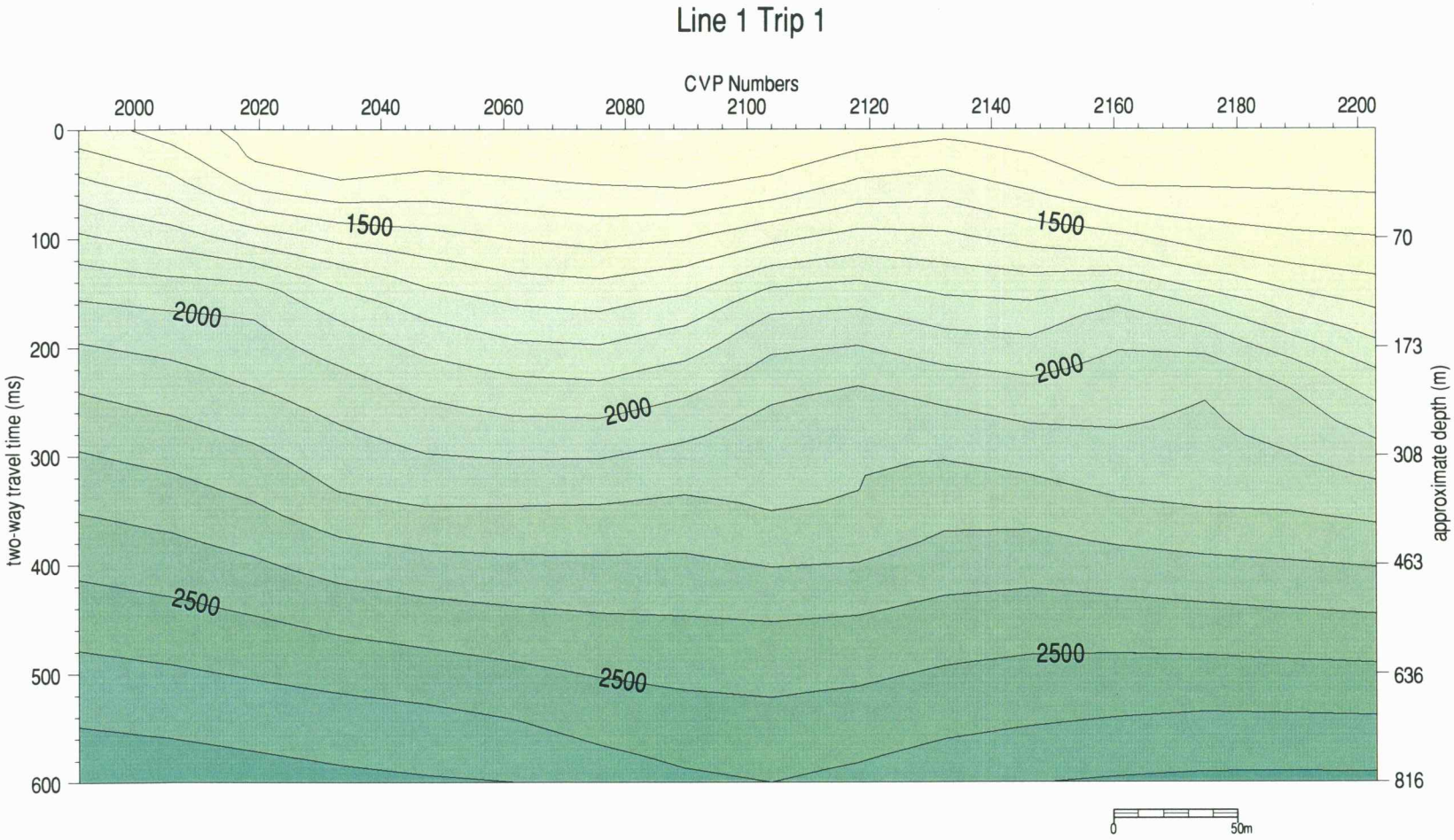

Figure 24. Stacking velocity field (m/s) from line1, trip1.

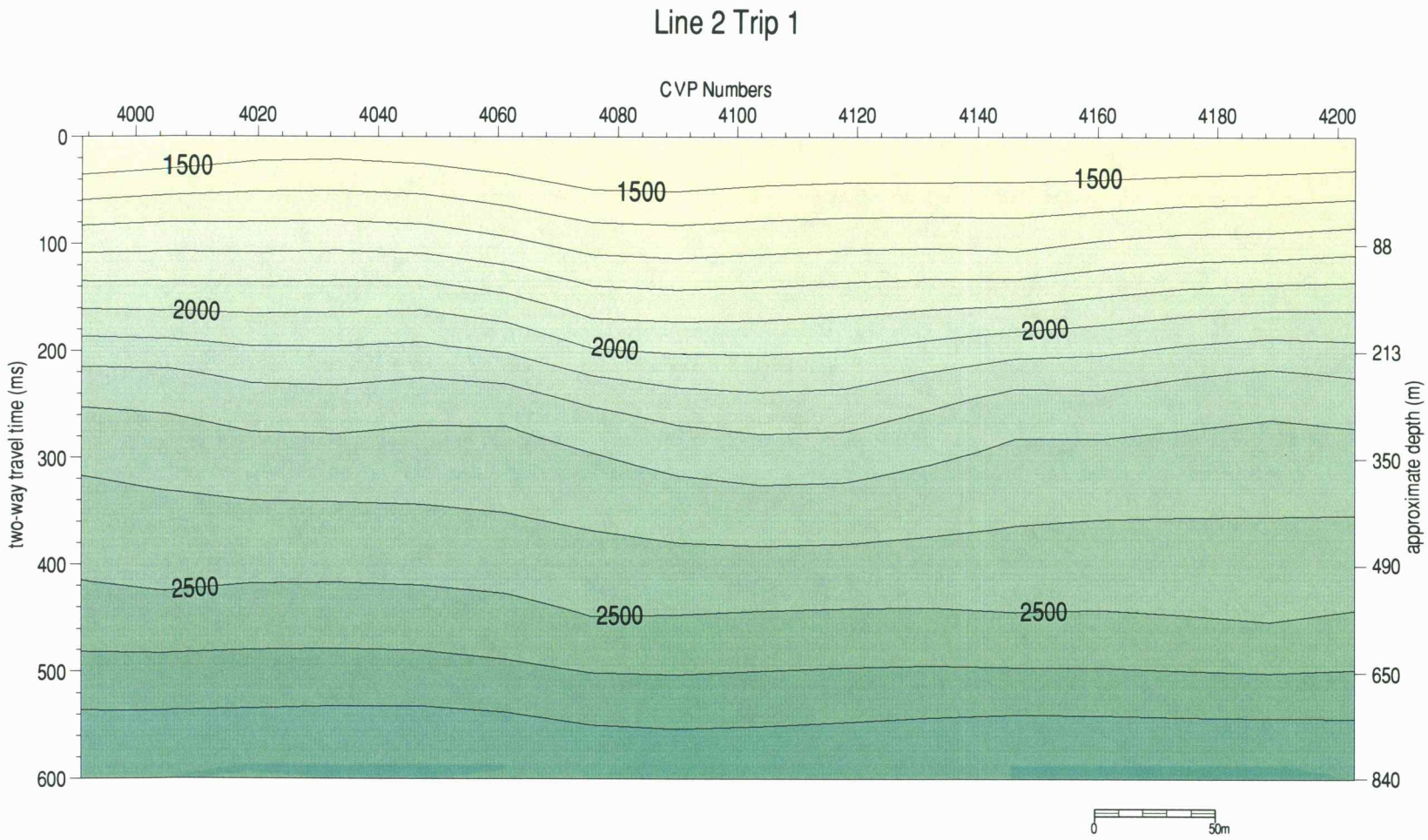

Figure 25. Stacking velocity field, in m/s, from line2, trip1.

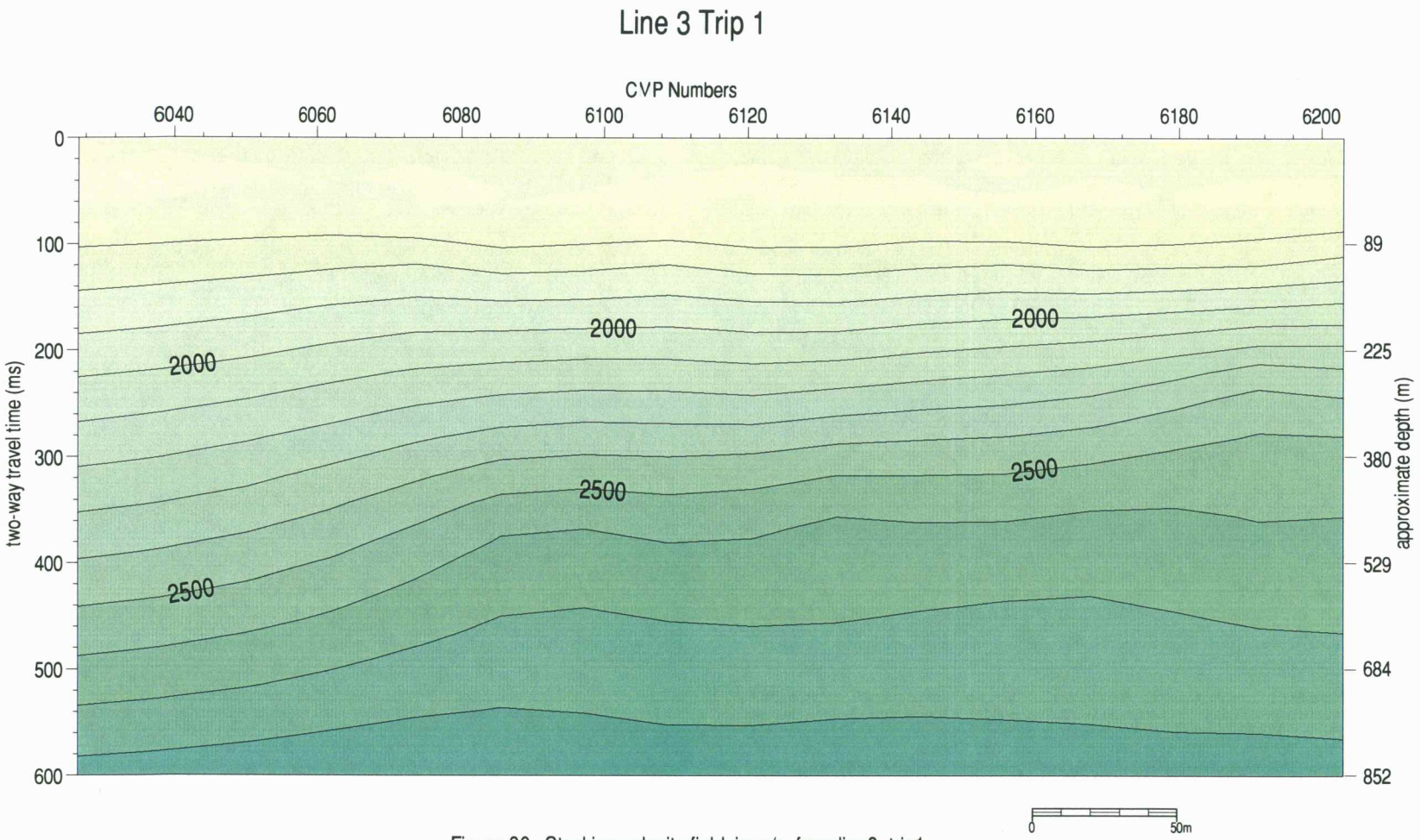

Figure 26. Stacking velocity field, in m/s, from line3, trip1.

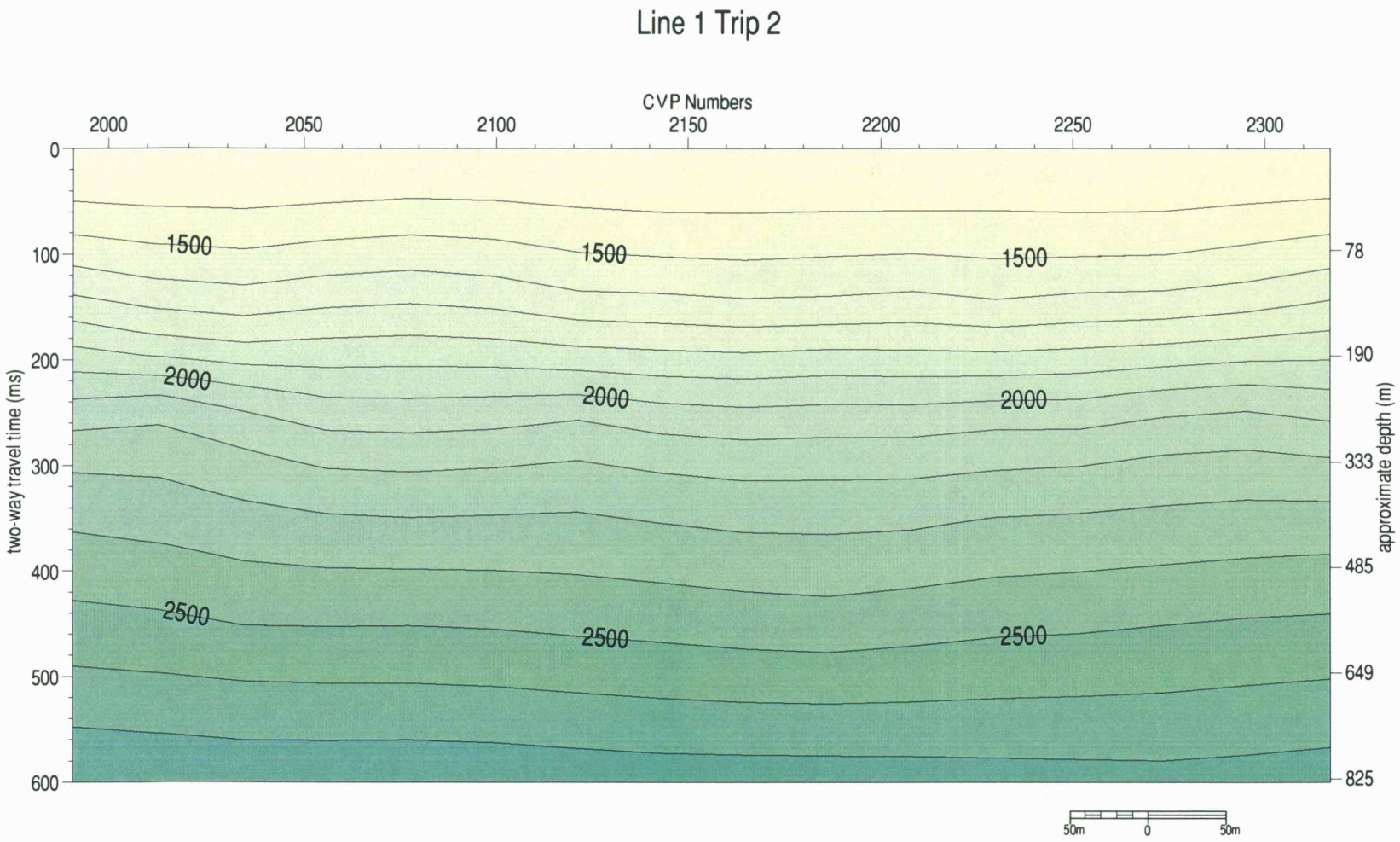

Figure 27. Stacking velocity field, in m/s, from line1, trip2.

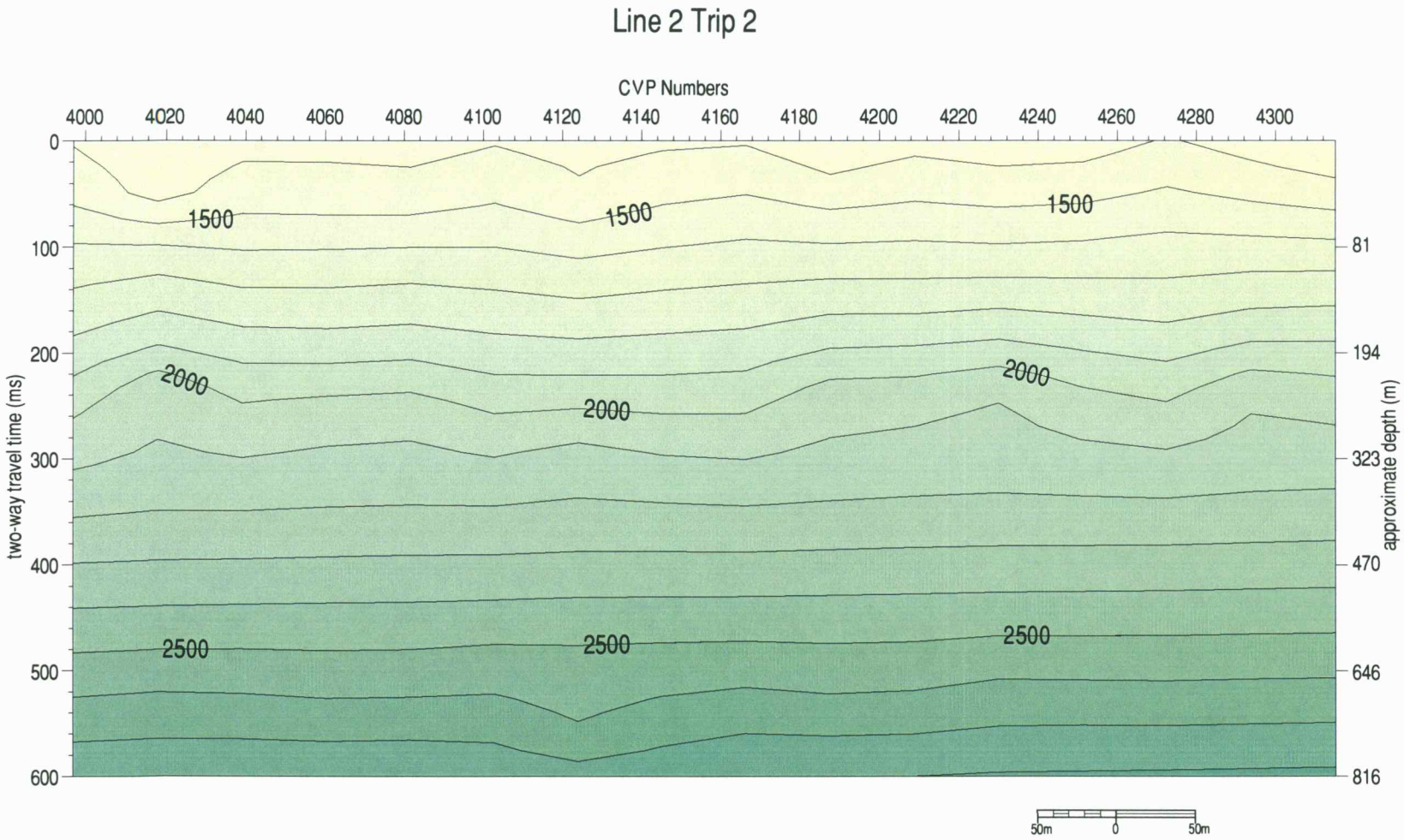

Figure 28. Stacking velocity field, in m/s, from line2, trip2.

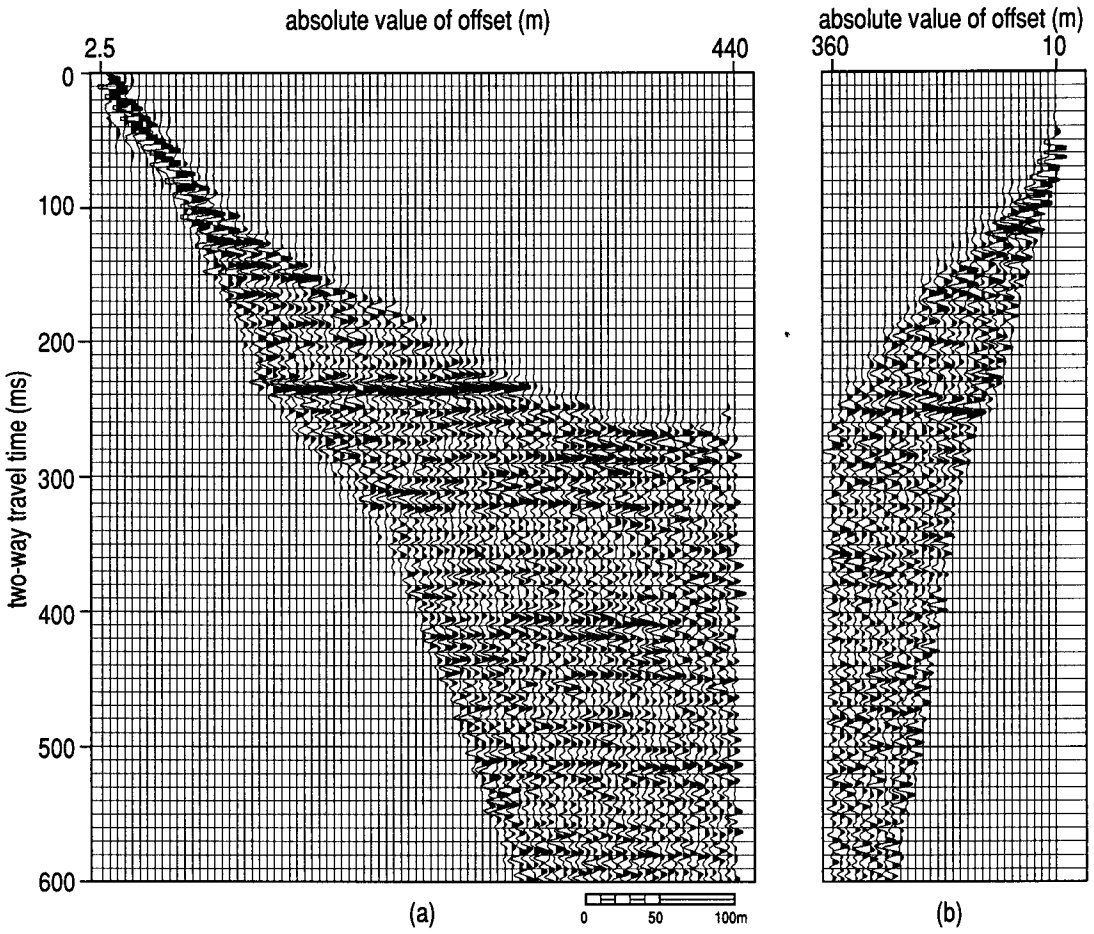

Figure 29. (a) NMO corrected CMP gather 4230; Line 2, Trip 2. (b) NMO corrected CMP gather 4060; Line 2 Trip 2.

Significant improvement in the overall signal-to-noise ratio of the second survey in comparison to the first one is due to higher fold content and pre-processing prior to vertically stacking shot gathers of the second survey.

The true, time-varying fold of the stack sections is significantly lower than the nominal fold calculated from acquisition parameters. This is due mainly to muting operations and NMO corrections applied to the data. To calculate the actual fold of the data, true-fold maps were created for each of the stack sections using the method described by Liberty and Knoll (1998). To generate these maps, raw data were sorted into CMP gathers and a value of one was assigned to data samples. To achieve this task using ProMAX™, two identical copies of raw unprocessed CMP gathers were merged placing identical traces side by side. Each trace was then divided by its adjacent counterpart, resulting in CMP gathers with traces with unit amplitude value per sample. Subsequently, mute and NMO corrections were applied to the data using the same flow and parameters used in processing the original data sets. The traces in the CMP gathers were then summed instead or stacked, resulting in one trace per CMP location containing data samples representing true fold as a function of time. The resulting data were output from ProMAX, converted into ascii format and contoured in Surfer™ to generate true-fold contour maps (plates 6 through 10).

The true-fold displays show symmetric fold distribution only for the first two lines of the first acquisition survey. The lack of shots at the south end of line 3 during that same survey resulted in higher fold values to lie towards the north (CMPs 6105 through 6120). The two lines acquired in the second survey display asymmetric fold distribution, with higher fold values towards higher CMP numbers. This asymmetry resulted from acquisition design, due to moving the source through the spread during the last shot points.

Analysis of the true-fold maps is of key importance in the interpretation of the stacked sections in this study. Lines 1 and 2 from the second acquisition survey display a visibly higher signal-to-noise ratio between CMPs 1090 to1120 and 2095 to 2130 respectively. Several coherent reflectors can be observed within these CMP ranges. However, these reflectors lose coherency and signal-to-noise ratio decreases away from these CMP locations. These locations coincide with the area of highest fold displayed in the true-fold maps. Because signal-to-noise ratio varies proportionally to the square root of fold, the improved coherency of these zones could be attributed to higher fold values rather than to changes in geology. To investigate the nature of these changes in lateral coherency, decimated stack sections were generated by dropping selected shot gathers which contributed traces to these CMP locations. As a result, stack sections with even fold distribution were obtained (plates 11 through 14). The signal-to-noise ratio of

the decimated stacks is very similar to the original stacks, possessing higher coherency at the same CMP locations. Therefore, lateral variations in the coherency of reflectors in this case are not derived from fold distribution but possibly to lateral variations in geology.

Experimental low fold 3-D survey

A low fold, minimal cost 3-D survey based on common offset and shallow seismic reflection technique was shot during the first trip to the study area. The goal of the survey was to gain insight into the potential of a minimal deployment 3-D survey to delineate major structural traits around the French Sinkhole and similar features elsewhere. The survey was designed to employ the equipment and crew used to acquired the 2-D lines. As a result, the study evaluates the effectiveness of planning a 3-D survey around the limitations of typical near-surface seismic investigations, adopting a small number of recording channels, restricted computational power, 2-D processing packages, small acquisition crews and low budgets.

The results of this study are discussed in the expanded abstract "Delineation of salt dissolution sinkholes using minimal deployment shallow 3-D seismic reflection surveying" presented at the 1997 Society of Exploration Geophysicists International Meeting in Dallas, Texas (Appendix C).

Synthetic Seismogram

A synthetic seismogram derived from a sonic log approximately 2 miles away from the French well correlates reasonably well with the seismic data. The synthetic seismogram was aligned with the seismic data to help tie reflections on the stacked sections with particular geologic interfaces interpreted from borehole logs (figure 3). This procedure helped separate primary reflections from multiples as well as unique packets of reflections that represent formation or even member groupings. Time-to-depth conversion of the seismic sections was another important use of the synthetic seismogram.

The French well was never logged for sonic transit times and the closest sonic log available from wells in the vicinity of the French site is from the Staub no. 1-24 well. The Staub well is located 1980ft from the South line and 4950ft from the East line of the Southwest ¼ of Section 24, Township 23 South, Range 14 West, approximately 2 miles southwest of the French well. Sonic and gamma ray logs were acquired throughout the interval from 4075ft, (TD of the Staub well), to 300ft of depth in 1991. To optimize the fit between the sonic and the seismic, the gamma ray curve from the Staub well was compared to the French curve and found to be very similar with a best match obtained by moving the Staub's curves 35ft towards the surface (figure 30). The close match between the gamma ray curves is a strong indication that

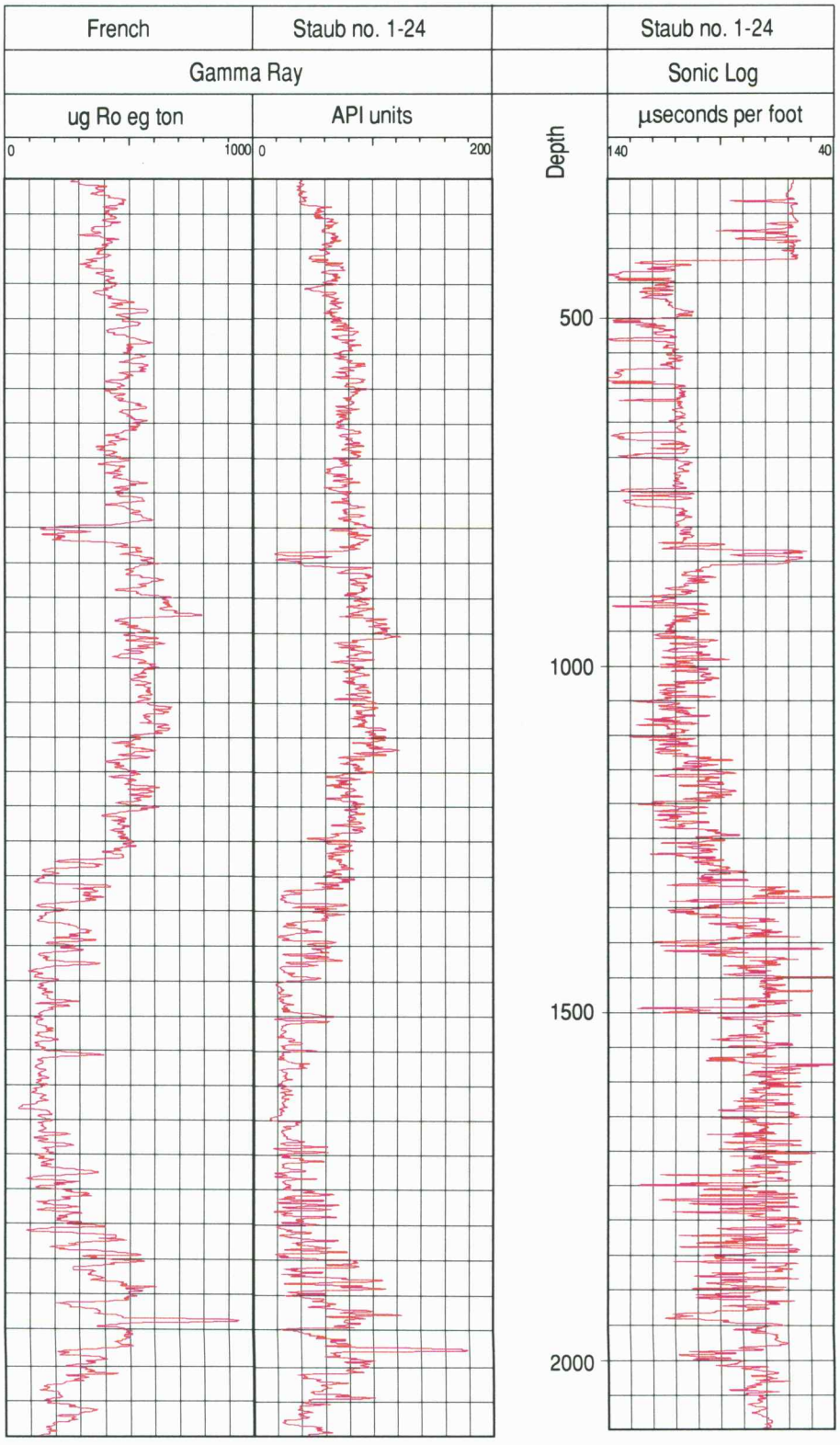

Figure 30. Gamma-ray and sonic logs from the French and Staub wells.

the sonic log from the Staub well will represent the acoustic properties at the French site fairly well.

The synthetic seismogram produced for this study is the product of convolving a Klauder seismic wavelet with the reflectivity series obtained from the sonic log when density is assumed to be constant. The Klauder wavelet was created using the corner frequencies of the sweep used in acquiring the seismic data. The synthetic traces were band-pass filtered so their spectral properties best matched the CMP stacks. The resulting synthetic seismogram is one-dimensional in nature assuming vertical incidence (zero-offset) and horizontal interfaces.

The sonic curve from the Staub well shows a distinctive change in transit time to approximately 50μs/ft (164μs/m) at the Stone Corral Anhydrite interval. This slow transit time reflects the high velocity nature of anhydrides, with sonic interval velocities averaging around 20,000ft/s (6,100 m/s). The sonic curve displays an additional change towards slower transit times at the Hutchinson Salt interval. Sonic transit times of halides average 67μs/ft (220μs/m) which translates into interval velocities of about 15,000ft/s (4,600m/s). Shales on the other hand have a wide range of transit times, from 62μs/ft to 167μs/ft (205-550μs/m, Sheriff et al., 1995) but, on average, will have higher transit time values (lower interval velocity) than halite or

anhydrite. In the Staub well, shale readings decrease slightly in transit time from about 110 to 100μs/ft with depth. The strong velocity contrasts between anhydrite-shale, halite-shale and anhydrite-halite are responsible for high impedance values and therefore, strong reflections are generated at these boundaries (figure 3).

Discrepancies observed between the synthetic and the actual data can be attributed in part to amplitude averaging of CMP stacked traces over a range of offsets and even to subtle dip effects not compensated for on synthetic seismograms (Sheriff et al., 1995). Furthermore, coherent and random noise were not considered in the creation of the synthetic data not to mention velocities obtained from sonic logs can be adversely affected by hole caving, inadequate penetration, invasion of formation by mudfiltrate and other factors.

Since the sonic log recorded instantaneous velocity as a function of depth, a simple transformation from depth to two-way-traveltime was used to match the synthetic seismogram with the CMP stacks (Plates 1 to 5). In the absence of a checkshot survey, an estimated replacement velocity was used to account for the material from the surface down to 300ft of depth. A constant velocity value was selected that aligned the Stone Corral wavelet on the synthetic with the Stone Corral reflection interpreted on the CMP sections.

Cumulative errors resulting from transforming interval velocity measurements from the sonic to average velocity caused mis-ties between events in the synthetic seismogram and the CMP stacks. No checkshot, uphole or VSP survey were available to correct the average velocity values calculated from the sonic and minimize these errors.

Seismic Interpretation

Several key reflecting interfaces important in understanding the stratigraphic and structural framework around the French well are the shallow Permian redbeds, the Stone Corral Anhydrite, the top of the Chase Group, and the top and bottom of the salt section (figure 31 to 35). Identification of these reflections on field files and tracking of them throughout the processing flow was of utmost importance in ensuring that they are in fact true reflections and not stacked coherent noise. The use of the synthetic seismogram previously described was key in providing a starting-point for the stratigraphic interpretation presented here.

The most striking feature common to all CMP sections is the faulted synform on the 250m deep Stone Corral Anhydrite. The Stone Corral is the strongest reflection in the data and possesses lateral continuity in all lines

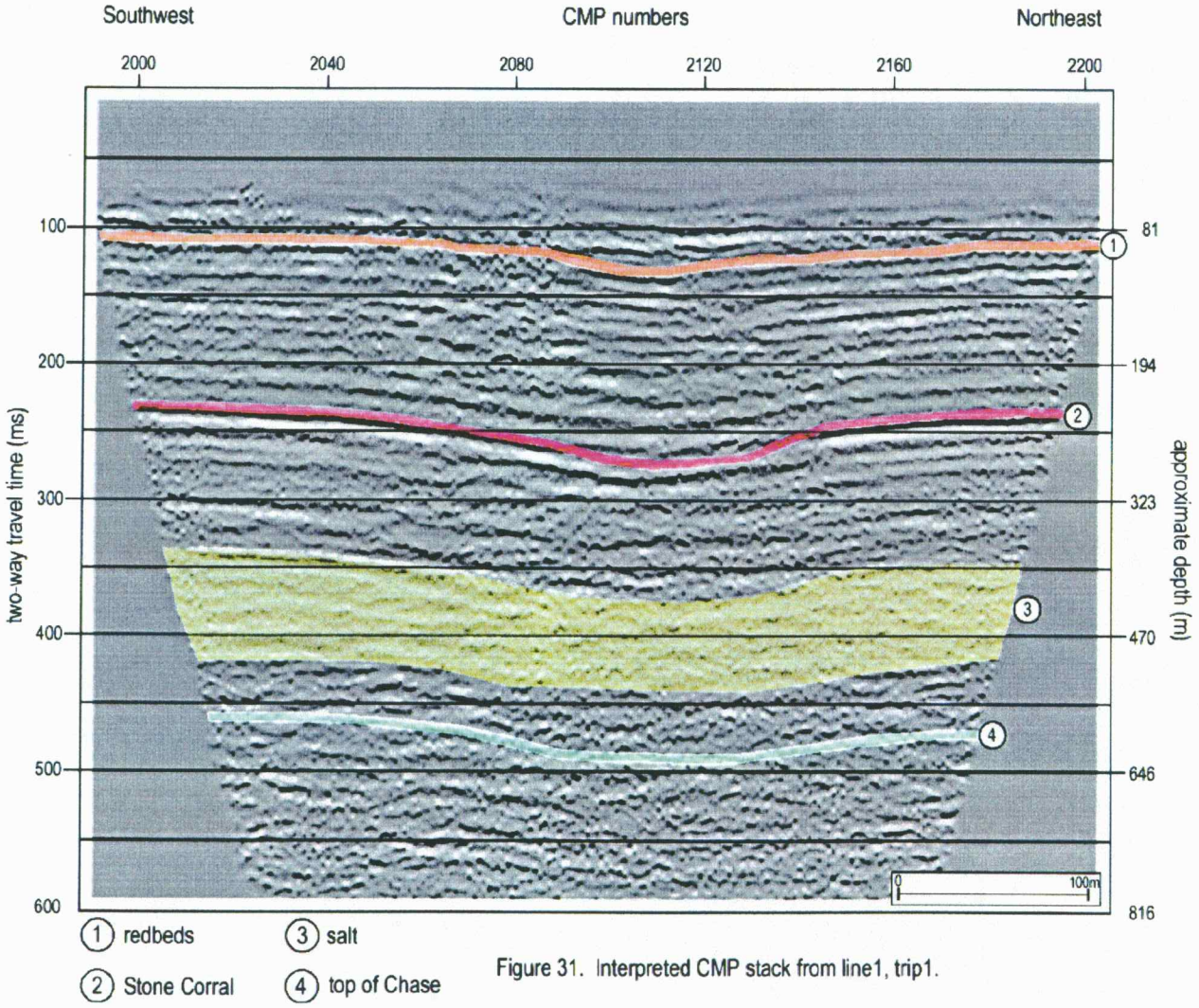

Figure 31. Interpreted CMP stack from line1, trip1.

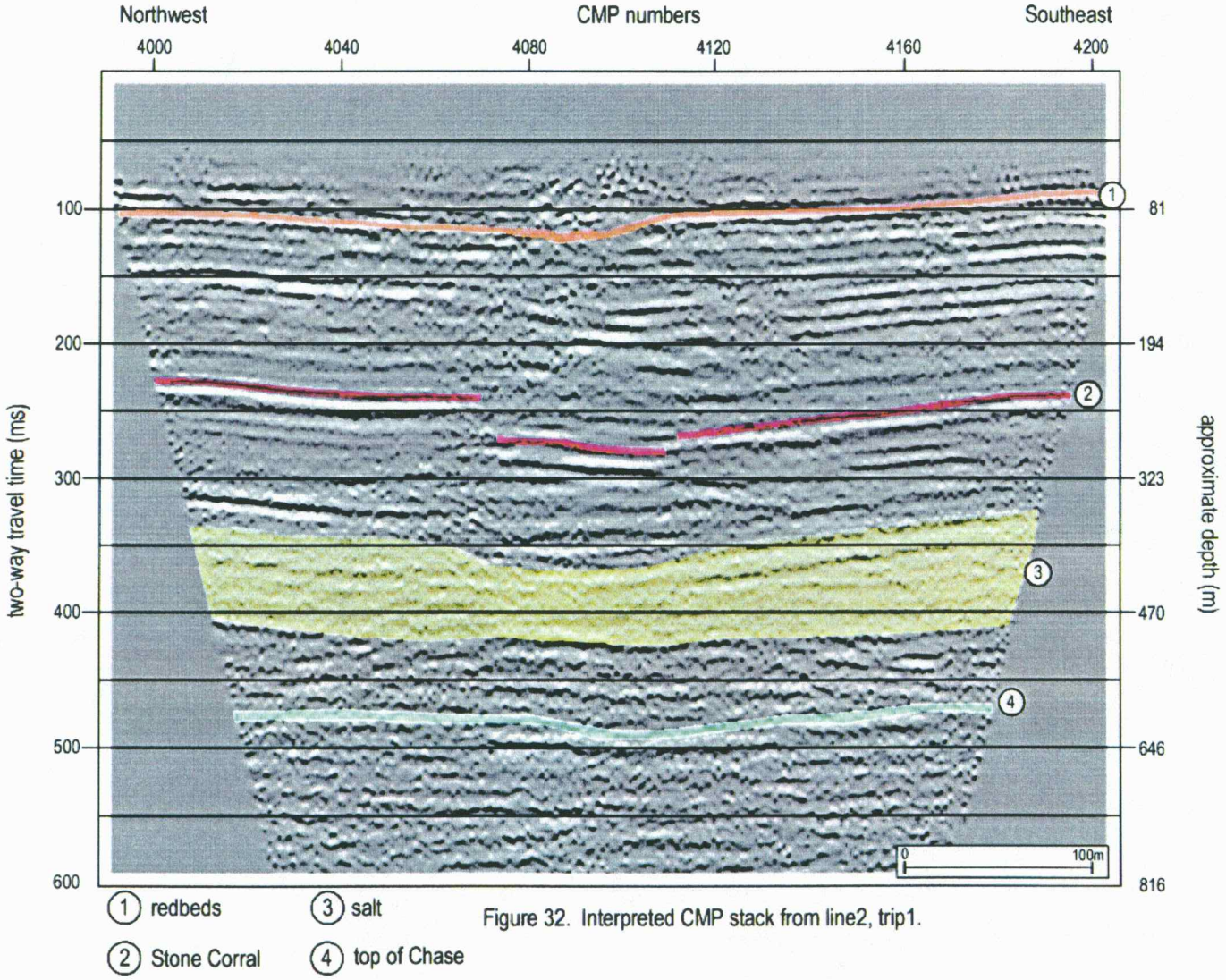

Figure 32. Interpreted CMP stack from line2, trip1.

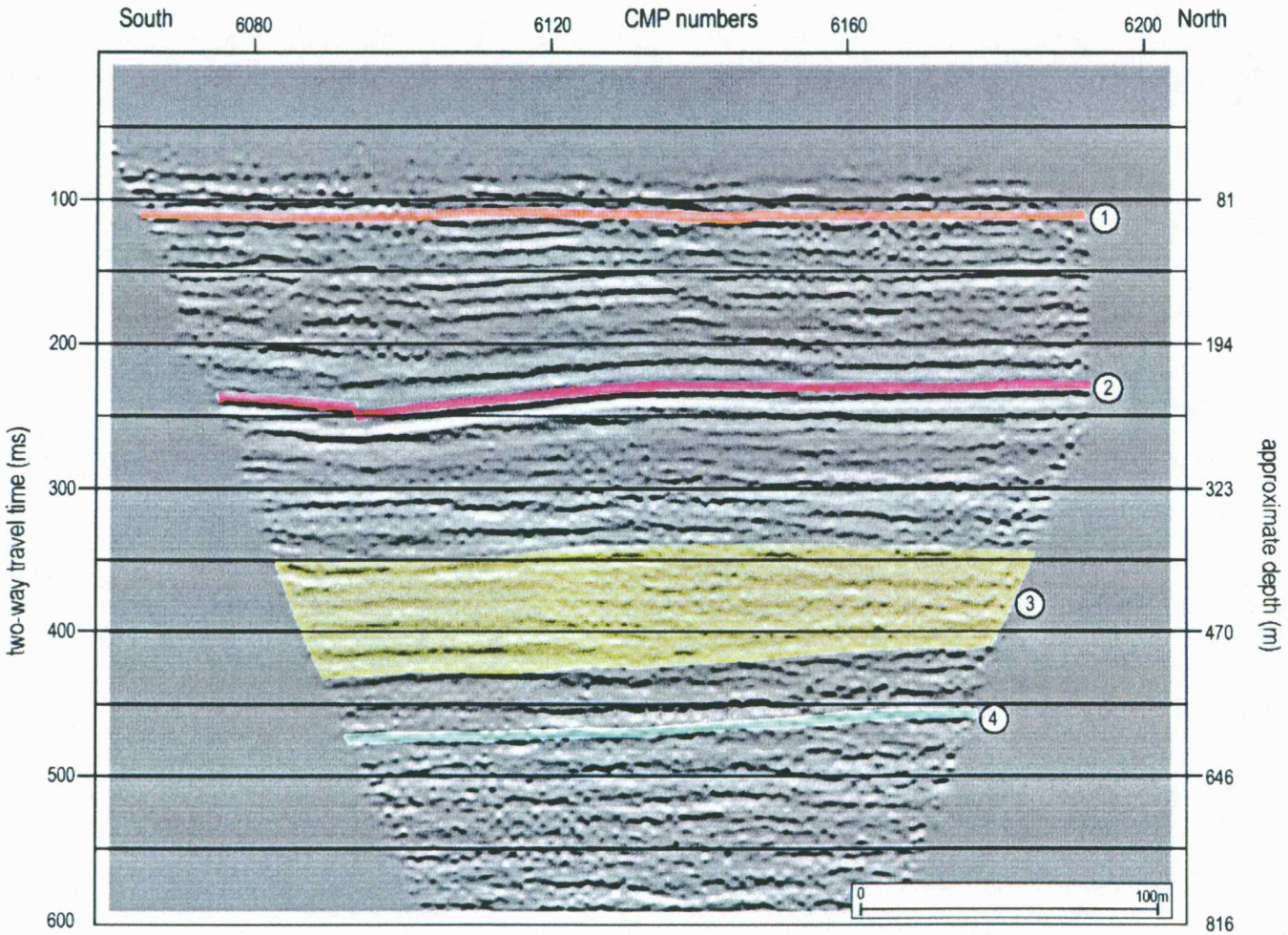

Figure 33. Interpreted CMP stack from line3, trip1.

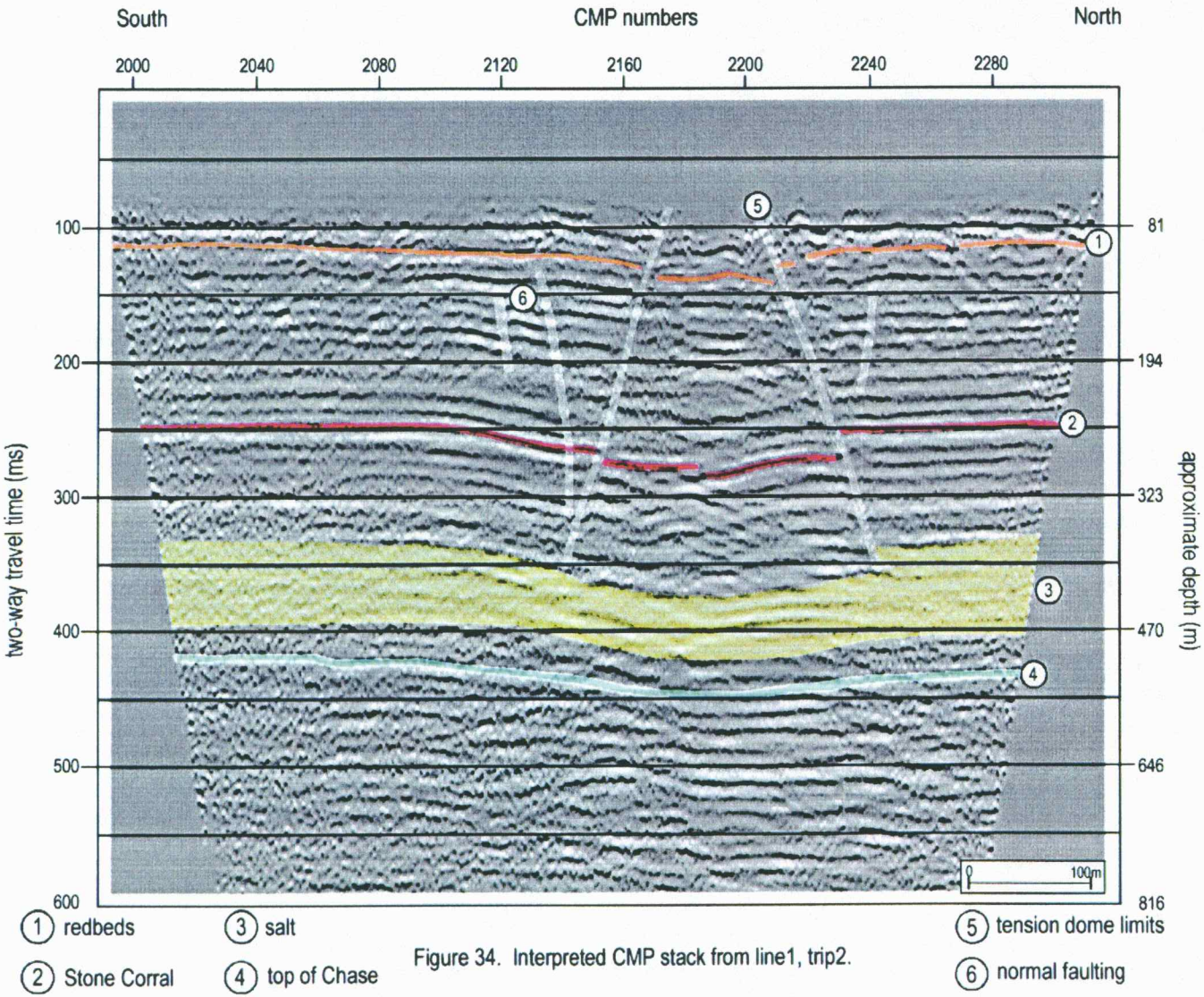

Figure 34. Interpreted CMP stack from line1, trip2.

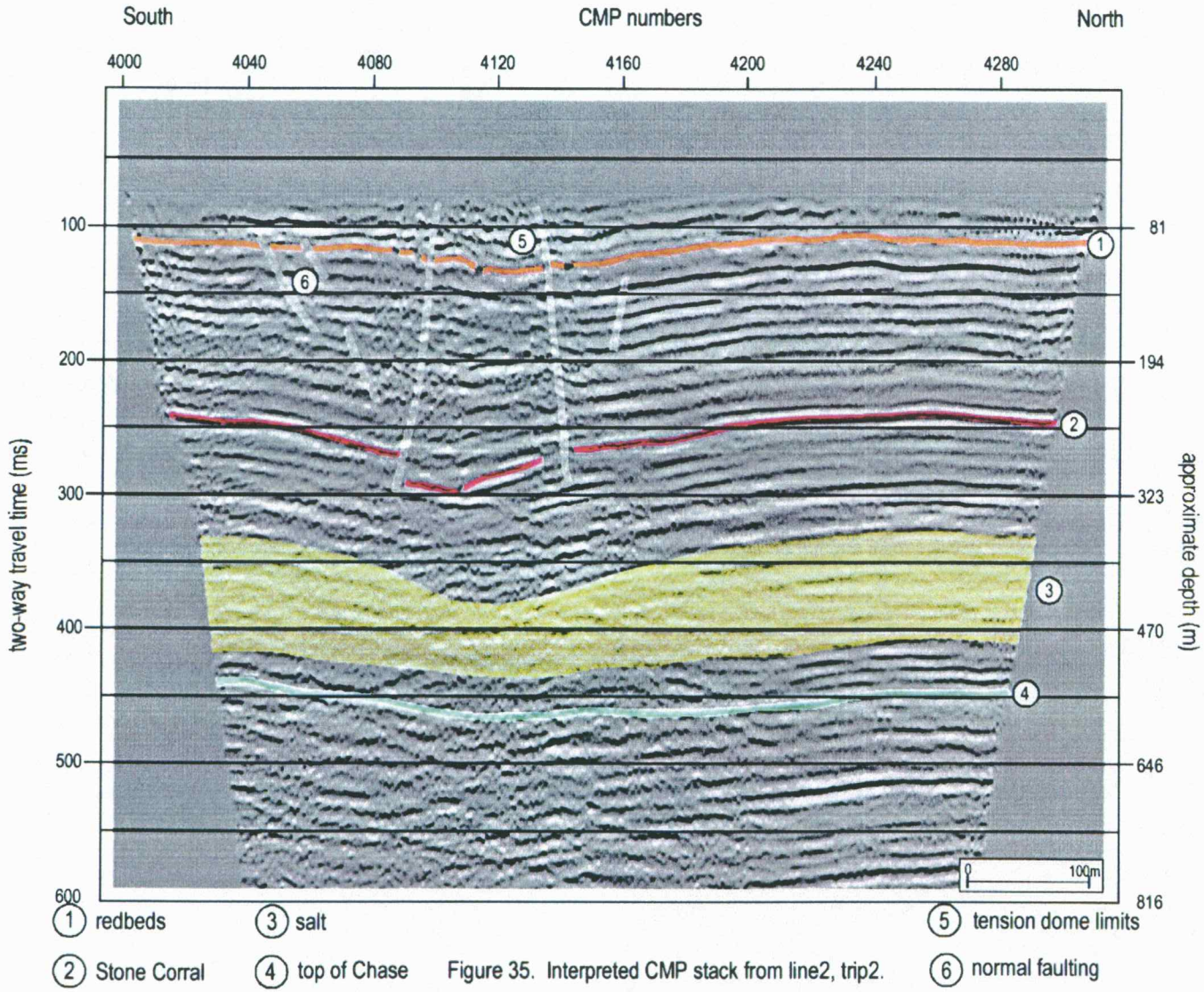

Figure 35. Interpreted CMP stack from line2, trip2.

despite structural complexities. Evidences of both brittle and plastic deformation of the Stone Corral are found on the stacks. A collapsed portion of the Stone Corral interval between CMPs 4090 and 4140 from line 2, trip2, centered at the disposal well located about 35m north of CMP 4110 is a striking example of the deformation character of these kind of collapse features (Steeples et al., 1986, Miller et. al 1997). The approximately 50m of vertical movement observed where the collapsed slab is broken into two segments between CMPs 4080 and 4140 represents the maximum displacement observed at this site. Deformation of the Stone Corral seems to extend from CMPs 4040 on the west side and 4200 on the east side of the profile. These CMP locations represent inflection points marking the limits of the synform that formed prior to roof failure and collapse.

The same collapsed synform occurs directly below the disposal well location around CMP 2192 on the north/south profile from the same acquisition trip. Accordingly, the downdropped portion of the Stone Corral shows signs of fracturing into smaller segments. The maximum vertical displacement of the Stone Corral Anhydrite on this line is of approximately 40m and occurs near the disposal well location. The CMP stacks from the first trip display these same structural traits but are not as evident due to the lower signal-to-noise ratio and lower resolution potential.

The reflection interpreted as the top of the salt occurs at approximately 325ms (390m of depth). This reflection does not possess the prominent amplitude characteristics of the Stone Corral reflection because the contrast between acoustic velocities of the Hutchinson salt and the overlying shale is much smaller than the contrast between the Stone Corral and the shales that overly it. Also, salt has a lower density (2.16g/cm^3) than anhydrite (2.96g/cm^3). This observation is confirmed by both the sonic at this site and previous studies in this area. Reflections from within the salt interval itself are from laterally persistent thin anhydrite and shale layers interbedded with halite that permeate the entire salt interval. These intra-salt reflections and the reflection originating from the top of the salt are discontinuous towards the center of the sink. Termination of the intra-salt reflections is likely related to the collapse of the less soluble anhydrite and shale units into voids left after dissolution of the salt (Miller et al., 1997). This central portion of the seismic sections without laterally coherent reflections within the salt unit is interpreted as part of the dissolved volume. Localized reflections from within this disturbed zone are probably due to remnants of intra-salt layers and shale beds from the "upper member" of the Wellington Formation that have fallen or slumped into the void created by salt dissolution.

The reflection from the top of the Chase Group is interpreted on the CMP sections at around 460ms (570m). As expected and consistent with

previous seismic studies, this reflection loses coherency below the disturbed zone. This loss of coherency is believed to be related to the attenuation of the seismic energy in the disturbed zone due to changes in the overall compaction, scattering, and non-uniform reflection raypaths. The reflection from the top of the Chase Group possesses a "draped" geometry similar to the reflections above it. This "pulldown" is likely caused by a drop in average velocity above the disturbed zone. Assuming the Chase Group is flat and using it as a datum to correct the seismic data, nearly 20ms of static drape can be accounted for between the top of the Chase Group and the ground surface.

Finally, many shallow reflections evident between the ground surface and Stone Corral Anhydrite exhibit a peculiar bridging character that seems to be very laterally discontinuous. The "sag" obvious in these "bridged" units becomes progressively less severe moving from the Stone Corral to the surface.

Structural Interpretation

The main structural features of the French sink are similar to the Panning, Crawford and Witt sinkholes described by Walters (1977) and discussed earlier in this study (figures 6, 7, and 8). Walters depicts failure planes bounding the primary collapse portions of these sinkholes that resemble reverse faults. These failure planes are centered on the disposal well and diverge downwards from the surface. Walters omits any discussion of geometry character of these structures. These wedge type structures suggest the volume of material dissolved encompasses an area much larger at depth than apparent at the ground surface.

The five CMP sections that are the focus of this study show signs of a similar wedge or dome-shaped collapse structure centered at the French well.

Similar structures have been described previously that formed as a result of cavern breakdown (Davies, 1951). Davies defines breakdown as the "failure en masse of the roof or walls of caverns". Analysis of the stress regime acting on cavern roofs and walls prior to the time of collapse provides a likely mechanism for the dissolution structures observed on the seismic data.

Lithostatic load is the key to the development of breakdown (Davies, 1951). Before a cavern forms, the vertical and horizontal components of stress acting at any point in the subsurface are in equilibrium. Once an opening forms, these forces are no longer in equilibrium and a new stress regime develops forcing the roof and walls into the opening once the strength of the rock is overcome. Vertical stresses cause beds to drape (sag) and separate at physical contacts in the area above the cavern. The extent of this separation and sag is defined in three dimensions by a tension dome (figure 36). The amount of sag depends on the strength of the material. Assuming horizontal beds of similar physical strength, sag is greatest around a vertical axis centered on the opening (or cavity) and lessens upwards with decreasing depths. After separation, lithostatic load cannot be transmitted within the tension dome, causing stress to be transferred to adjacent rocks and to the walls of the cavity. Rock outside the tension dome has no direct impact on the mechanics of breakdown, it is the weight of the rock units within the dome that causes collapse. Failure general occurs first on a sagging beam closest to the wall where shear forces are the greatest (figure 37).

Collapse of rocks within the tension dome can be confined to the lowermost unit forming the ceiling where layer sag can extend to the point of failure. Depending on the rock properties and void specifics, massive breakdown result in the failure of successive beds within the dome. In the

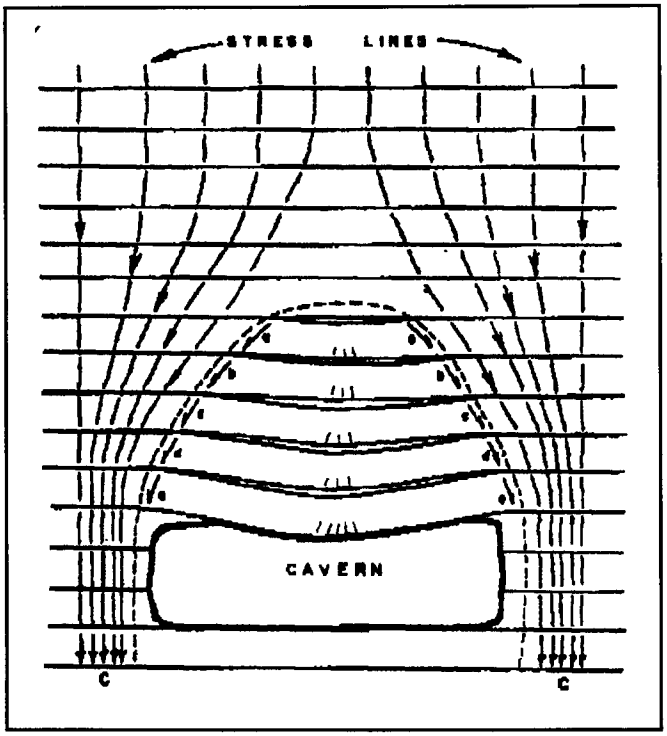

Figure 36. Tension dome and distribution of stress line around a cavern opening in horizontal strata (Davies, 1951).

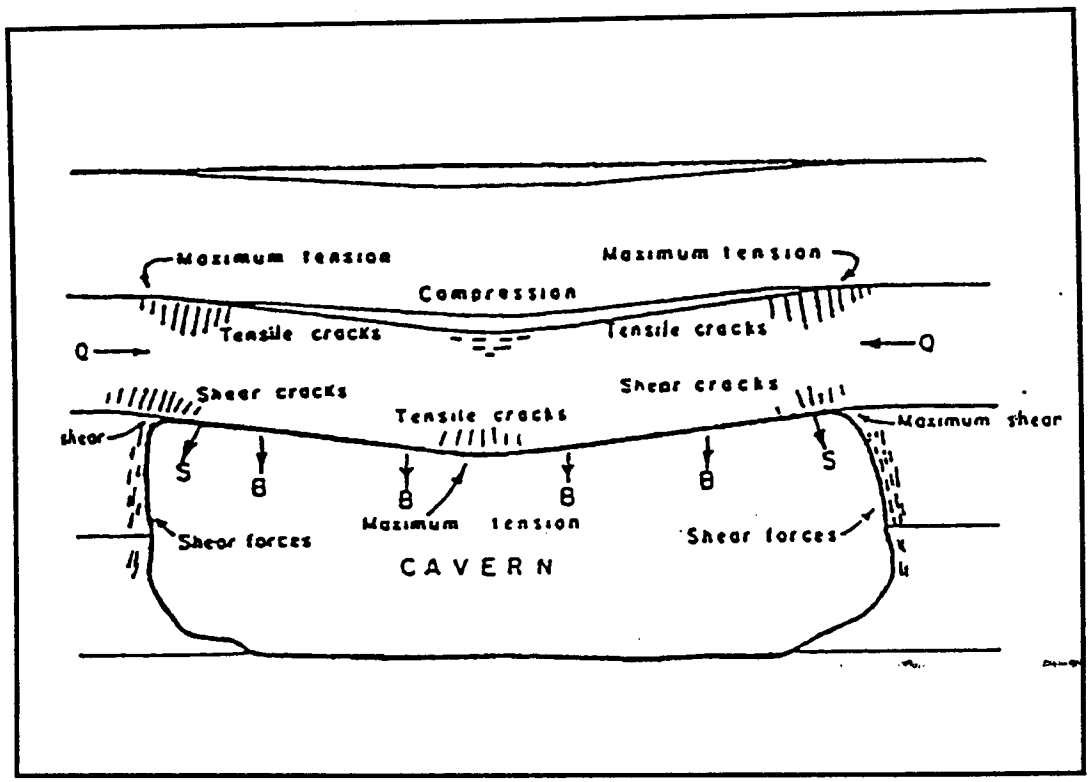

Figure 37. Shear and compressional stresses acting in a sagging beam (Davies, 1951).

latter, it is possible for failure to start in different locations within the dome. Depending on material properties and stress levels the lowest bed may collapse progressing gradually upwards into the overlying units or collapse can be initiated by failure of any unit within the dome. Most breakdowns can be attributed to the latter mechanism where a sagging bed within the dome fails rapidly, transferring its weight to the bed below. Failure of underlying units follows much like dominos due to increased load. Such a sequence of failures extends over a considerable vertical distance and typically culminates in roof collapse. Failure of intermediate layers within the dome are a plausible mechanism for catastrophic subsidence rates observed in select sinkholes throughout central Kansas.

Reflections in the vicinity of the French well represent beds that have undergone deformation and failure as defined by an arched boundary generally consistent with a tension dome (Davies 1951). This boundary is marked by a decrease in signal-to-noise ratio, apparent bed offset, and loss of coherency attributed to attenuation and scattering of energy along the planes (or in this case "zones") of failure. The dome extends vertically from the salt interval to the top of the section, is roughly symmetric in shape and appears generally centered on the French well (figure 34 – line1, trip2). The beds within this dome have undergone differing amounts of plastic and brittle deformation attributed to differences in strength of the various lithologies

within the dome. Lithologies can be ranked from weak to strong according to strength at room temperature and low confining pressure (Davis, 1984) (figure 38). Lithologies present at the French site most susceptible to ductile deformation are, in increasing order, shale, anhydrite and salt. Thus, the Stone Corral Anhydrite is more prone to ductile deformation than the overlying Harper shales and the underlying Ninnescah shales. An example that bares this out is shown in figure 31 (line1, trip1) between CMPs 2080 and 2140 and 250 and 280ms where the Stone Corral reflection possesses more deformation than the reflection a shale-sandstone interface within the Harper Formation directly above it.

In all five CMP stacks evidence exists supporting failure of the Stone Corral Formation along the tension dome boundary which marking the area of greatest shear stress. Lines 2 and 3 of the second trip and line 2 of the first trip show tensional cracks on the lower surface of the sagging anhydrite layer representing additional evidence supporting failure in the area of maximum tension (figure 37). This area lies near the center of the sagging anhydrite layer and is associated with the formation of tension cracks on its lower surface.

General Ranking of Lithology according to strength, based on tests at room temperature and low confining pressure	
Strongest	Quartzite
	Granite
	Quartz-Cemented Sandstone
	Basalt
	Limestone
	Calcite-Cemented Sandstone
	Schist
	Marble
	Shale/Mudstone
	Anhydrite
Weakest	Salt

Figure 38. Classification of common rocks according to strength (Davis, 1984).

Conclusions

The French sink was formed as a direct result of dissolution of the Hutchinson salt by brine disposal practices at the French "A" no. 1 well. The dissolution cavity and resulting tension dome controlling the subsidence mechanisms includes a volume no less than 1,000,000m^3. Since about 30 percent of this volume contains altered shale and anhydrite layers, the amount of dissolved salt can be estimated at 700,000m^3. Considering the amount of time the French was used as a disposal well, the amount of brines injected, and the typical salinity values for brines in the area, disposal practices alone can not account for all the dissolved salt.

After casing and grout failure, the French well bore served as a conduit for previously confined or perched groundwater to reach the salt interval. Fresh water moving through the well bore was probably introduced within the Permian redbed sequence. In general, the Stone Corral acts as an impermeable layer preventing water from shallower aquifers from reaching the salt, however, once a well penetrates it, a potential path of communication is established.

Two stages of dissolution are inferred from the stack. An initial one that was responsible for forming a cavity large enough to instigate the collapse of

the overlying units, which for the most part is confined to the tension dome. Initial activation of the subsidence process likely occurred when the gradual outward movement of the dissolution front to the point of roof rock failure. Collapse likely originated in units directly above the cavity, progressing slowly upward towards the surface. A second stage or mechanism of dissolution is inferred from deformation of units outside the area delimited by the tension dome. This later stage of dissolution probably involved movement of freshwater through pathways opened by failure within the tension dome during the first stage, especially in the immediate proximity of the fracture planes. Normal faulting is characteristic of this later stage of dissolution and consistent with the gradual outward progression of subsidence.

Information on the hydrostatic level at the French is crucial for understanding the dynamics of dissolution. Dissolution would be easily facilitated if the hydrostatic level of the borehole was below the salt interval. This scenario would provide a 100% man-made flow-through system with a continuous source of unsaturated brines in contact with the salt and a ready outlet for saturated brine to leave the salt area. Without a man made outlet (borehole) for saturated brine to leave the salt interval, a natural feature such as a fault, fracture, or paleo-sinkhole must be present. No evidence exists to support a natural escape route for brines.

The active dissolution front seems to extend outward from the center of the sink a radial distance between 200m and 250m. The Schulz #2 and Sutton 1-B wells (figure 11) located approximately 200m south and west of the French well respectively, were reported to have communication with the French during plugging procedures. A large void was encountered at the salt interval during plugging of the Sutton 1-B well by the KCC. Dissolution is occurring within confined, preferential halite horizons in the salt unit, advancing faster laterally then vertically across the salt interval.

References

Barbier, M. G., Bondon, P., Mellinger, R., and Viallix, J., 1976. MiniSosie for land seismology: Geophys. Prosp., 24, 518-527.

Baumgardner, Jr., R., W., Hoadley, A. D., Goldstein, A. G., 1982. Formation of the Wink Sink, a salt dissolution and collapse feature, Winkler County, Texas: Bureau of Econ. Geol., Report of Investigations, no. 114, 1-38.

Davies, W. E., 1951. Mechanics of cavern breakdown: National speleological socitey,13: 36-43.

Davies, W. E., 1949. Features of cave breakdown: National Speleological Society, 11:34-35.

Doveton, J. H., 1994. Geologic log Interpretation, SEPM, Short Course no. 29,1-169.

Ege, J. R., 1984. Formation of solution-subsidence sinkholes above salt beds: U. S. Geological Survey Circular 897, 1-11.

Fader, S. W., 1975. Land subsidence caused by dissolution of salt near four oil and gas wells in central Kansas: U. S. Geol. Surey, Water-Resources Investigations 27-75, 1-28.

Jennings, J. N., 1985, Karst Geomorphology: Basil Blackwell

Johnson, K., 1997. Evaporite karst in the United States: Carbonates and Evaporites, v 12, no. 1, 2-14.

Knapp, R. W., et al., 1989. Seismic reflection surveys at sinkholes in central Kansas: Preceedings, Symposium on Geophysics in Kansas, C. W. Steeples, ed., Kansas Geol. Survey Bull. 226, 95-116.

Liberty, L. M. and Knoll, M., 1998. Time varying fold in high-resolution seismic reflection data: a recipe for optimized acquisition and quality control processing and interpretation:

Martin, R. B., 1968. Relationship between quality of water in the Arbuckle Group and major structural features in central and eastern Kansas: M. S. thesis, University of Kansas, 1-79.

Martinez, J. D., Johnson, K. S., Neal, J. T., 1998. Sinkholes in Evaporite rocks: American Scientist, 86, 38-51.

Mayne, W. H., 1962. Horizontal data stacking techniques: Geophysics, 27, 927-938.

Miller, R. D., 1992. Normal moveout stretch mute on shallow –reflection data: Geophysics, 57, no. 11, 1502-1507.

Miller, R. D., and Xia, J., 1996. Shallow high resolution seismic reflection to delineate upper 400m around a collapse feature in central Kansas [Exp. Abs.]; in Technical Program Abstracts and Biographies: Soc. Explor. Geophys. 66th Ann. Mtg., 892-895.

Miller, R. D., Villella, A. C., Xia, J., 1997. Shallow high-resolution seismic reflection to delineate upper 400m around a collapse feature in central Kansas: Environmental Geosciences, 4, no. 3, 119-126.

Sheriff, R. E., and Geldart, L. P., 1995. Exploration Seismology, second edition: Cambridge University Press.

Sheriff, R. E., 1991, Encyclopedic Dictionary of Exploration Geophysics: Soc. Expl. Geophys.

Steeples, D. W., Knapp, R. W. and McElwee, C. D., 1986. Seismic reflection investigation of sinkholes beneath interstate highway 70 in Kansas: Geophysics, 51, no.2, 295-301.

Steeples, D. W., and Miller, R. D., 1990. Seismic reflection methods applied to engineering, environmental, and groundwater problems: Soc. Explor. Geophys. Volumes in Geotechnical and Environmental Geophysics, Stan Ward, vol1: Review and tutorial, 1-30.

Villella, A. C., 1997. Delineation of salt dissolution sinkholes using minimal deployment shallow 3-D seismic reflection surveying [Exp. Abs.]; in Technical Program Abstracts and Biographies: Soc. Explor. Geophys. 67th Ann. Mtg.,

Walters, R. F., 1977. Land subsidence in central Kansas related to salt dissolution: Kansas Geol. Survey Bull. 214, 1-82.

Walters, R. F., 1991. Gorham Oil Field: Kansas Geol. Survey Bull. 228, 1-112.

Watney, W. L., Berg, J. A. and Paul, S., 1988. Origin and distribution of the Hutchinson Salt (lower Leonardian) in Kansas: Midcontinent SEPM Special Publication No. 1.:113-135.

White, W. B., 1988. Geomorphology and hydrology of karst terrains: Oxford University Press.

Yilmaz, O., 1987. Seismic Data Processing: Soc. Expl. Geophys.

Zeller, D. E., 1968, The stratigraphic succession in Kansas: Kansas Geol. Survey Bull. 189, 1-81.

Plate 1 - CMP Stack From Line 1 Trip 1

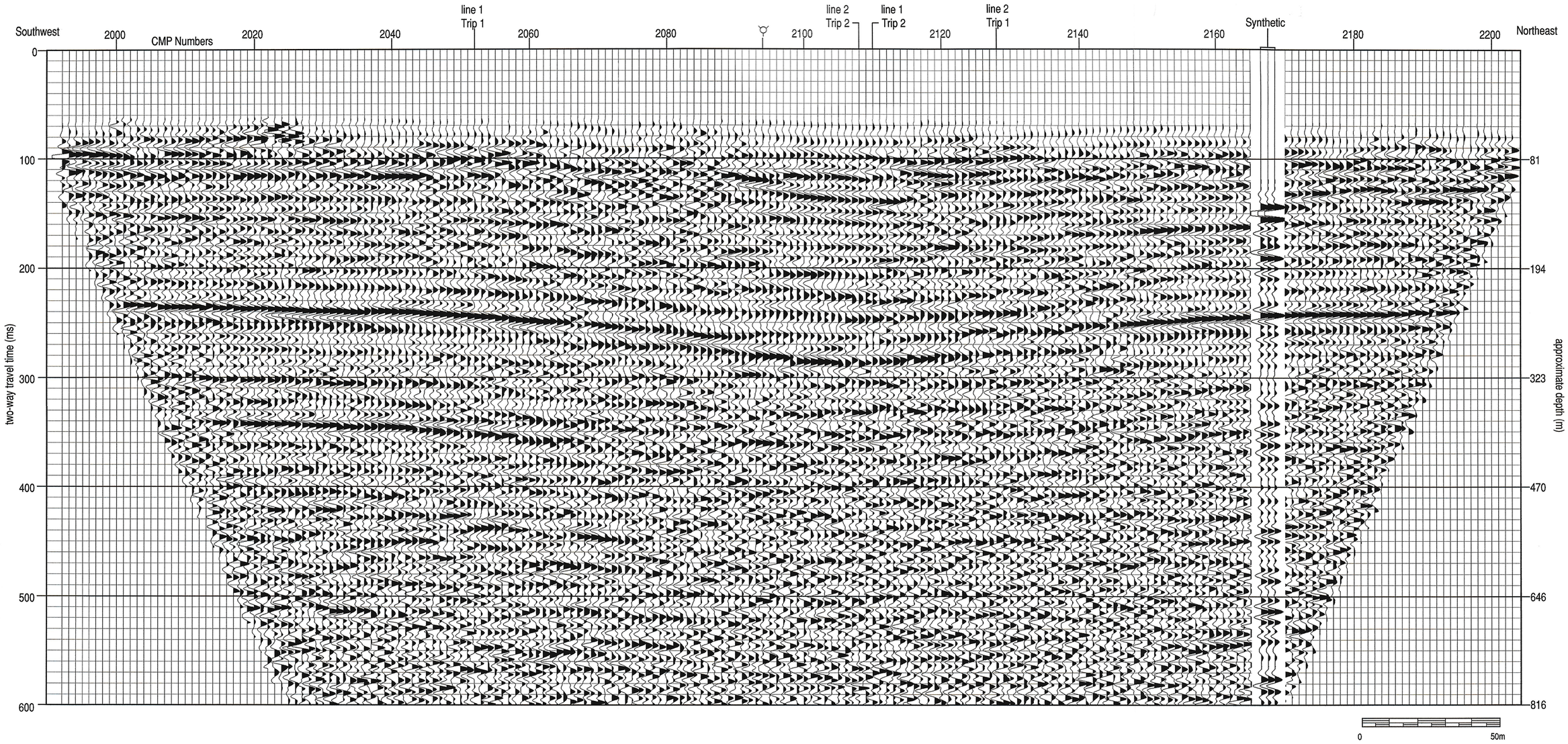

94c

94c

Plate 2 - CMP Stack From Line 2 Trip 1

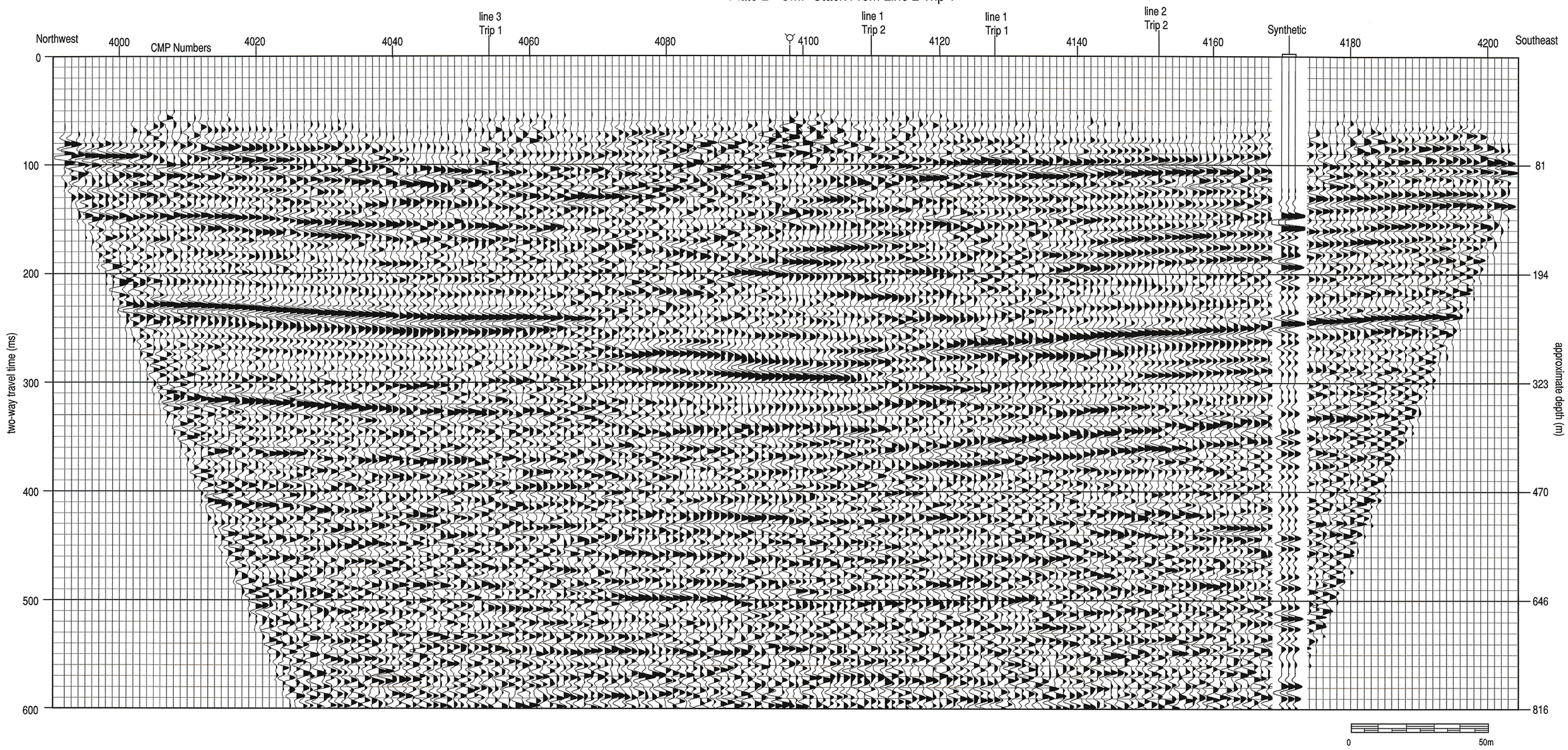

94 b

94 b

Plate 3 - CMP Stack From Line 3 Trip 1

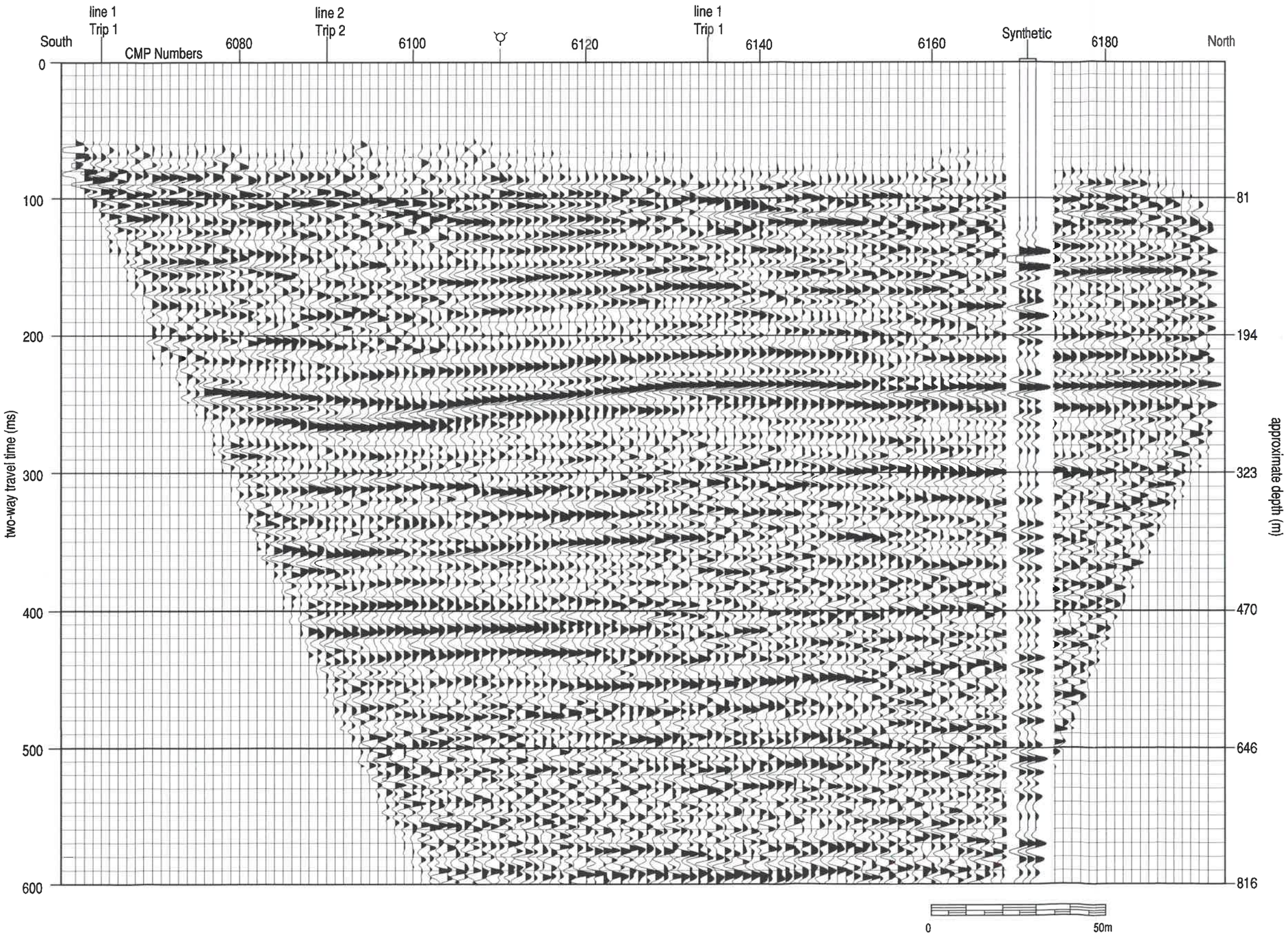

94a

Appendix 1. Type log for Stafford County.

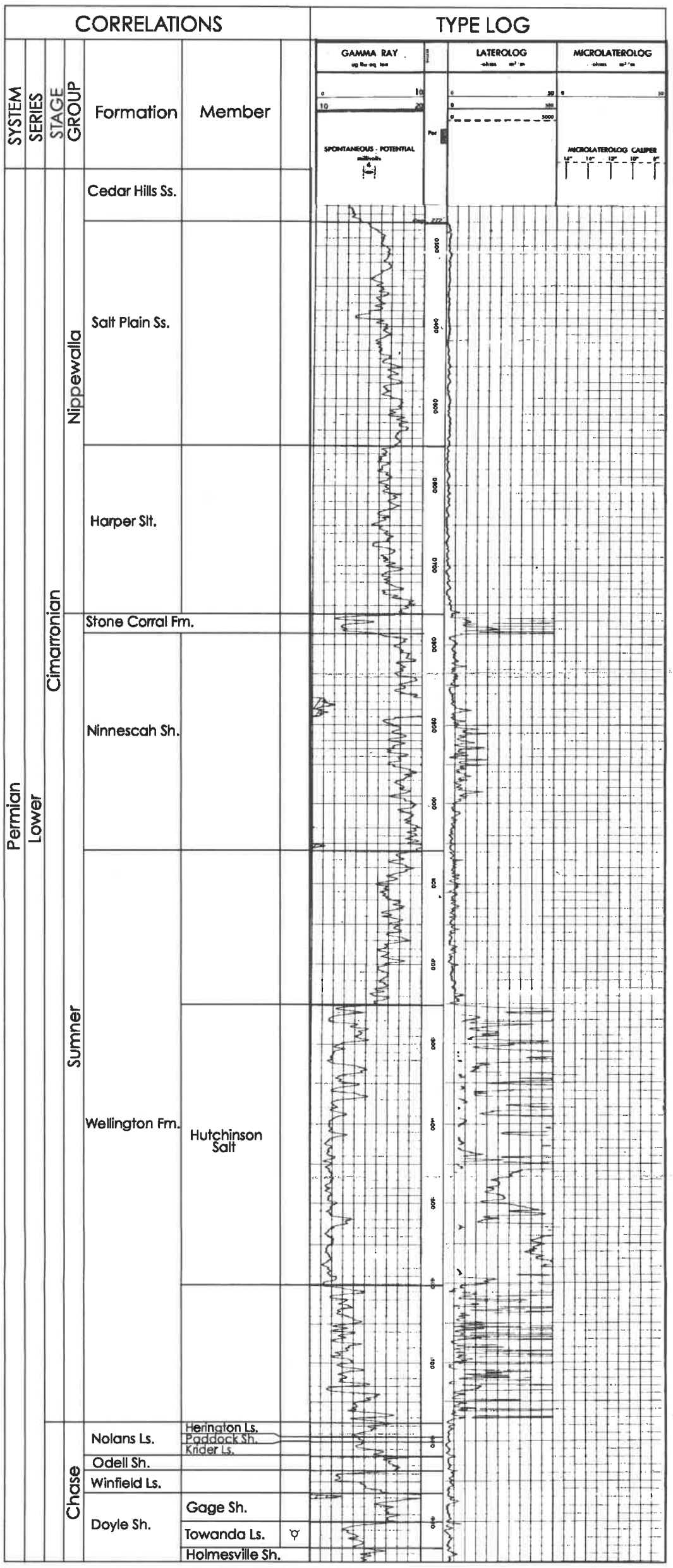

Appendix 2. Topographic map of the study site

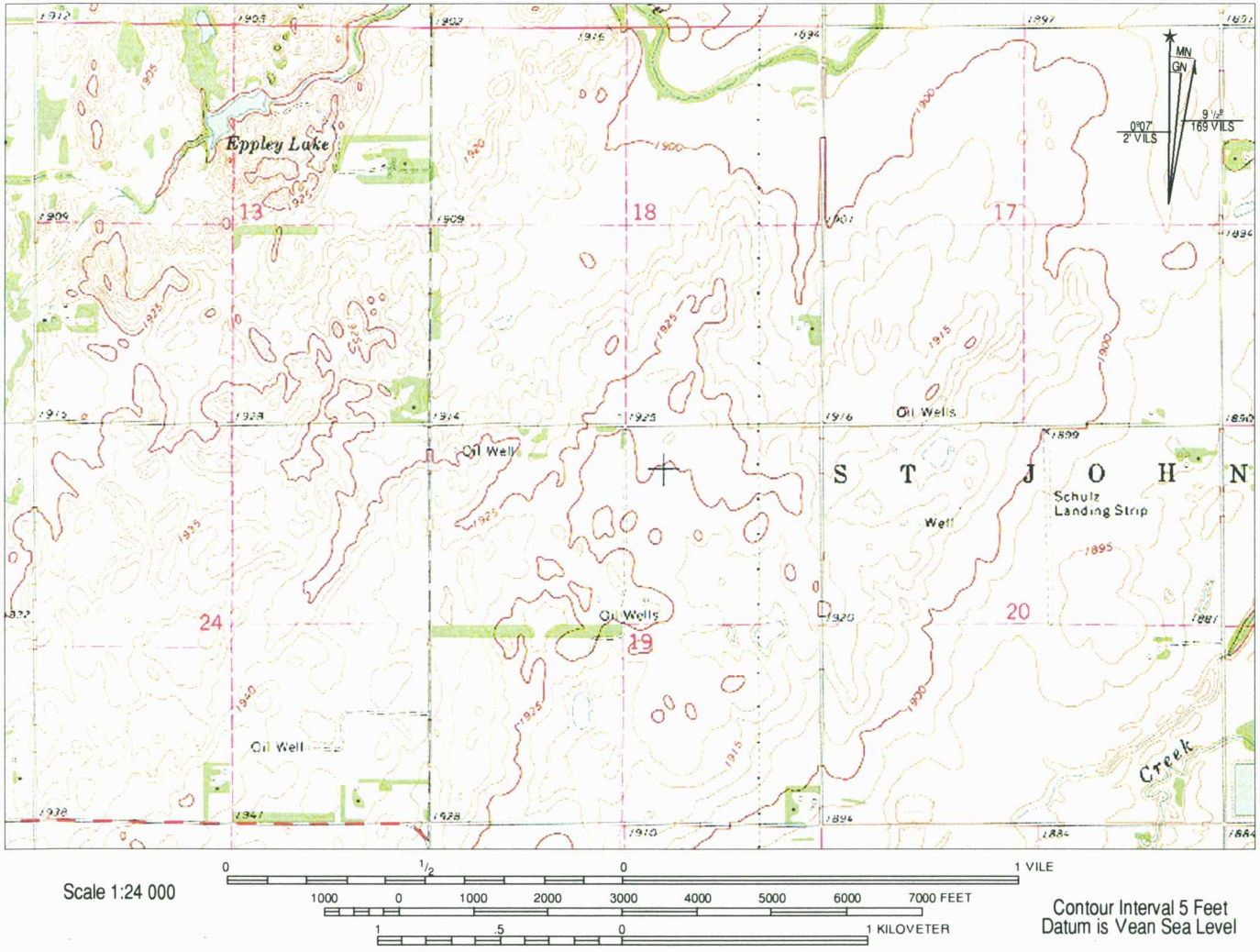

Scale 1:24 000

Contour Interval 5 Feet
Datum is Vean Sea Level

Appendix 3 - SEG Expanded Abstract

Delineation of salt dissolution sinkholes using minimal deployment shallow 3-D seismic reflection surveying

Ana C. Villella, Jianghai Xia, and Richard D. Miller, Kansas Geological Survey*

SUMMARY

The advantages of 3-D seismic imaging are well founded for petroleum applications. Significant potential exists for this technique in delineating targets critical to shallow site characterization. The high cost and high technology nature as well as many assumptions appropriate for deeper petroleum problems are not realistic or feasible for near surface applications. A low fold, minimal cost 3-D survey designed around common offset and shallow seismic reflection techniques at a salt dissolution sinkhole in central Kansas provided valuable insight into the effectiveness and potential of minimal deployment 3-D surveys to delineate major structural features. Volumetric display enhanced the interpretability of this low cost but effective 3-D survey.

INTRODUCTION

Salt dissolution sinkholes are a common hazard in areas of petroleum disposal wells and solution mining in southcentral Kansas (Walters, 1977). The structural framework of these sinkholes is often complex and can rarely be understood from their surface expression. Hazards during the plugging of leaking wells and selection of appropriate grout horizons in problematic disposal wells are aspects of the remediation process where quick and cost effective images of the subsurface are important and feasible with seismic reflection techniques.

Two-dimensional seismic reflection surveys throughout Kansas have imaged the subsurface expression of sinkholes with some success (Miller et al., 1985; Knapp et al.,1989; Miller et al.,1996). Nevertheless, the irregular nature of the dissolution cavities impedes examination of 3-D structures with the 2-D lines alone. Control on fault orientation, structural relationships and differential growth predictions are a few of the problems not accounted for in previous studies.

Recent attempts have been made to apply 3-D petroleum techniques to near surface investigations (House et al., 1996; Siahkoohi and West, 1996; Lanz et al., 1995). The high cost of this technology makes it economically unfeasible for many shallow targets. Furthermore, complete evaluation of the method as it relates to near surface targets has been proposed to reduce and hopefully eliminate misuse and/or overselling of the technique for shallow applications.

This study evaluates a survey designed to investigate a sinkhole using common tools available for most near surface seismic reflection investigations, with a focus on particular issues:

- minimized cost
- minimized data with minimal detriment to image
- quick appraisal of structure
- use of lowcost 2-D software
- extrapolate between 2-D lines

The result is a low fold 3-D survey acquired using a fixed patch, sorted into 3-D CMPs and processed using 2-D algorithms.

DISCUSSION

Geology and previous seismic work:
The French sinkhole in southcentral Kansas is the focus of this study. The French Sink was formed in the vicinity of a disposal well which inadvertantly placed unsaturated brines in contact with evaporite sequences of the Hutchinson Salt Member of the Permian Wellington Formation. Dissolution of the salt beds caused the flexure and failure of the overlaying rocks, resulting in surface subsidence.

Several 2-D seismic surveys have been successful imaging the subsurface around sinkholes formed by dissolution of the Hutchinson Salt throughout Kansas. A recent survey conducted by the Kansas Geological Survey at the French Sink (Miller et al., 1996) produced images of the shallow subsurface with higher resolution and signal-to-noise than any of the previous investigations. In most studies, the most prominent reflections come from anhydrite layers within the salt sequence, and from the Stone Corral Formation above the salt. At the French site, the Stone Corral reflection can be observed at 240ms (240m) and reflections from the top of the salt identifiable at 310ms (400m). The high signal-to-noise ratio and potential resolution of 2-D CDP stacks from the French Sink reveals a conjugate set of normal and reverse faults centered on the disposal well.

Data acquisition :
The Stone Corral Formation is a seismic marker bed the survey was designed to target. Expanding the imaged depth window to include layers less than 60m deep and as deep as 600m was possible through careful parameter design and on-site testing. A fixed spread of 96 receivers was laid out in a square around the water filled sinkhole with 5 m spacing between stations. Shot locations were along the sides of two squares stepping out symmetrically 50 and then 100m from the square receiver spread (fig 1). The source was an IVI Minivib programmed to deliver three individually recorded up-sweeps from 30 to 300Hz. The pilot was real time telemetried to the seismograph with each of the three sweeps recorded individually on the seismograph with their pilot, correlated and vertically stacked.

Data were recorded on two 48-channel, 24-bit Geometric Strata View seismographs networked for simultaneous 96-channel recording. Shot gathers were stored correlated in SEG2 format. Three 40Hz L28E Mark Products geophones were grouped in a 1ft circle. The simple design of this survey was intended to evaluate the effects of reducing the number of shot locations allowing data to be acquired in half a day. Crop land use in the southern portion of the study area prevented access to a few shot locations causing a slightly irregular fold distribution (fig 2).

Processing:
The basic processing flow was consistent with routine 2-D shallow reflection methodologies. Data were sorted into and processed as fifteen 2-D lines with source and receiver locations along each CMP line spatially distributed around the entire patch. This source receiver geometry resulted in low fold and irregular distribution of CMP locations which required resorting to an optimal bin size of 2.5m by 15m (fig 2). This rectangular binning preserved the integrity of the spatial resolution while increasing the CMP fold and velocity analysis control. The data were analyzed and moved out using two dimensional routines iterating between N-S and E-W directions until stack response was satisfactory.

RESULTS

This 3-D data set contains reasonable signal-to-noise ratio despite its low fold content (fig 3). The final stack sections are interpreted to possess structural features consistent with the 2-D lines. The Stone Corral reflection can be traced throughout the data volume exhibiting signs of both flexure and fault disturbance (fig 4). The lack of reflections at depths shallower than the Stone Corral event did not allow for confirmation of normal and reverse fault styles previously suggested on 2-D sections. This loss of coherent energy at shallow depths can be attributed to insufficient close offsets and reduced signal-to-noise ratio (likely due to fold) in comparison to the 2-D data. Fault deformation is also supported by diffractions produced at the edge of faulted Stone Corral blocks. A maximum vertical drop of about 20ms is interpreted at the center of the sink. Such diffractions are only present at lines sorted along the N-S direction, suggesting a preferential E-W direction of faulting. It is most likely these Fresnel zone-related diffractions were not observed in any of the 2-D lines since CDP locations were outside the area of maximum vertical displacement. Remarkable arrival patterns in response to bed termination and layers smaller than the radius of the first Fresnel zone are interpreted on some sections.

CMPs sparsely sampled the subsurface of a 220m by 220m patch centered on the sinkhole. Asymmetry in their distribution was caused by absence of shot points in the southeastern corner of the study area. The inability to shoot over the water filled sinkhole resulted in poor imaging of the center of the structure. Spatial sampling was satisfactory in light of the few number of shot points and recording channels.

The 2-D processing in both N-S and E-W directions helped define lateral variations in stacking velocity. 3-D volume display of the data assisted considerably in the interpretation of major structural features.

CONCLUSION

This study resulted in a low fold 3-D profile with reasonable stacking response. Consistency between interpretations of the 2-D and 3-D stacks is encouraging. The tradeoff between data redundancy and spatial sampling in the 3-D survey did not seem to significantly compromise the quality of the stacked sections. The lower signal-to-noise ratio of the 3-D profile allowed confirmation of only major structures observed in the 2-D lines. The greater spatial distribution of this survey assisted extrapolation of 2-D interpretations. Low cost and short turnaround were definite advantages. This survey minimized many of the more expensive and in some cases advantagious aspects of 3-D surveying to represent a good low-fold, low cost compromise. Plans are underway to double the number of shots and increase the layout to include 4 unique patches in hopes to evalution improvements and eventually determining optimum 3-D program for the objectives of this project.

REFERENCES

Ege, J.R., 1984, Formation of solution-subsidence sinkholes above salt beds: U.S. Geological Survey Circular 897, 11 pp.

House, J.R., T.M. Boyd, and F.P. Haeni, 1996, Haddam Meadows, Connecticut: A case study for the acquisition, processing, and relevance of 3-D seismic data as applied to the remediation of DNAPL contamination; In P. Weimer and T.L. Davis, eds., AAPG Studies in Geology #42 and SEG Geophysical Development Series #5: AAPG/SEG, Tulsa, p. 257-266.

Knapp, R.W., Steeples, D.W., Miller, R.D. and McElwee, C.D., 1989, Seismic reflection surveys at sinkholes in central Kansas: Geophysics in Kansas, D.W Steeples, ed., Kansas Geological Survey Bulletin 226, p. 95-116.

Lanz, E., A. Pugin, A. Green, and Horstmeyer, 1996, Results of 2- and 3-D high-resolution seismic reflection surveying of surficial sediments: Geophys. Res. Lett. 24, 491-494.

Miller, R.D., Steeples, D.W. and Treadway, J.A., 1985, Seismic reflection survey of a sinkhole in Ellsworth County, Kansas: Technical Program Abstracts and Biographies, 55th Annual Meeting, Society of Exploration Geophysicists, Washington DC, p.154-156.

Miller, R.D. and Xia, J., 1996, Shallow high resolution seimic reflection to delineate upper 400m around a collapse feature in central Kansas: Technical Program Expanded Abstracts with Author's Biographies, 66th Annual Meeting, Society of Exploration Geophysicists, Denver CO, p.892-895.

Walters, R. F., 1977, Land Subsidence in central Kansas related to salt dissolution: Kansas Geological Survey Bulletin 214, 82p.

Siahkoohi, H.R., and G.F. West, 1996, 3-D seismic imaging of complex structures in glacial deposits [Exp. Abs.]: Soc.of Explor. Geophys. 1, 873-876

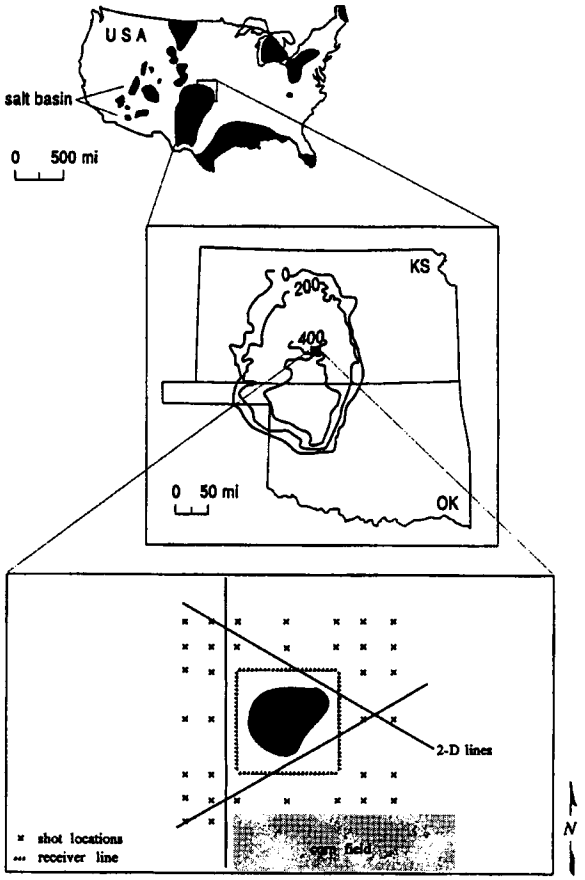

Fig 1. Site map showing relative locationsof (a) major salt basins in the United States (Ege, 1984) with (b) a generalized isopach map of the Hutchinson Salt Member in Kansas and Oklahoma (Walters, 1977), and (c) the relative location of the seismic reflections to the sinkhole.

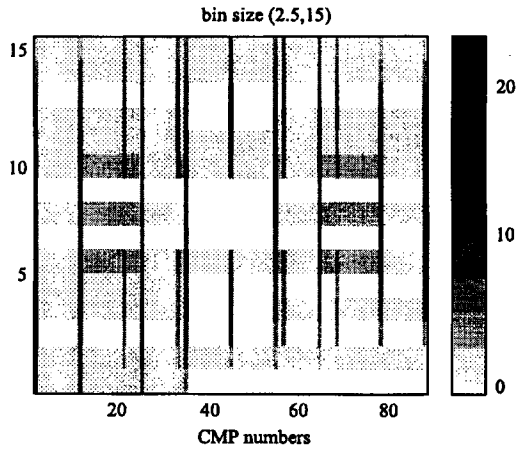

Fig2. Foldmap showing optimal bin size of 2.5m by 12m.

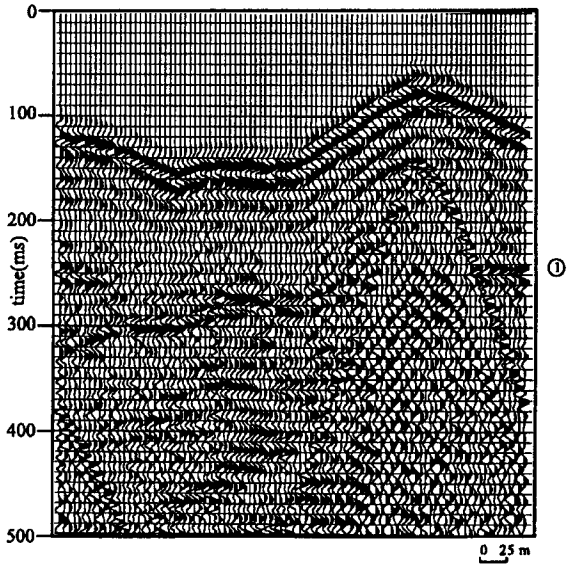

Fig 3. Filtered shot gather with Stone Corral anhydrite identified ①.

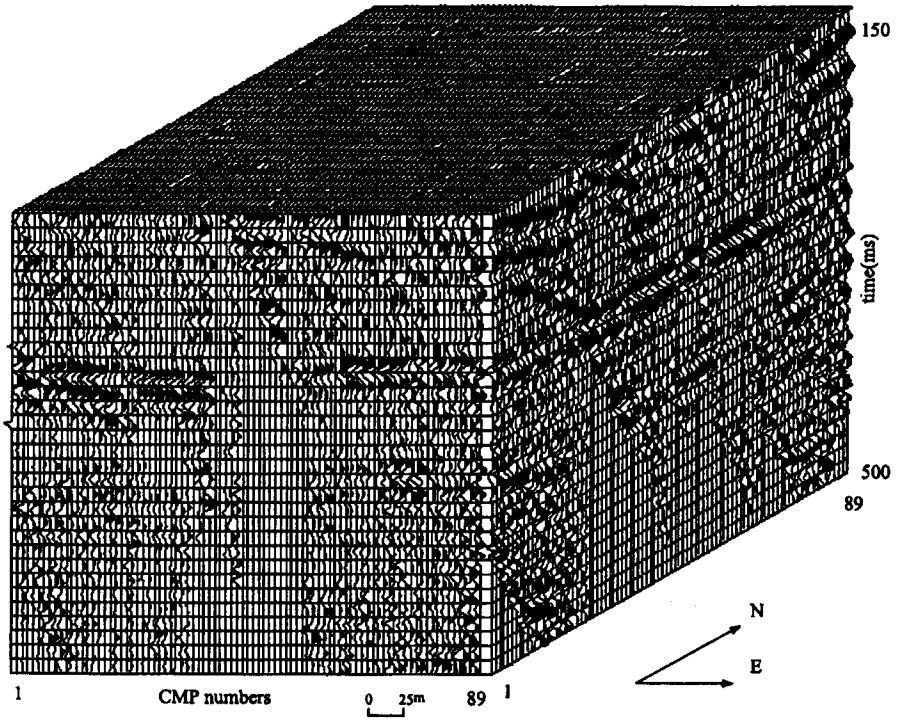

Fig4. Volumetric representation of CMP stack data.

Plate 4 - CMP Stack From Line 1 Trip 2

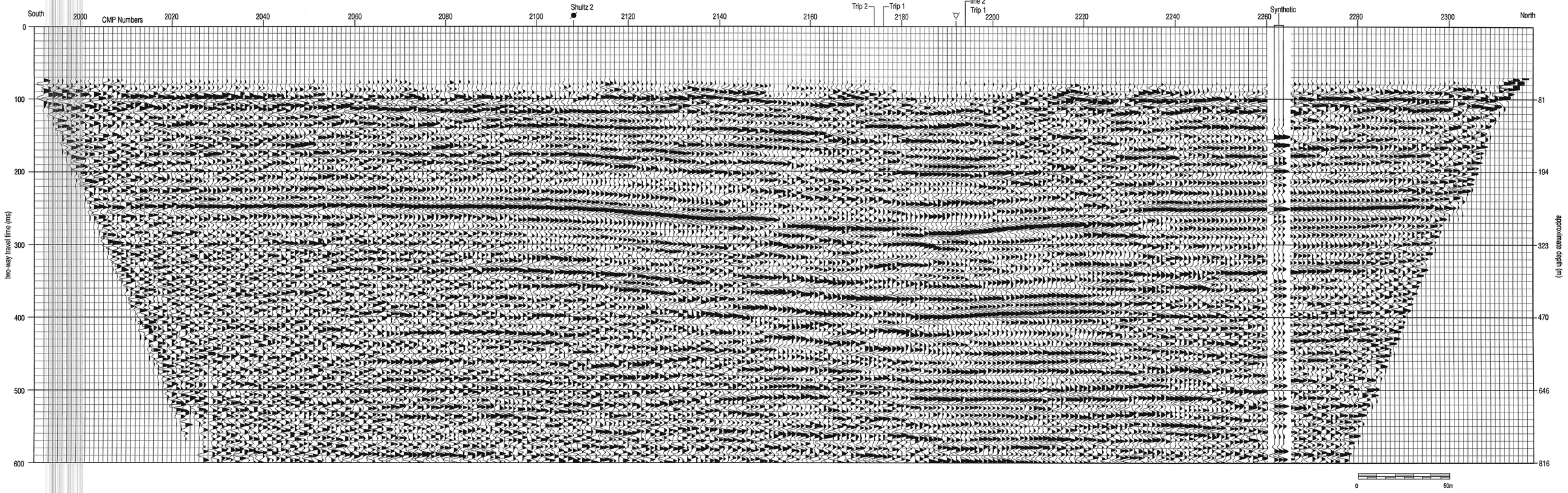

Plate 5 - CMP Stack From Line 2 Trip 2

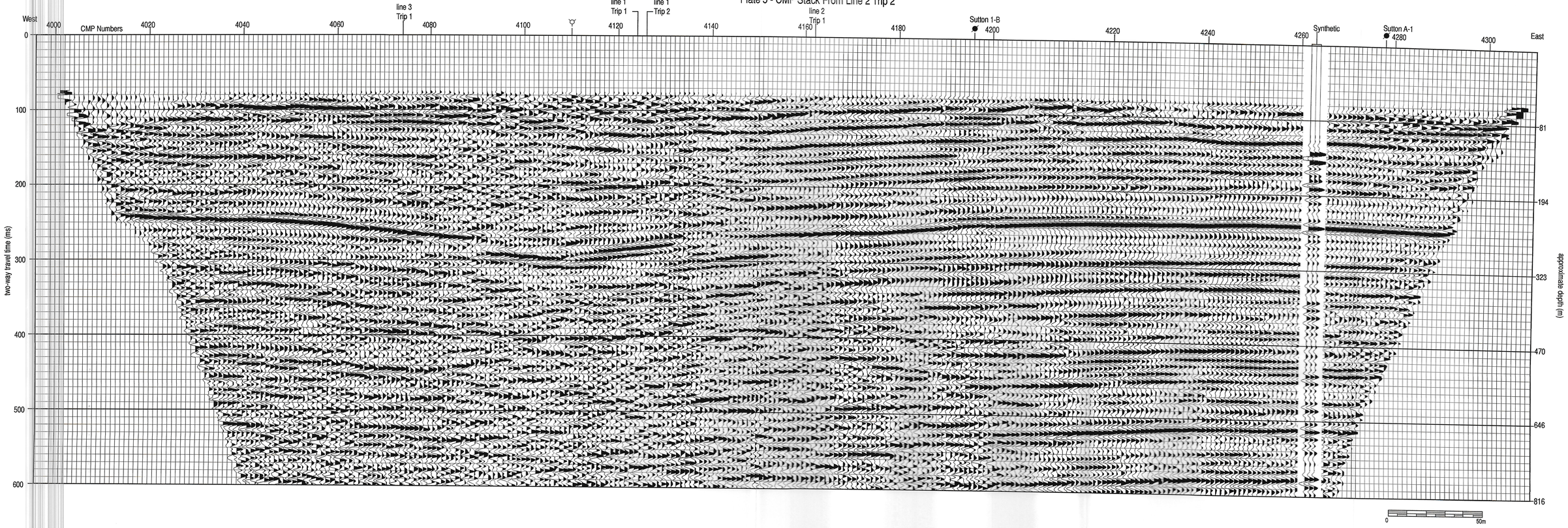

Plate 6 - True-Fold Map From Line 1 Trip 1

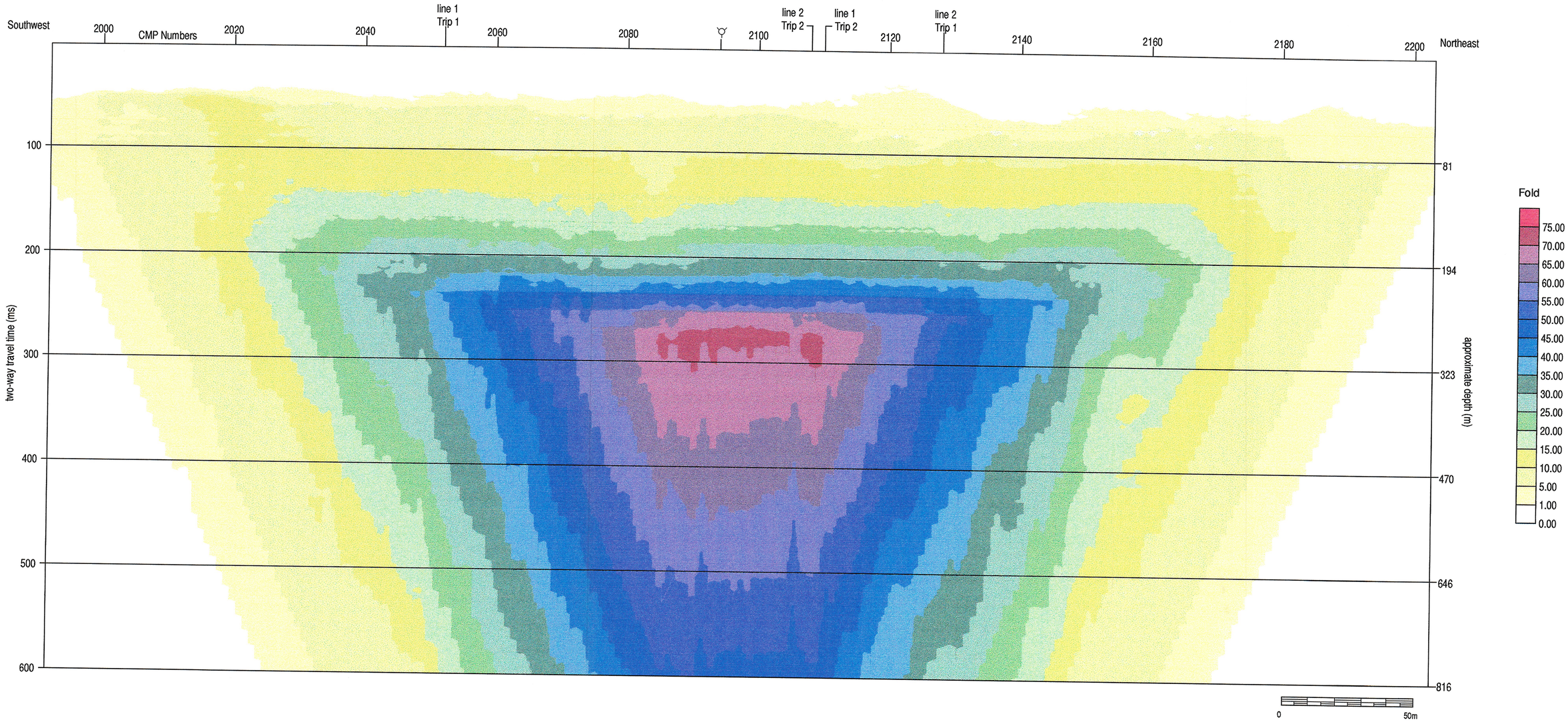

Plate 7 - True-Fold Map From Line 2 Trip 1

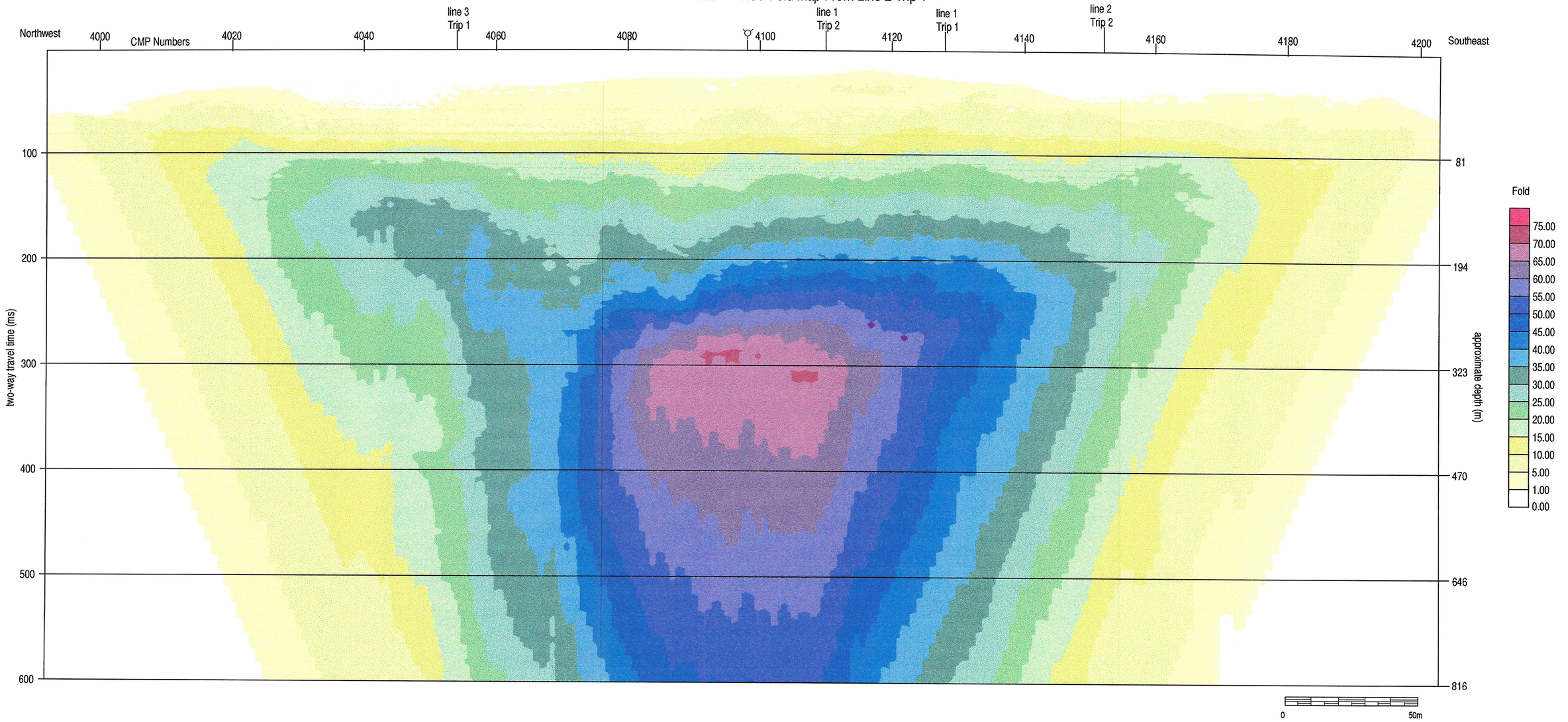

Plate 8 - True-Fold Map From Line 3 Trip 1

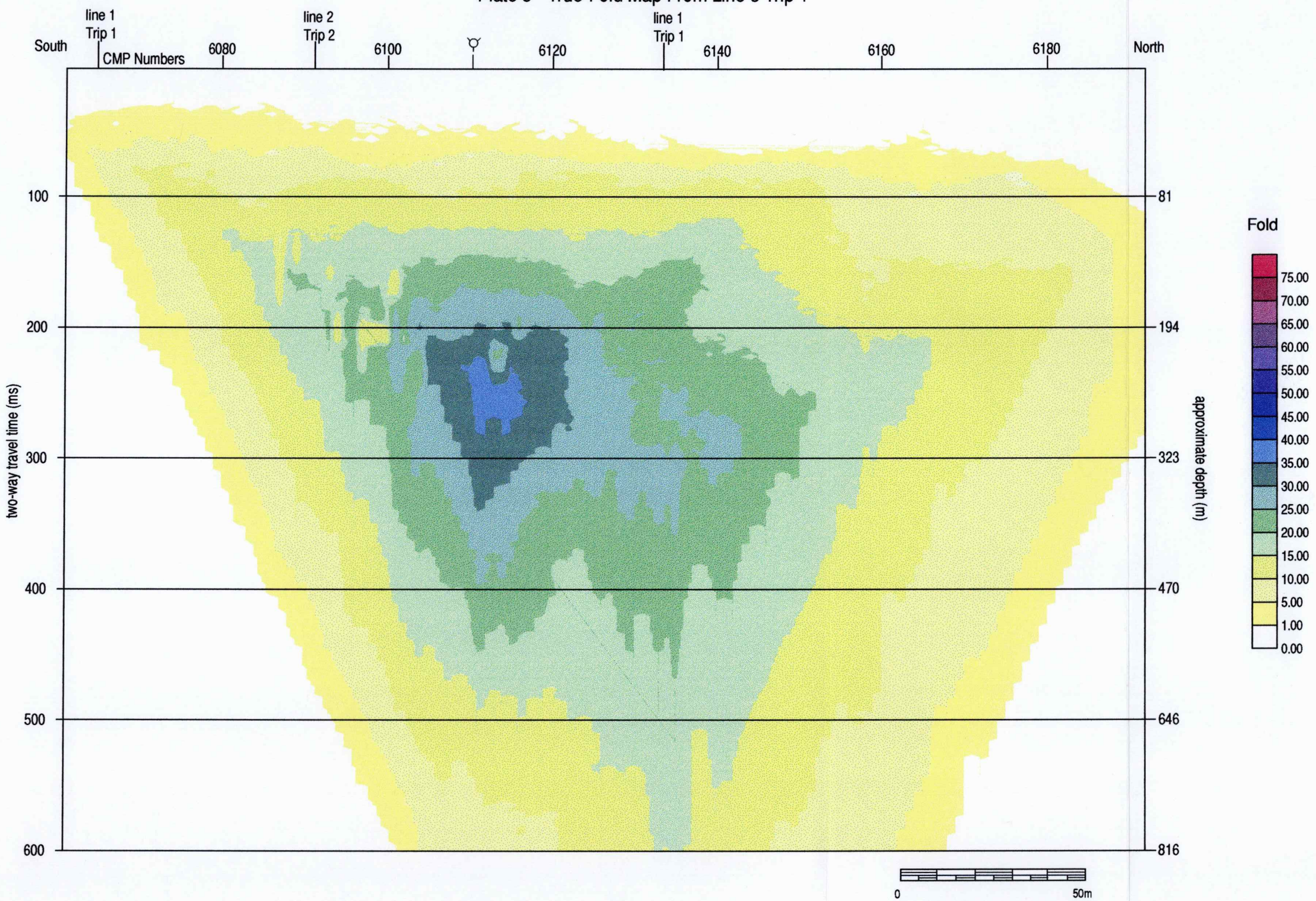

Plate 9 - True-Fold Map From Line 1 Trip 2

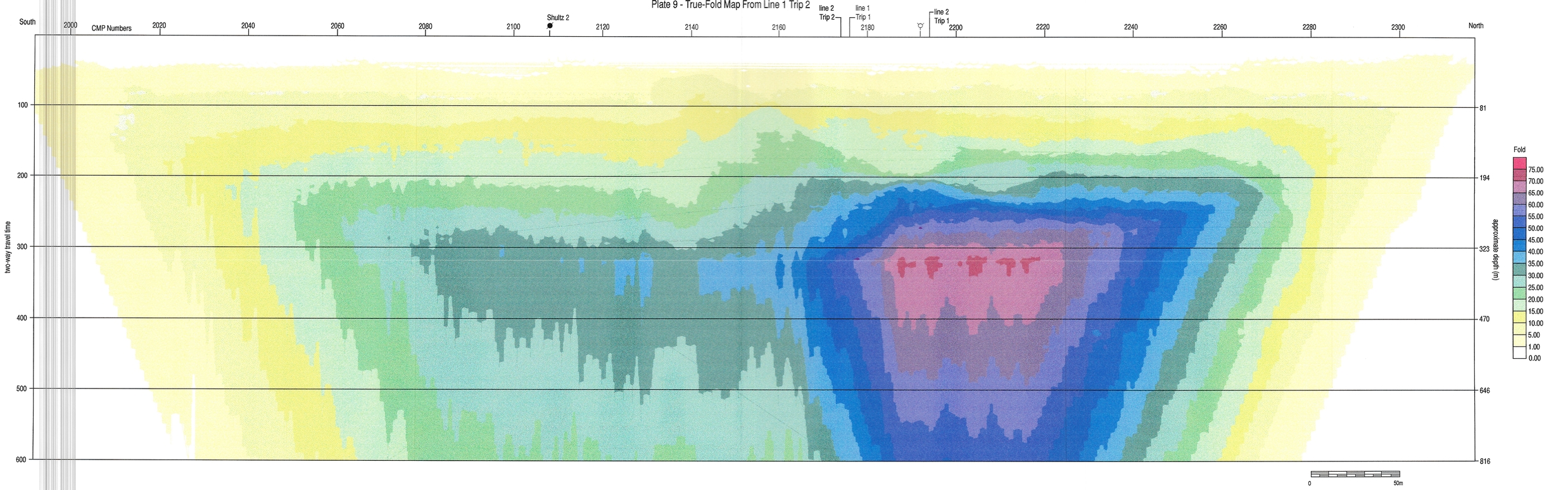

Plate 10 - True-Fold Map From Line 2 Trip 2

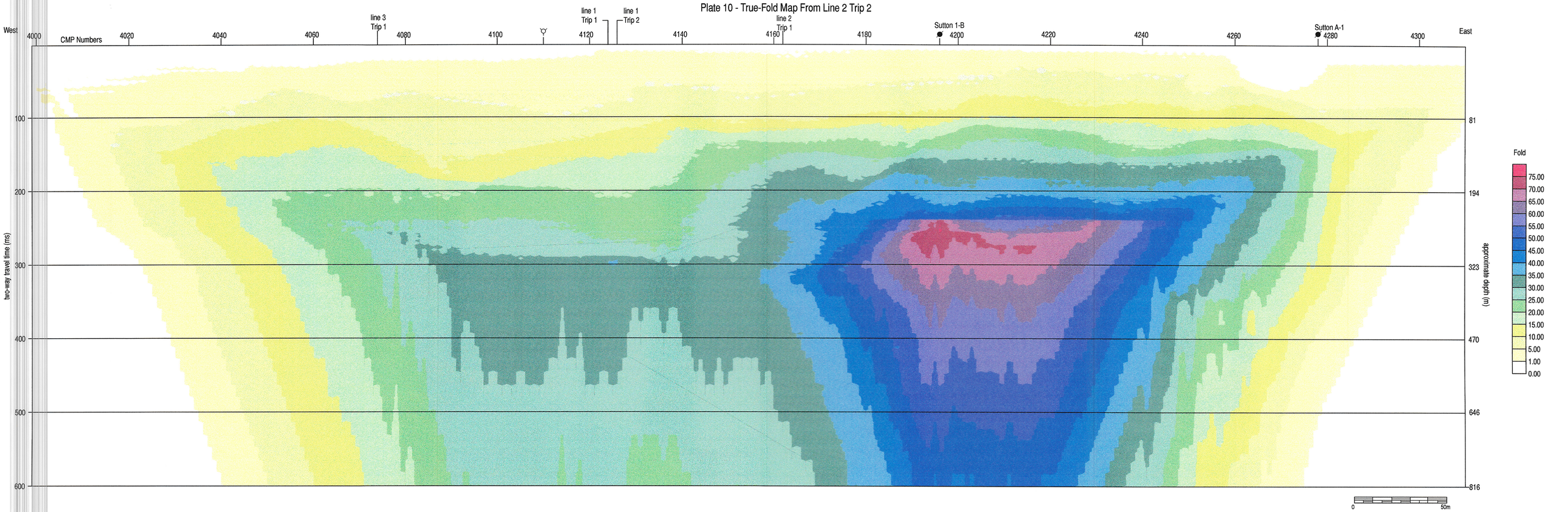

Plate 11 - Decimated CMP Stack From Line 1 Trip 2

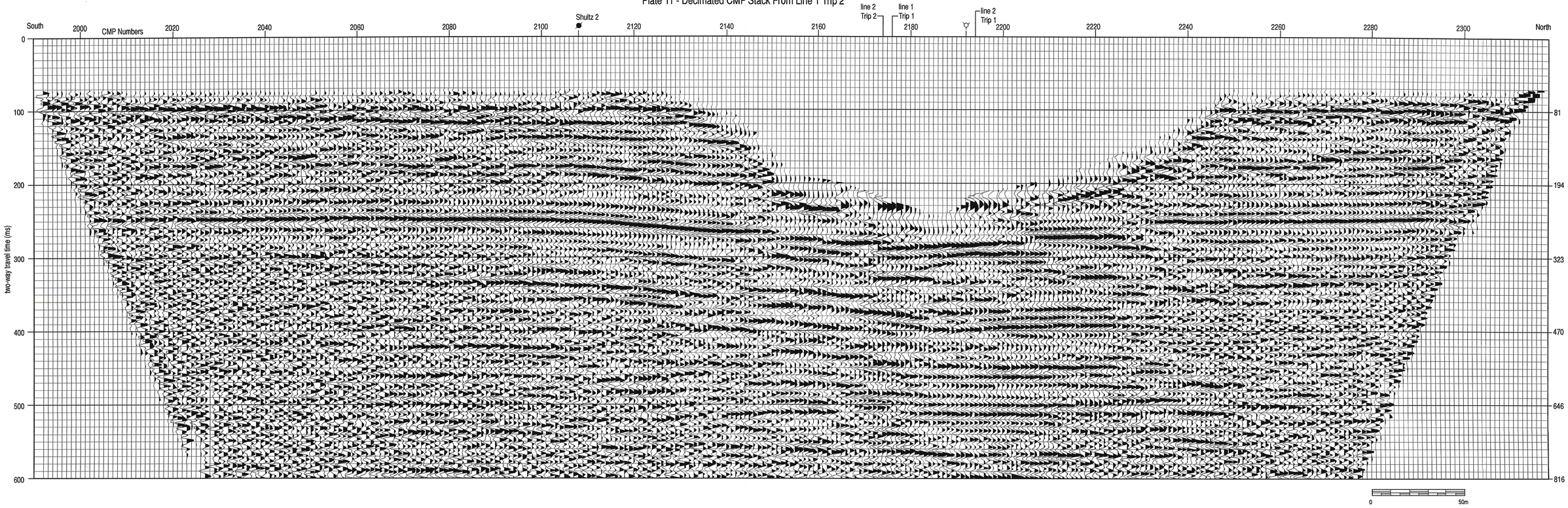

Plate 12 - Decimated True-Fold Map From Line 1 Trip 2

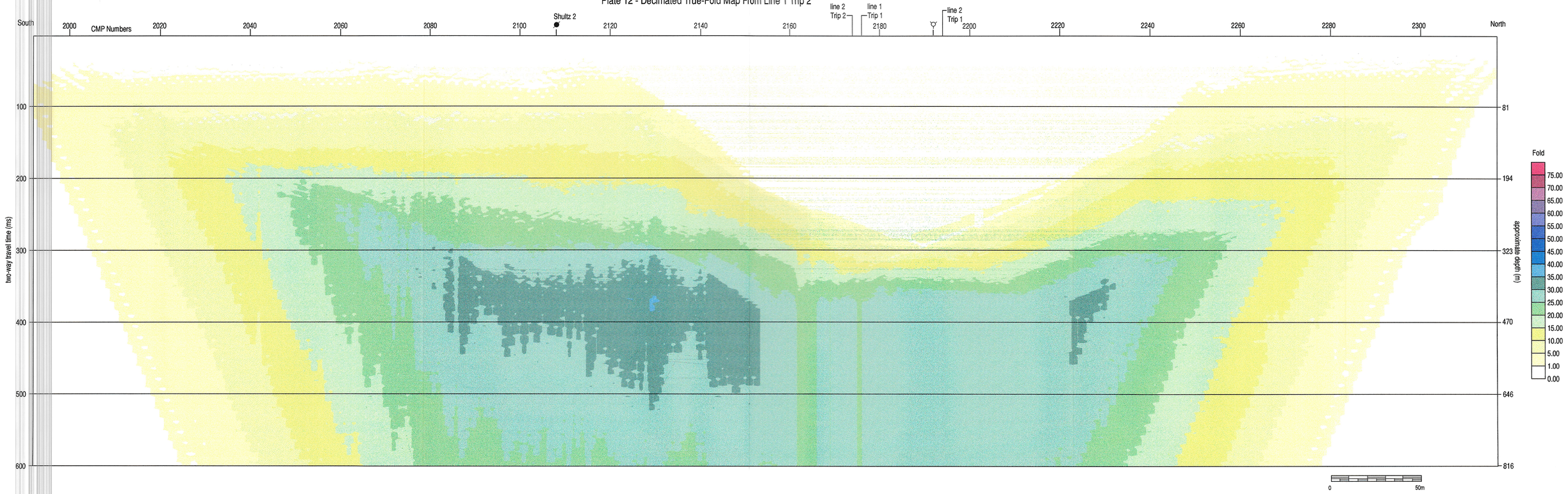

Plate 13 - Decimated CMP Stack From Line 2 Trip 2

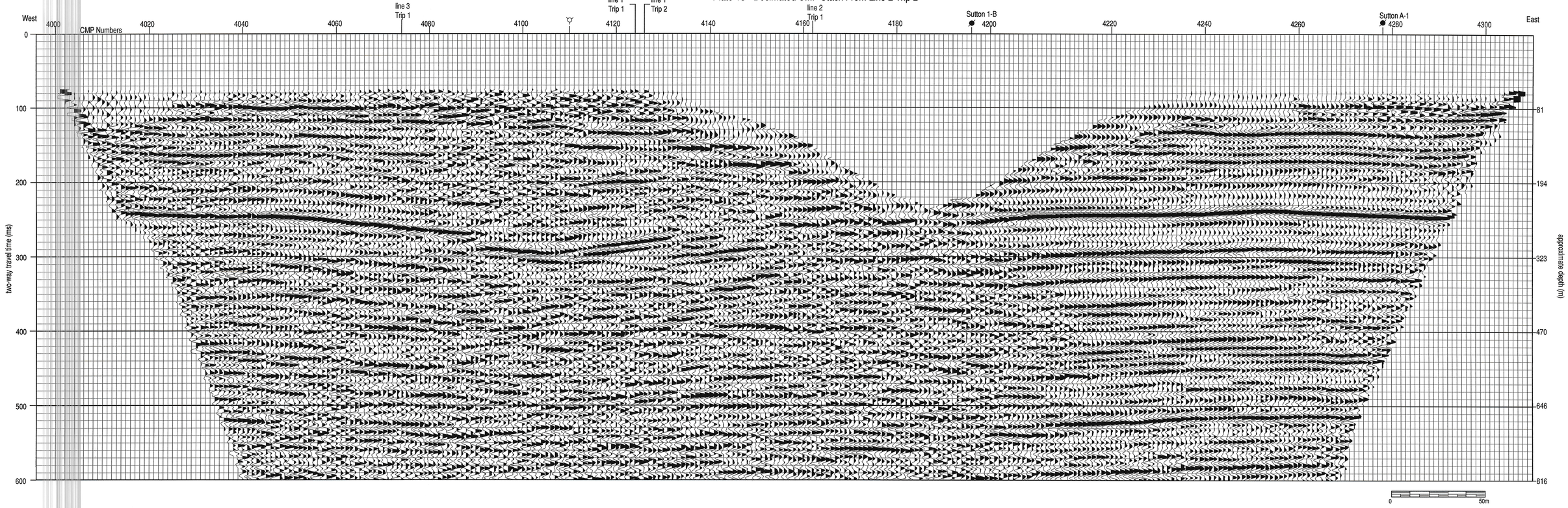

Plate 14 - Decimated True-Fold Map From Line 2 Trip 2